

**Acoustic characterization of seafloor and
benthic habitats using single and multi-beam
backscatter data**

A Thesis submitted to Goa University for the Award of the Degree of

DOCTOR OF PHILOSOPHY

in
Marine Sciences

By

Haris. K

Research Guide

Bishwajit Chakraborty

Goa University

Taleigao, Goa

2015

To umma and uppa

Statement

As required under the University ordinance OB-9.9 (v-vi), I state that this thesis entitled *Acoustic characterization of seafloor and benthic habitats using single and multi-beam backscatter data* is my original contribution and it has not been submitted on any previous occasion.

The literature related to the problem investigated has been cited. Due acknowledgements have been made wherever facilities and suggestions have been availed of.

HARIS. K

CSIR-National Institute of Oceanography, Goa.

23 June 2015

Certificate

This is to certify that the thesis entitled *Acoustic characterization of seafloor and benthic habitats using single and multi-beam backscatter data*, submitted by Haris. K to the Goa University for the degree of Doctor of Philosophy, is based on his original studies carried out under my supervision. The thesis or any part thereof has not been previously submitted for any other degree or diploma in any university or institution.

BISHWAJIT CHAKRABORTY

CSIR-National Institute of Oceanography, Goa.


23 June 2015

Vita

K. Haris

*Geological Oceanography Division
CSIR-National Institute of Oceanography
Dona Paula, Goa, India 403004*

 +91 (0) 832 2450494

 Mobile +91 9545385384

 harihassainar@gmail.com, kharis@nio.org

Education

- 2012–Present **Ph.D. in Marine Science**, *Goa University, Goa, India (Thesis submitted).*
- 2008–2010 **M.Tech. in Ocean Technology**, *Cochin University of Science and Technology, Kerala, India (8.69 CGPA).*
- 2006–2008 **M.Sc. in Physics**, *Aligarh Muslim University, Aligarh, India (66 %).*
- 2003–2006 **B.Sc. in Physics**, *Calicut University, Kerala, India (88 %).*

Experience

- 2015–Present **Project Assistant III**, *CSIR-National Institute of Oceanography, Goa, India.*
- 2011–2015 **Senior Research Fellow**, *CSIR-National Institute of Oceanography, Goa, India.*
- 2010–2011 **Project Assistant II**, *CSIR-National Institute of Oceanography, Goa, India.*

Achievements

- Complimentary EGU membership for the calendar year 2014.
- Senior Research Fellowship (SRF) for doctoral studies by *CSIR*, India, in Earth, Atmospheric, Ocean and Planetary Sciences, 2011.
- Merit scholarship by *AMU Alumni Association of Northern California*, 2006–2008.
- State Merit Scholarship (SMS) by *Govt. of Kerala*, India, 2003–2006.

Professional Interests

- High-frequency seafloor acoustics
- Hydroacoustics
- Scaling and multifractal studies
- Underwater ambient noise and Bioacoustics

Professional Training / Courses

- GulfEx 11** Participated in *GulfEx 11* program of APL, University of Washington, a shallow water experiment at Gulf of Mexico, Florida, USA (April 2011).
- Training on** Multibeam Echo-sounder (EM 302 & EM 1002) & Seafloor Information System: Delivered by Kongsberg Maritime AS, Norway at the CSIR-NIO, Goa, 05–09 May 2010.
- Course on** Underwater Acoustics: Lectures by Prof. Gopu Potty, University of Rhode Island at the NIOT, Chennai, 1–8 February 2011.
- Scientific cruise** Shipboard experience (over 50 days) to acquire multi-beam echosounder data.

Publications

 Peer reviewed Journals (Publications from the thesis)

- **K. Haris**, B. Chakraborty, C. De, R. G. Prabhudesai, and W. A. Fernandes, “Model-based seafloor characterization employing multi-beam angular backscatter data - A comparative study with dual-frequency single beam,” *Journal*

of the Acoustical Society of America, 130(6), 3623–3632 (2011).

- **K. Haris**, B. Chakraborty, B. Ingole, A. Menezes, and R. Srivastava, “Seabed habitat mapping employing single and multi-beam backscatter data: A case study from the western continental shelf of India,” *Continental Shelf Research*, 48, 40–49 (2012).
- B. Chakraborty, **K. Haris**, G. Latha, N. Maslov, and A. Menezes, “Multifractal approach for seafloor characterization,” *IEEE Geoscience and Remote Sensing Letters*, 11(1), 54–58 (2014).
- **K. Haris** and B. Chakraborty, “Stochastic formalism-based seafloor feature discrimination using multifractality of time-dependent acoustic backscatter,” *Nonlinear Processes in Geophysics*, 21, 101–113 (2014).
- **K. Haris**, B. Chakraborty, A. Menezes, W. A. Fernandes, and M. Naik, “Seafloor micro-roughness, benthic macro-fauna, and sediment substrate: A study of their interrelationship using high-frequency echo-sounding systems,” *Indian Journal of Geo-Marine Sciences*, Special issue on Ocean Acoustics and Indian Ocean Application (in press, 2015).

 Peer reviewed Journals (Other publications)

- B. Chakraborty, A. K. Saran, D. Sinai Kuncolienker, R. A. Sreepada, **K. Haris**, and W. A. Fernandes, “Characterization of *Hippocampus Kuda* (Bleeker, 1852)- yellow seahorse feeding click sound signal in a laboratory environment: An application of probability density function and power spectral density analyses,” *Bioacoustic*, 23, 1–14 (2014).
- B. Chakraborty, S. M. Karisiddaiah, A. Menezes, **K. Haris**, G. S. Gokul, W. A. Fernandes, and G. Kavitha, “Characterizing slope morphology using multifractal technique: a study from the western continental margin of India,” *Natural Hazards*, 73, 547–565 (2014).
- **K. Haris**, B. Chakraborty, A. Menezes, R. A. Sreepada, and W. A. Fernandes, “Multifractal detrended fluctuation analysis

to characterize phase couplings in seahorse (*Hippocampus kuda*) feeding clicks,” *Journal of the Acoustical Society of America*, 136(4), 1972–1981 (2014).

- B. Chakraborty, A. Menezes, S. Dandapath, W. A. Fernandes, S. M. Karisiddaiah, **K. Haris**, and G. S. Gokul, “Application of hybrid techniques (Self-Organizing Map and Fuzzy Algorithm) using backscatter data for segmentation and fine-Scale roughness characterization of seepage-related seafloor along the western continental margin of India,” *IEEE Journal of Oceanic Engineering*, 40(1), 03–14 (2015).

Conference proceedings

- B. Chakraborty and **K. Haris**, “Seafloor roughness estimation employing bathymetric systems: An appraisal of the classification and characterization of high-frequency acoustic data,” *Advances in Ocean Acoustics* (Proceedings of the 3rd International Conference on Ocean Acoustics, Beijing, China, 21-25 May 2012, Invited paper on *Thirty Years of Progress in Ocean Acoustics and Selected Topic*), *American Institute of Physics*, USA, 1495, 283–296 (2012).
- **K. Haris** and B. Chakraborty, “Application of high-frequency echo-sounders for seafloor and associated benthic habitat characterization,” XIX National Symposium on Ultrasonics, CSIR-NPL, Delhi, 30–31 October 2012. Proceedings published in the *Journal of Pure and Applied Ultrasonics*, 35, 87–94 (2013).
- **K. Haris** and B. Chakraborty, “Acoustic characterization of continental shelf seafloor and benthic habitats using single and multibeam backscatter data,” (Proceedings of the 1st International Conference & Exhibition on Underwater Acoustics, Corfu, Greece, 23–28 June 2013), 1045–1050 (2013).
- B. Chakraborty and **K. Haris**, “Remote acoustic seafloor characterization using numerical model and statistical based stochastic multifractal,” (Proceedings of the 1st International Conference & Exhibition on Underwater Acoustics, Corfu,

Greece, 23–28 June 2013, Invited paper on structured session *Sediment Backscattering*), 1013–1020 (2013).

- W. A. Fernandes, B. Chakraborty, **K. Haris**, K. Vijayakumar, D. Sundar, R. A. A. Luise, M. M. Mahanty and G. Latha, “How biological (fish) noise affects the performance of shallow water passive array system,” (Proceedings of the *International Symposium on Underwater Technology UT-2015, NIOT, Chennai, 23–25 February 2015*), Underwater Technology (UT), 2015 IEEE.
- A. A. A. Menezes, M. Naik, W. A. Fernandes, **K. Haris**, B. Chakraborty, S. Estiberio and R. B. Lohani, “Fine scale analyses of a coralline bank mapped using multi-beam backscatter data,” (Proceedings of the *International Symposium on Underwater Technology UT-2015, NIOT, Chennai, 23–25 February 2015*), Underwater Technology (UT), 2015 IEEE.

Research Supervisor

Dr. B. Chakraborty Chief Scientist, Geological Oceanography Division, CSIR-National Institute of Oceanography, Goa, India, 403004. ✉ bishwajit@nio.org

Personal Information

Permanent Address Kunnath House, Othukkungal Post, Malappuram Dt., Kerala, India, 676528

Date of birth 20 February 1986

Sex Male

Nationality Indian

Acknowledgements

“No one has ever become poor by giving.”

Anne Frank

I wish to express my profound gratitude to my mentor and guru, Dr. Bishwajit Chakraborty for his guidance during the course of this study. I have been fortunate to be associate with Dr. Chakraborty who could provide a self-liberating environment to learn, work and explore on my own. Dr. Chakraborty has been exceptionally supportive throughout the period. I had a wonderful experience working with him. Without his generosity and sincerity, it would not have been easy to complete the thesis.

I am grateful to Mr. Andrew Menezes and Mr. William Fernandes for their invaluable and openhanded support provided to process and analyze the data. Several figures illustrated in the thesis bear their painstaking effort and skill.

The single-beam and multi-beam echosounder data utilized in the research work was acquired with the support from the members of the survey group, CSIR-National Institute of Oceanography (CSIR-NIO). I wish to express my greatest appreciation to scientists, officers, crew and seamen in charge for the respective scientific cruises during the heydays. Financial support for the project was provided by the Council of Scientific and Industrial Research (CSIR), Department of Information Technology (DIT) and Ministry of Earth Sciences (MoES), Government of India.

I express my gratitude to the editors and reviewers of the *Journal of the Acoustical Society of America*, *Continental Shelf Research*, *IEEE Geoscience and Remote Sensing Letters*, *Nonlinear Processes in Geophysics* and *Indian Journal of Geo-Marine Sciences* for their meticulous remarks to improve our manuscripts. The stochastic multifractal formalism presented in the thesis was intrigued by the

comments of an anonymous reviewer of *IEEE Geoscience and Remote Sensing Letters*. Inclusion of this formalism has significantly improved this thesis, and I am grateful to all the reviewers. I am also indebted to Prof. Shaun Lovejoy (McGill University, Canada) and Dr. Espen A. F. Ihlen (Norwegian University of Science and Technology, Norway) for making available multifractal analyses codes in the public domain. Thanks are due to the developers of *Google* search engine to access pedagogical materials online.

I would like to thank Dr. Pawan Dewangan, member of the Faculty Research Committee for reviewing my half-yearly reports. I also thank Dr. P. Vethamony who guided me during the Master's dissertation and introduced me to the research field.

I also wish to express my sincere thanks to the former and present Directors of CSIR-NIO, Dr. S. R. Shetye and Dr. S. W. A. Naqvi, for providing all the necessary infrastructure and facilities to carry out this study. I wish to offer my special thanks to Prof. G. N. Nayak and Mr. Yashwant for helping with office formalities in the Goa University.

Special thanks are due to Dr. Anil Chaubey and Dr. M. T. Babu for their kind financial assistance to participate 1st International Conference & Exhibition on Underwater Acoustics, Corfu, Greece. I acknowledge National Institute of Ocean Technology (NIOT), CSIR and Office of Naval Research Global (ONRG) for funding my deputations abroad. The meeting and conference attended was an avenue to present my research work and also to interact with leading scientists working in the field of Underwater Acoustics, particularly Dr. Darrell Jackson and Christian de Moustier.

All the work consolidated in this thesis was carried out at CSIR-NIO and I express my gratitude for the support received from the various departments especially HRM, NICMAS and ITG. I duly acknowledge with much gratefulness the research fellowship awarded by CSIR.

Colleagues and friends have been generating good ambience around me always. I greatly value their friendship and sincerely appreciate their uplifting engagements.

The space indented for the acknowledgement would be inadequate to catalogue their names. The moment shared with them will be cherished forever.

None of this would have been possible without the love and goodwill of my family. The thesis would not have emerged without the blessings of my *Umma* and *Uppa*. The thesis is dedicated to them. My heartfelt gratitude to *Kakka*, *Poochi*, *Immatty*, *Kunchol* and *Labi* for their encouragement and poignant support.

HARIS. K

CSIR-National Institute of Oceanography, Goa.

23 June 2015

Contents

Statement	iii
Certificate	iv
Vita	v
Acknowledgements	x
Contents	xiii
Acronyms	xvi
Symbols	xviii
List of Figures	xxi
List of Tables	xxiv
1. Introduction	1
1.1. Motivation.....	1
1.2. Research objectives.....	7
1.3. Thesis outline.....	7
2. Study area and data processing methodology	13
2.1. Study area.....	13
2.2. Single-beam data acquisition and processing.....	14
2.3. Multi-beam data acquisition and processing.....	17
2.3.1. Heading and position correction.....	19
2.3.2. Bathymetry slope and seafloor insonified area correction.....	19
2.3.3. Lambert's law removal and corrected angular backscatter data.....	20
2.3.4. Backscatter image data processing.....	20
2.4. Sediment sampling.....	21

3. Model-based seafloor characterization	24
3.1. Introduction.....	24
3.2. Model-data comparison.....	26
3.2.1. Computation of scaling parameter to calibrate the data.....	26
3.2.2. Two-stage parametric optimization.....	29
3.3. Inversion results and discussion.....	29
3.3.1. Mean grain size (M_ϕ).....	32
3.3.2. Seafloor roughness parameters (γ_2 and w_2).....	34
3.3.3. Sediment volume scattering parameter (σ_2).....	36
3.4. Concluding remarks.....	38
4. Seabed habitat mapping	40
4.1. Introduction.....	40
4.2. Results and discussion.....	43
4.2.1. Ground-truth data.....	44
4.2.2. Backscatter and grain size.....	44
4.2.3. Grain size and benthic habitat.....	48
4.2.4. Interrelationship between backscatter, grain size, and benthic macro-fauna abundance.....	50
4.3. Concluding remarks.....	56
5. Benthic habitat characterization using geoacoustic inversion results	57
5.1. Introduction.....	57
5.2. Results and discussion.....	60
5.2.1. Backscatter and mean grain size.....	61
5.2.2. Macrobenthos-sediment relationship.....	62
5.2.3. Macrobenthos-roughness relationship.....	64
5.3. Concluding remarks.....	67
6. Multifractal approach for seafloor	68
Part 1. Application to multi-beam image data	68
6.1. Introduction.....	68
6.2. Data sets.....	72
6.3. Strange attractors.....	73

6.4. Stochastic multifractal formalism.....	75
6.4.1. Moment scaling function and universal multifractals.....	75
6.4.2. Fractionally Integrated Flux model.....	76
6.5. Results and discussion.....	79
6.5.1. Strange attractors based technique.....	79
6.5.2. Stochastic multifractal field based technique.....	82
6.6. Concluding remarks.....	83
Part 2: Application to single-beam echo envelope data	85
6.7. Introduction.....	85
6.8. Multiscaling.....	88
6.9. Results and discussion.....	90
6.9.1. Sediment distribution.....	90
6.9.2. Multifractal phase transition.....	91
6.9.3. The universal multifractal parameters.....	93
6.9.4. Possible influence of seafloor backscattering process.....	98
6.9.5. Relationship with fractal dimension.....	98
6.9.6. Comparison with inversion results.....	100
6.10. Concluding remarks.....	103
7. Summary	104
Appendix	107
Bibliography	109

Acronyms

ANN	Artificial Neural Network
APL-UW	Applied Physics Laboratory, University of Washington
ASCII	American Standard Code for Information Interchange
BS	Backscatter strength
CSIR	Council of Scientific and Industrial Research
CSIR-NIO	CSIR-National Institute of Oceanography
DEM	Digital Elevation Model
DIT	Department of Information Technology
EEZ	Exclusive Economic Zone
FIF	Fractionally Integrated Flux
GIS	Geographic Information System
GPS	Global Positioning System
HB	Hard body organisms
HRM	Human Resource Management
ITG	Information Technology Group
MBES	Multi-beam echosounder
MoES	Ministry of Earth Sciences
NICMAS	National Information Centre for Marine Sciences
NIOT	National Institute of Ocean Technology
NNW	North-northwest
ONRG	Office of Naval Research Global
PC	Principal Components
PCA	Principal Component Analysis
PROBASI	PROcessing BAcKscatter SIGnal

SAX	Sediment Acoustics Experiment
SB	Soft body organisms
SBES	Single-beam echosounder
SOC	Self-Organized Criticality
SONAR	SOund Navigation And Ranging
SSE	South-southeast
WCMI	Western continental margin of India
WCSI	Western continental shelf of India
1D	One-dimension
2D	Two-dimension
3D	Three-dimension
4D	Four-dimension

Symbols

A	Beam-insonified area
B	Degree of asymmetry related to multifractal spectrum
BS_0	Mean backscattering coefficient
BS_{data}	Angular backscatter strength
BS_{model}	Model predicted backscatter strength
c	Sound speed in water
C_1	Sparseness of the field
d	Standard dimension of the space
$D(q)$	Generalized fractal dimension
$\Delta D(q)$	Width of the generalized fractal dimension
EL	Time average of the received backscatter signal envelope
E/S	Error-to-signal ratio
f	Frequency of the measure
$f(\alpha)$	Singularity spectrum
$\Delta f(\alpha)$	Stability of the multifractal spectrum
Gup	Receiving sensitivity of the echo-sounder
h	Water depth
h_{ref}	Reference water depth
H	Degree of smoothness
i	Image box representing bathymetry and backscatter
I_λ	Intensity field of bathymetry and backscatter in the image box
k_w	Acoustic wavenumber
K_c	Cutoff wavenumber

$K(q)$	Moment scaling function
ΔK	Bragg wavenumber
l	Smallest scale in the image box representing bathymetry and backscatter
L	Largest scale in the image box representing bathymetry and backscatter
m	Mass of the measure corresponds to bathymetry and backscatter
M_ϕ	Sediment mean grain size in phi unit
$n(\varepsilon)$	Number of image box representing bathymetry and backscatter
q	Order of the moment
q_c	Critical moment
q_s	Theoretical value of the critical moment
R	Vertical water depth in meter
R^2	Correlation coefficient
S	Backscatter strength
S_s	Surface roughness coefficient
S_v	Volume scattering coefficient
SL	Source level of the echo-sounder
TL	Two-way transmission of the signal in water
TS	Target strength
TVG	Time variable gain
U_A	Depth corrected backscatter signal
U_g	Mean grain size diameter of the sediment samples
V_{tot}	Gain utilized in the echo-sounder
w_2	Seafloor roughness spectrum strength
W	Width of the multifractal spectrum
α	Degree of multifractality

α_b	Attenuation coefficient of the signal in water
α_{max}	Maximum singularity index
α_{min}	Minimum singularity index
β	Power law exponent
$\chi(q, \varepsilon)$	Partition function that describes the probability of ‘containing the object’
ε	Length of the image box representing bathymetry and backscatter
ϕ_i	Scale by scale conserved multifractal flux
φ	Incidence angle
γ_2	Seafloor roughness spectrum exponent
λ	Scale ratio of the image box representing bathymetry and backscatter
λa	Acoustic wavelength
θ_g	Grazing angle
σ_2	Sediment volume scattering parameter
σ_v	Sediment volume scattering coefficient
$\tau(q)$	Mass exponent function

List of Figures

1.1	General procedure for acoustic based seafloor studies.....	4
1.2	Dichotomy in the framework of low-order deterministic and high-order stochastic chaos.....	5
1.3	A scheme for quantifying dominant roughness creating processes on the seafloor.....	6
2.1	Study regions with type of data collected in the central part of the WCMI.....	14
2.2	Graphical abstract of the SBES data processing methodology.....	17
2.3	Graphical abstract of the MBES data processing methodology.....	21
3.1	The acoustic and sediment sample data acquisition locations with respective sediment types used for inversion modeling.....	25
3.2	Computation of scaling parameter to calibrate MBES data.....	28
3.3	Flow chart representing 4D inversion procedure for seafloor parameter computation.....	30
3.4	Model-data comparison for three geologically distinct sediment provinces.....	32
3.5	Scatter plot of multi-frequency inversion results.....	34
4.1	Study area selected for seabed habitat mapping with acoustic and sediment sample data acquisition locations.....	42
4.2	The relationship between the backscatter at three frequencies and weight percentage of sediment types.....	46
4.3	Generic representation of backscatter strength versus incidence	

angle (after Lurton, 2002) illustrating the physical processes involved in seafloor backscattering.....	47
4.4 Correlation between the benthic macro-fauna and weight percentage of sediment types.....	49
4.5 GIS-based classification representing the animal-sediment relationship.....	50
4.6 Clustering of benthic macro-fauna, multi-frequency backscatter, and sediment types.....	52
4.7 GIS-based classification representing the backscatter-animal-sediment interrelationship at 33 kHz.....	53
4.8 GIS-based classification representing the backscatter-animal-sediment interrelationship at 210 kHz.....	53
4.9 Depth wise spatial variations of biomass, backscatter, and benthic density.....	54
4.10 GIS-based classification representing the distribution of total organic carbon in relation to the benthic macro-fauna and sediment types.....	55
5.1 Study area with graphical representation of the methodology.....	59
5.2 GIS-based sediment distribution and benthic macro-faunal abundance map of the study area.....	60
5.3 Scatter plot demonstrating the success of inversion modeling carried out.....	61
5.4 location wise clustering of measured and derived inversion parameters.....	63
5.5 GIS-based image classification representing the variation of w_2 in relation to the benthic macro-fauna and sediment types at 33 and 210 kHz.....	65
5.6 GIS-based image classification representing the variation of σ_2 in relation to the benthic macro-fauna and sediment types at 33 and 210 kHz.....	66

6.1	The backscatter map of the study area indicating some of the main structural features of the region of the WCMI.....	71
6.2	Backscatter (in digital number: 0–255) and bathymetry seafloor seepage blocks selected from the multifractal analyses.....	72
6.3	Schematic representation of generalized correlation dimension function $D(q)$ and multifractal spectrum $f(\alpha)$	74
6.4	Log/log curves of the normalized trace moment (M) as functions of the scale ratio $\lambda=L/l$	78
6.5	Block wise generalized correlation dimension $D(q)$ and multifractal spectrum $f(\alpha)$ plots for backscatter and bathymetry data...	80
6.6	Results of strange attractor and stochastic multifractal formalisms.....	81
6.7	GIS-based sediment distribution map of the study area with graphical abstract of the methodology implemented.....	87
6.8	Log/log plot of the normalized trace moments as a function of the scale ratio $\lambda=L/l$ at 33 and 210 kHz.....	89
6.9	Comparison between the empirical and theoretical moment scaling function $K(q)$ as a function of q	92
6.10	Frequency wise scatter plot of the measured M_φ and computed codimension parameter C_1 at 33 and 210 kHz.....	95
6.11	A quantitative comparison between the scale invariant multifractal parameters (α , C_1 , and H) at 33 and 210 kHz.....	96
6.12	Comparison of the computed multifractal parameters (α , C_1 , and H) at frequencies 33 and 210 kHz.....	97
6.13	3D scatter diagram showing clustering among M_φ , C_1 and w_2 at 33 and 210 kHz.....	102
A.1	The figure depicts the validity of the composite-roughness approximation as a function of the acoustic frequency and spectral strength w_2	108

List of Tables

2.1	Location wise distribution of sediment type, biomass and benthic macro-fauna.....	23
3.1	Summary of the seafloor parameters derived from three acoustic frequencies, 33 and 210 kHz (SBES) and 95 kHz (MBES).....	31
6.1	Summary of universal multifractal parameters.....	93

Chapter 1

Introduction

1.1 Motivation

Ocean Acoustics is the science of sound waves in the seas and has become an imperative tool for underwater remote sensing. Advances in the field of *Ocean Acoustics* has propelled researchers to investigate oceanic features, seafloor habitats and associated processes. Sound propagation modeling has augmented studies related to oceanographic processes including coastal upwelling, sediment plume movement, eddies and frontal systems, coastally trapped waves, and internal solitary waves. Likewise, technological innovations in active sonar based high-frequency single-beam (SBES) and multi-beam echosounder system (MBES) have mutually facilitated effective management of living and non-living resources along with mapping of the seafloor.

Space based satellite remote sensing is one of the conventional techniques for oceanographic research studies. Many dynamical properties of the open ocean and the variability of the changes in the coastal zones can be mapped and effectively monitored using the remote sensing techniques. However, space based marine remote sensing methods do not provide adequate resolution for precise measurements as the light and electromagnetic waves attenuate rapidly in seawater. Prospectively, application of the acoustic remote sensing techniques, using high-frequency SBES and MBES sonar imageries can generate significant data for ocean multidisciplinary studies including seafloor characterization and benthic habitat studies (Anderson *et al.*, 2008; Brown *et al.*, 2011). The acoustic remote sensing methods are primarily concerned with identifying, classifying and mapping surficial

geological features of the seafloor. These procedures are well recognized as a useful tool in oceanography to characterize the seafloor over a wide area and facilitate preliminary geological analyses.

Considering the relevance of marine environmental management, cost-effective methods to study the seafloor at large spatial scales are needed. Studies investigating the distribution of seafloor sediments and benthic habitat usually involve overt collection of samples using sediment grabs or diving methods for characterizing the sediment substrate, associated benthic species and to assess the benthic density. Such methodologies provide the most accurate representation, however such studies are time consuming and restricted to relatively small areas of the seafloor. Alternatively, the acoustic remote sensing method employing SBES and MBES is being widely used to explore the seafloor and the benthic habitat environment owing to the rapid data acquisition advantages.

The seafloor characterization and classification methodologies are traditionally grouped into two categories, namely model-based techniques and empirical methods, as can be gleaned from different seminal scientific literature¹ (Fig. 1.1). The model-based techniques often utilize physics-based acoustic backscatter models to differentiate the seafloor sediments by optimizing the comparison between the measured and the modeled signals. The empirical methods rely on the statistical and artificial neural network-based approaches to correlate the features derived from the data with the sediment type.

Several issues still remain relative and ambiguous to both model and statistical based techniques used to characterize seafloor microroughness (Jackson and Richardson, 2007 and references therein). It has been previously presumed that the seafloor roughness scattering is a stationary Gaussian random process with power law dependence over a wide range of spatio-temporal scales (having single power law exponent). This postulation is counterintuitive and need to be reformulated for

¹ The related literatures are duly cited in the respective chapters.

the development of nonlinear techniques² based modeling and analyses methods to adequately describe seafloor roughness variation over all measured scales (Fig. 1.2). The standard bathymetry map at a coarse resolution can be conveniently characterized in a “deterministic” framework. However, the fine resolution SBES and MBES data reveals small scale features of the seafloor and calls for the application of “stochastic” formalism to carry out the analyses³. The proposition, with the support of concurrent environmental measurements will help to fathom out dominant roughness creating processes including hydrodynamic and biological activities on the seafloor⁴ (Fig. 1.3).

The thesis consolidated here, aims at establishing and documenting quantitative (model-based and empirical) methods for remote acoustic characterization of the seafloor and the associated benthic habitats using high-frequency echo-sounding systems. The technologically advanced seafloor studies offer the prospect of acquiring new data, novel insights and delving into new research challenges. The versatility and improved understanding of the technology portrayed in the thesis should be of interest to multidisciplinary researchers.

² The advantages of nonlinear technique based multifractal analyses over standard statistical approaches have been reported in Lovejoy *et al.* Nonlinear Geophysics: Why We Need It, 2009a. The multifractal analysis characterizes the local scale properties of the data in addition to its global properties. Correspondingly, it is possible to quantify the statistical distribution of the local singularities (i.e. local multifractal exponents) present in the data.

³ The schematic diagram, illustrating the range of spatial resolutions required to conveniently characterize seafloor morphology using the deterministic and stochastic formalisms are available in Goff and Jordan (1988).

⁴ The hydrodynamic (currents, waves) and biological processes (bioturbation) have predictable and profound effects on the formation of seafloor microtopography and resulting acoustic response. Analyzing the data collected using 12 kHz MBES, deep-towed 30 kHz sonar, and stereophotography, Fox and Hayes (1985) in their seminal work noted the adequacy of single power law exponent to characterize seafloor roughness spectra over a wide range of scales (on the Atlantic coast continental rise). Much recent comparison of the roughness spectra (Briggs *et al.*, 2005) computed from MBES and stereophotographs in the northeastern Gulf of Mexico indicated the occurrence of multiple power laws and related exponents. The power law applied to wavelengths (<10 cm) was attributed to the biogenic features and resulting roughness that may be relatively stable in time. The power law exponent utilized to characterize wavelengths (>100 cm) was related to lasting morphological features on the seafloor. The portion of the spectrum within 10–100 cm wavelength was ascribed to wave-generated ripple that can vary considerably with time (Jackson and Richardson, 2007). Therefore, the assumption of single power is inadequate to characterize seafloor roughness over a wide range of spatio-temporal scales.

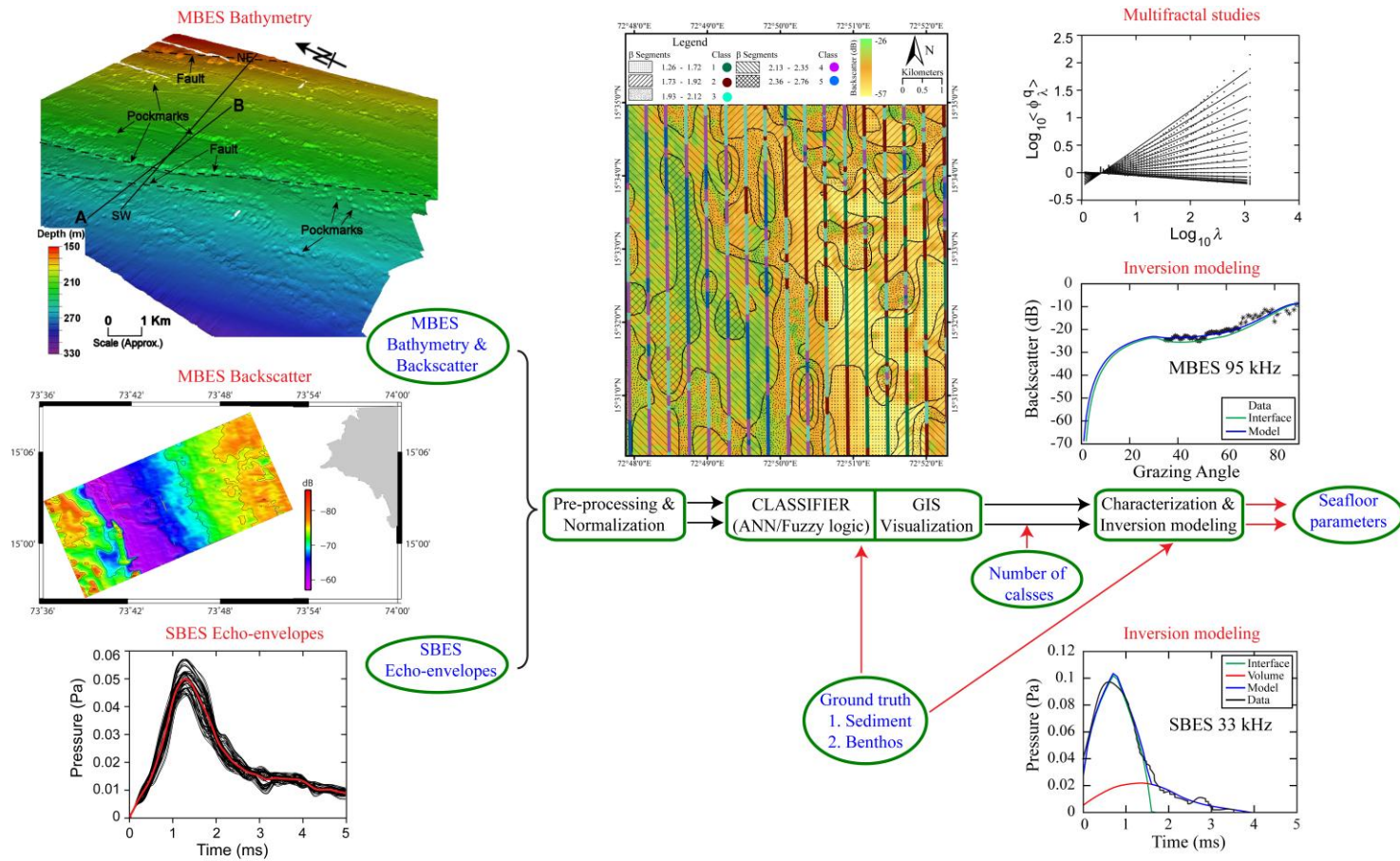


Fig. 1.1 The figure illustrates general procedure for acoustic based seafloor studies describing model-based techniques and empirical methods.

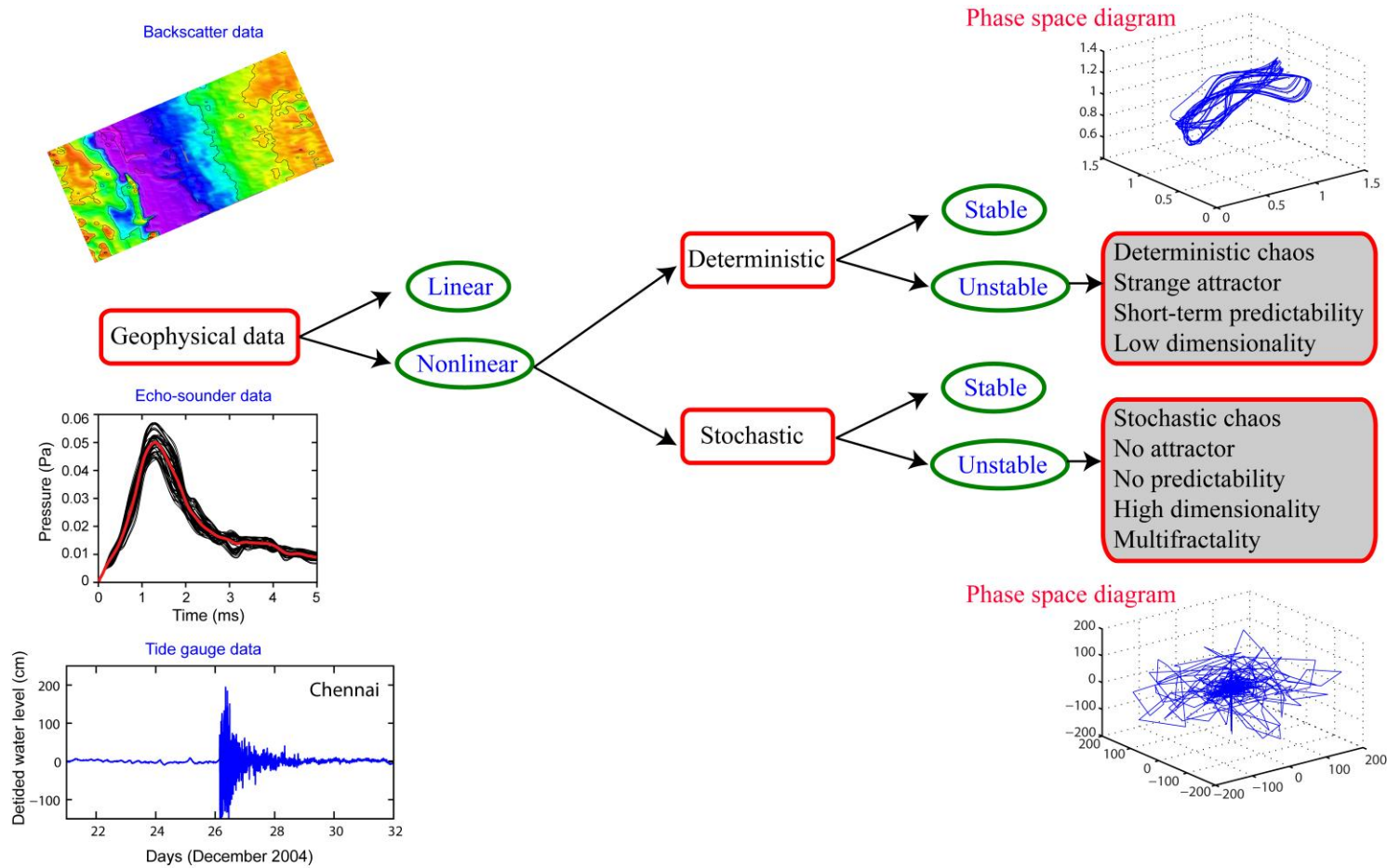


Fig. 1.2 Schematic diagram depicting the dichotomy in the framework of low-order deterministic and high-order stochastic chaos for the adequate characterization of geophysical data sets.

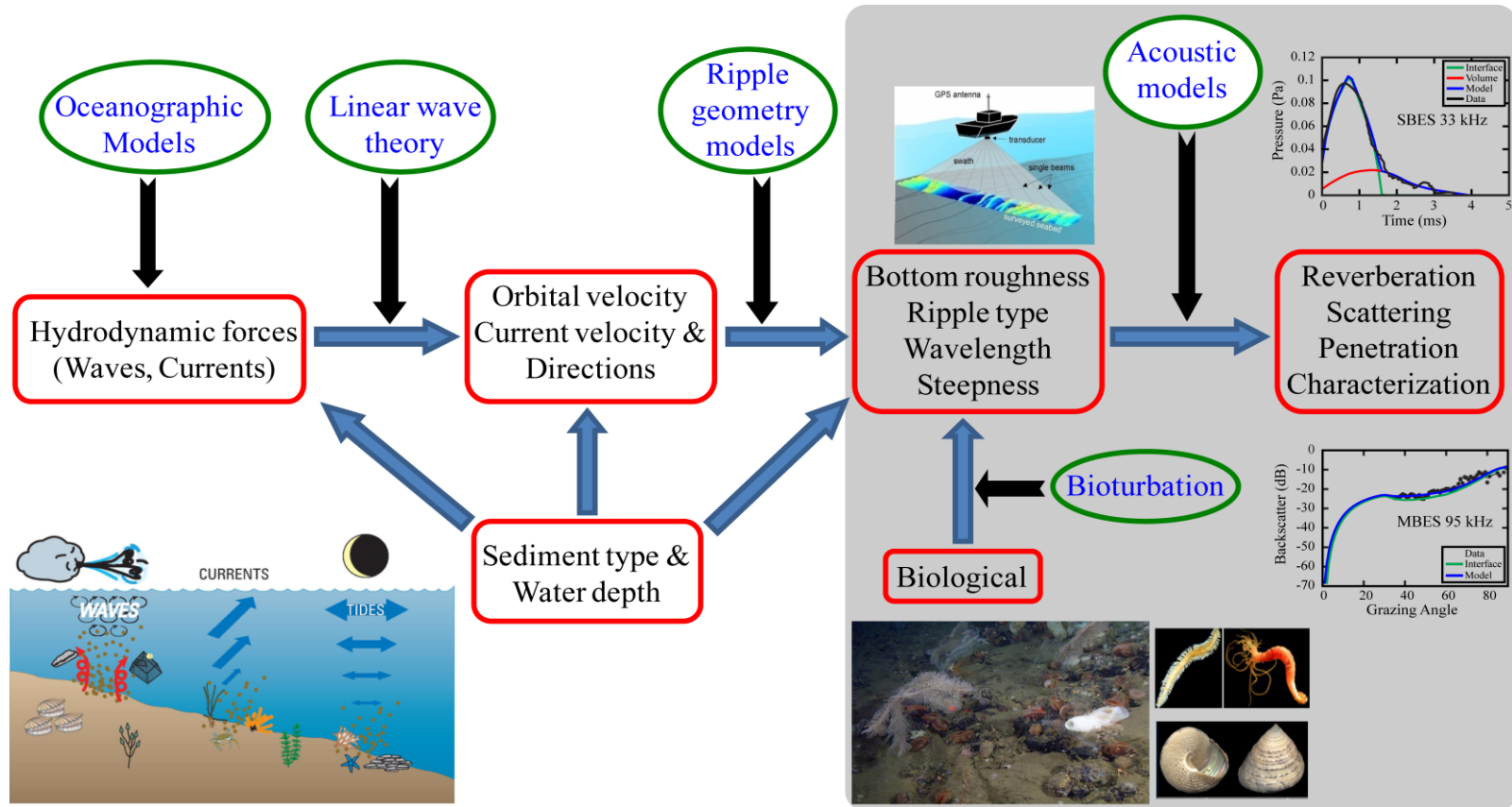


Fig. 1.3 A scheme for quantifying dominant roughness creating processes including hydrodynamic and biological activities on the seafloor (modified after Jackson and Richardson, 2007).

1.2 Research objectives

The doctoral research reported here highlights the potential utilization of SBES and MBES data acquired from the central part of the western continental margin of India (WCMI), to address the following specific scientific and technical objectives:

- Model-based seafloor characterization employing multi-beam angular backscatter data;
- Seabed habitat mapping employing single and multi-beam backscatter data;
- Multifractal approach based seafloor characterization and feature discrimination.

1.3 Thesis outline

The thesis elaborating the doctoral research carried out has been organized as follows:

Chapter 1: Introduction

The introduction chapter reminiscence the background studies carried out and briefly describes the established procedure for seafloor studies using high-frequency SBES and MBES. The chapter also enunciates the motivation and objectives of the doctoral research.

Chapter 2: Study area and data processing methodology

Chapter 2 describes the study area, with the description of acoustic and sediment data sets including benthic macro-fauna. Concise overviews of acoustic data processing methodologies are also recapped in this chapter.

Chapter 3: Model-based seafloor characterization

The backscatter data acquired using the echo-sounding systems can be matched with the theoretical scattering models to interpret the fine scale seafloor information embedded in data (Jackson *et al.*, 1986; Chakraborty *et al.*, 2000; Sternlicht and de

Moustier, 2003a, b; De and Chakraborty, 2011; Williams *et al.*, 2012). The numerical approach employed for extracting information from the data is commonly referred to as “inversion modeling”. Inversion modeling primarily involves physics based approach to calculate seafloor roughness parameters, namely, the sediment mean grain size (M_ϕ); spectral parameters at the water-seafloor interface (γ_2 , w_2); and sediment volume parameter (σ_2). Accordingly, in this chapter, the composite roughness scattering theory developed by Jackson *et al.* (1986) has been implemented to characterize seafloor sediment provinces off Goa, utilizing the angular backscatter data derived employing MBES operable at 95 kHz. Distinct interclass separations between the sediment provinces are evident from the spatial variability of computed inversion results, particularly the sediment mean grain size (M_ϕ) and sediment-water interface roughness (w_2). The seafloor parameters derived from the 95 kHz MBES data are consistent with the ground-truth data as well as with the inversion results obtained using 33 and 210 kHz SBES data at the same locations. The results highlighted in this chapter have been reported in Haris *et al.* (2011).

Chapter 4: Seabed habitat mapping

Seafloor benthic habitats are physically distinct areas of the seabed that are associated with particular species, communities, or assemblages with its coexisting diversity. The benthic habitat maps can conveniently illustrate the nature, distribution and extent of the distinct physical environment and the associated species communities. Correspondingly, the acoustic backscatter computed from MBES and SBES operable at 95 kHz and 33/210 kHz, respectively, have been used to study the distribution of sediment texture and benthic macro-fauna abundance along the central part of the WCMI (off Goa)⁵. Concurrent acoustical, physical, and biological parameters were measured to characterize the continental shelf seafloor. Two distinct feeding groups were observed from the study area: namely, “deposit feeders” (majority of polychaete worms and related soft body species like nematode,

⁵ The interaction effects of the dual-frequency SBES backscatter signal with the seafloor sediment substrate and benthic biota along the WCMI was first initiated by Chakraborty *et al.* (2007).

oligochaetes, nemertinea, and echurids) mainly in shallow region and “filter feeders” (hard body bivalves and gastropods) in deeper depths. The relationships between processed acoustic backscatter strength, grain size, and benthic macro-fauna abundance have been demonstrated by applying Principal Component Analyses (PCA), and Geographic Information System (GIS) based seafloor maps. The clustering analysis explains that the backscatter values at three frequencies are strongly correlated with both substrate type and faunal functional group assemblages on the seafloor. The preferences of deposit feeders (soft body benthic macro-fauna) in the fine-sediment regions and filter feeders (hard body benthic macro-fauna) in coarse sediment regions were linked to the variations in sediment granulometry as well as backscatter strengths in the study area. This study further underscores the versatility of high-frequency echo-sounding systems to map seafloor sediment distribution and associated benthic habitat across large areas of seafloor (Haris *et al.*, 2012).

Chapter 5: Benthic habitat characterization using geoacoustic inversion results

In this chapter, the spatial variability of sediment geoacoustic inversion results, derived from dual-frequency SBES and MBES have been further analyzed to demonstrate the interrelationship among the sediment texture and benthic macro-fauna abundance. The correlation among the derived acoustical and biological parameters has been identified from the spatial map generated using ArcGIS and validated by applying PCA. Distinct interclass separation of the sediment provinces is revealed by the spatial variability in the computed inversion results, demonstrating a strong correlation with the backscatter and biologically active faunal functional group assemblages on the seafloor. The results obtained are indicative of bioturbation by benthic animals, resulting in variability in the data that should be taken into account to optimize the model-data matching procedure during inversion (Haris *et al.*, 2015).

Chapter 6: Multifractal approach for seafloor characterization: Part 1

Seafloor bathymetry and the associated backscattering data of submerged objects have an extremely wide range of spatio-temporal scales necessitating application of power law to carry out the analyses (Fox and Hayes, 1985). The power law behavior in such instances requires multifractal analyses in order to determine the fractal statistics of both seafloor backscatter and bathymetry image data (Fig. 1.2). It is imperative to treat such data as a scale invariant field requiring multifractal measures and exponent functions, rather than a unique scaling exponent, such as fractal dimension. Besides, the continuous form of seafloor heterogeneity (due to bioturbation, sediment deposition, seafloor seepages, or hydrodynamic processes) has received the most attention and calls for the application of more versatile statistical techniques for determining seafloor roughness statistics. Accordingly, the work described in this chapter demonstrates multifractal techniques based characterization of pockmark seepage associated seafloor along the central part of the WCMI. Six representative blocks of backscatter and bathymetry co-registered image data were used to characterize the seafloor. Two distinct multifractal formalisms have been applied to determine the characteristics. The first formalism employs data analyses using generalized dimension $D(q)$, and multifractal singularity spectrum $f(\alpha)$ linked shape parameters, based on the “strange attractors” (Fig. 1.2) that exhibit multifractal scaling (Halsey *et al.*, 1986). The second approach is designed as “stochastic” multifractal fields that connect the image block quantification to the three fundamental parameters namely, degree of multifractality α , sparseness C_1 and degree of smoothness H (Schertzer and Lovejoy, 1987). The present investigation using the two multifractal formalisms to characterize the seafloor backscatter and bathymetry data provides comparative results that can be expounded upon. The results described in this chapter have been reported in Chakraborty *et al.* (2014).

Multifractal approach for seafloor characterization: Part 2

The success of the model-based inversion procedure (described in Chapter 3) depends on the scattering theory employed in the forward backscatter model and requires detailed understanding of the scattering mechanism. The study of sound interaction with the seafloor and the corresponding inversion modeling impose a challenging task, particularly with the existence of diversity in the benthic habitat of the area (detailed in Chapter 4 and 5). The scattering process of acoustic wave is influenced by the presence of benthic fauna (Fig. 1.3) responsible for modifying the small-scale morphological features and the density fluctuations within the sediment volume (in addition to the hydrodynamic processes). Incorporation of the number density of biological organisms and their collective activities (i.e. burrowing and home building) in the forward backscatter model complicate the inverse modeling even further. In order to further expand the seafloor feature discrimination, an empirical method that uses the scaling and multifractality of the dual frequency SBES echo-envelopes at 33 and 210 kHz has been introduced. The reason for using multifractal framework is to build on the fact that the layers of seafloor imprints a fractal signature on the echo signal along with the self-similarity of sediment ripples of various sizes. Moreover, acoustically soft sediments are penetrated more deeply by acoustic signals and produce longer and corrugated echoes than hard sediments, evidencing fractal structures.

In the second part of this chapter, dual-frequency echo-envelope data acquired using the normal-incidence SBES, have been examined to study its scale invariant properties. The scaling and multifractality of the SBES echo-envelopes (at 33 and 210 kHz) were validated by applying stochastic based multifractal analyses technique. The analyses carried out substantiate the hierarchy of multiplicative cascade dynamics in the echo-envelopes, demonstrating a first-order multifractal phase transition. The resulting scale invariant parameters (α , C_1 , and H) establish gainful information that can facilitate the distinctive delineation of the sediment provinces in the central part of the WCMI. The “universal multifractal” parameters (Gagnon *et al.*, 2006) among the coarse and fine sediments exhibit subtle difference

in α and H , whereas the codimension parameter C_1 representing the sparseness of the data is varied. The C_1 values are well clustered at both the acoustic frequencies, demarcating the coarse and fine sediment provinces. Statistically significant correlations are noticeable between the computed C_1 values and the ground truth sediment information. The variations in the multifractal parameters and their behavior with respect to the ground truth sediment information are in good corroboration with the previously computed sediment geoaoustic inversion results obtained at the same locations (Haris *et al.*, 2014).

Chapter 8: Summary

The concluding chapter summarizes the salient findings of the thesis.

Chapter 2

Study area and data processing methodology

2.1 Study area

The acoustic and sediment data acquired from two study regions (Fig. 2.1) selected in the central part of the WCMI are utilized for the research work carried out in this thesis. The sediment substrates in the study areas were generally ranging from clayey silt to sand. The seafloor mapping experiments were conducted by CSIR-National Institute of Oceanography (CSIR-NIO) using hull-mounted calibrated high-frequency SBES and MBES in calm weather conditions. The shallow water SBES data was acquired under a project granted by Department of Information Technology (DIT), Government of India. The MBES data from shallow and outer slope area were collected as a part of Exclusive Economic Zone (EEZ) mapping program of Ministry of Earth Sciences (MoES), Government of India.

The seafloor depths in the shallow study region generally varied between 29 and 109 m (Fig. 2.1). The deep water study area extended over 105 km² with water depths ranging from 145 m in the northeast to 330 m in the southwest. The average slope of the study area was 0.90°. A number of deep seated faults, basement highs, reefs, and ridge systems were reported earlier along the WCMI (Bhattacharya and Chaubey, 2001). The faults in the region were parallel to the Dharwar Precambrian

orogenic trend and 112 pockmarks (Dandapath *et al.*, 2010) were reported from the study area close to NNW-SSE trending fault zone.

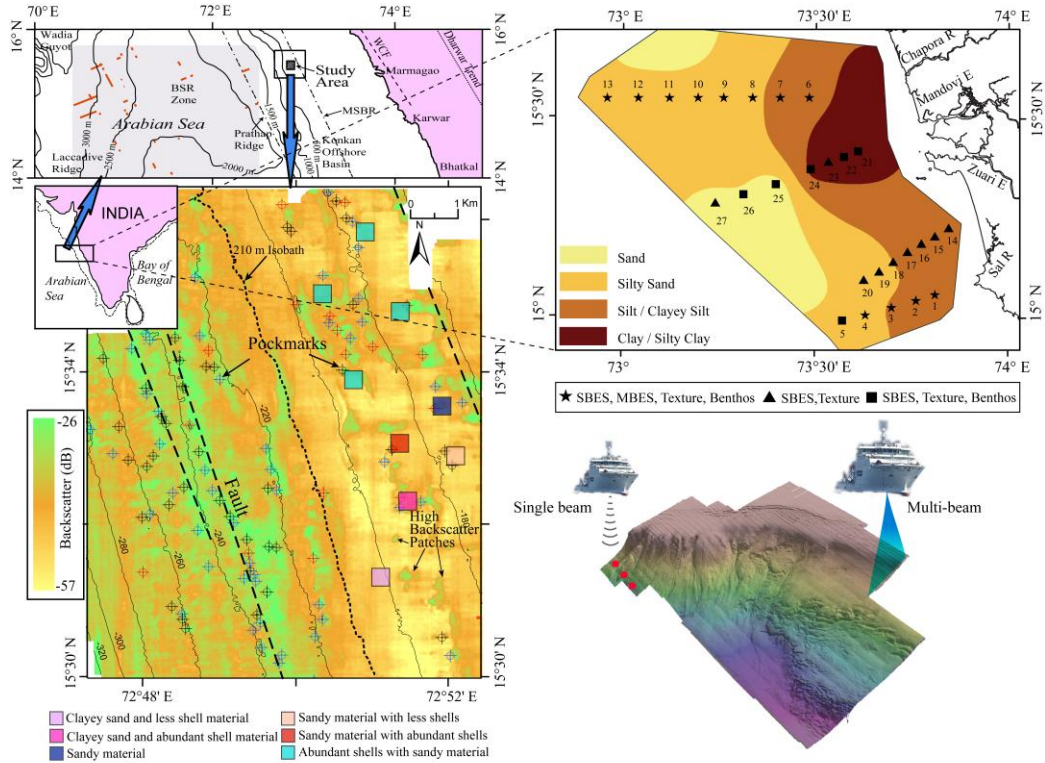


Fig. 2.1 The figure represents study regions with type of data collected in the central part of the WCMI. The acoustic data were acquired using RESON-NS 420 dual-frequency SBES and EM 1002 MBES. The ground truth sediment information was collected using a Van-Veen grab.

2.2 Single-beam data acquisition and processing

The dual-frequency (33 and 210 kHz) echo data were acquired over substrates ranging from clayey silt to sand in the central part of the WCMI, using a hull-mounted normal incidence RESON-NS 420 SBES. The beam width of the echosounder transducer for 33 and 210 kHz are 20° and 9° respectively, with corresponding pulse lengths of 0.97 and 0.61 ms. The raw analog output on the

receiver circuit board was tapped and connected to a PCL 1712L 12-bit A/D converter with a sampling frequency of 1 MHz. The echoes were recorded along with the information of the echo-sounder adjustments and ship position obtained from the GPS system. Figure 2.1 shows the SBES data acquisition locations.

The recorded echo data were converted from binary to ASCII format restricting to a range -5 to $+5$ V. Hilbert transform was employed to obtain the echo-envelope from the echo trace at each location. The shape of the echo-envelope is generally influenced by various factors including natural variability of the seafloor, transducer heave, and noise due to echo-sounder instability (Haris *et al.*, 2012). Therefore, several post processing steps such as visual check, echo alignment and echo averaging were performed for obtaining good averaged echo-envelopes (Fig. 2.2).

The first step taken in the post processing was to select good echo-envelopes (with minimum distortion) by removing the saturated and clipped echo-envelopes through visual inspection. This was achieved by careful selection of the echo-envelopes, characterized by a well-defined initial rise and amplitude followed by a slow decay. The data having voltage response saturates at $+5$ V and those with prominent multi peaks were discarded. Precisely, an echo-envelopes displaying only one important peak, with amplitude between 2.5 and 5 V were qualified for further processing steps. Due to the transducer heave motion and small variations of seafloor depth over consecutive pings (while recording the backscatter data), initial rise times of the echo-envelopes are not identical. Hence, it was imperative to align all the echo-envelopes before carrying out further processing. The alignment was based on identifying and indexing a temporal feature on the echo-envelope. The initial rise time and the time of peak amplitude were considered as an important temporal feature of the echo. After identifying the temporal feature, all echoes within the ensemble were adjusted with time to align with the selected feature (Fig. 2.2). The aligned echo-envelopes were averaged to obtain stable acoustic signals to compute the values of universal multifractal parameters associated with different sediment provinces. The echo-envelopes were first averaged using 20 successive envelopes with 95% overlap (in a moving average sense with sequences 1–20, 2–21, and so on,

utilizing all the consistent echo-envelopes available in the dataset). The voltage form of the aligned data were converted to pressure signal using the hydrophone sensitivity values provided by the transducer manufacturer. The resulting aligned pressure curves were finally ensemble averaged to obtain a representative stable acoustic signal at each location (De, 2010; Haris *et al.*, 2014).

Apart from the processing steps described above, the echo-envelope data necessitated additional correction for the sonar footprint dimension prior to the analyses. The footprint diameter enlarges in proportion to the water depth, correspondingly the backscatter area and echo duration increases. As a result, an echo recorded at a greater depth is expanded in time and an echo recorded at a lesser depth is compressed along the time axis (when compared to a reference depth). Consequently, the acoustic returns from the same seafloor sediment type lying at different depths do not have the same shape (De and Chakraborty, 2009). Accordingly, a first-order correction was applied to remove the influence of the depth on the time spread (Pouliquen, 2004). The time spread of the echo-envelope was multiplied by a factor h_{ref}/h , where h_{ref} is the reference depth of 50 m (approximate average of all the spot depths) and h is the depth at the position of the individual echo data (De and Chakraborty, 2010, 2012). The procedure followed is equivalent to the depth-dependent correction described by van Walree *et al.* (2005).

Finally, to compute the backscatter strength (in dB) from the depth corrected backscatter signal of the dual-frequency echo-sounder, we follow Urick (1983), as referenced in Chakraborty *et al.* (2007):

$$\langle 10\log_{10} S \rangle = \langle 20\log_{10} U_A \rangle - V_{tot} - Gup - SL + \langle 40\log_{10}(R) \rangle + 2\alpha_b R - 10\log_{10} A \quad (2.1)$$

where S is the backscatter strength, U_A the depth corrected backscatter signal obtained from particular locations, and V_{tot} the system gain utilized in the echo-sounder. For the source level (SL) and receiving sensitivity (Gup), two different sets of values were used for two frequencies (33 and 210 kHz). Similarly, for the attenuation coefficient (α_b), two values corresponding to 33 and 210 kHz were used with R and A as the vertical depth (m) and the beam-insonified area respectively.

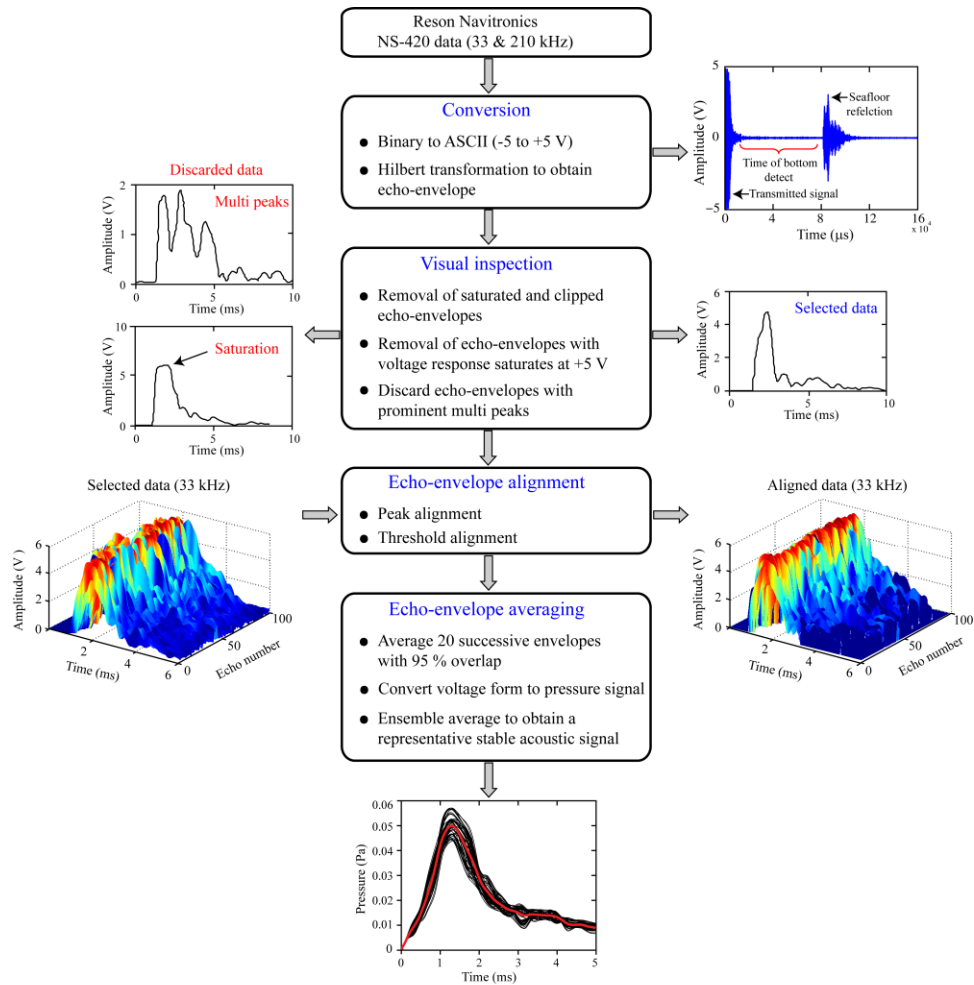


Fig. 2.2 Graphical abstract of the SBES data processing methodology.

2.3 Multi-beam data acquisition and processing

The 95 kHz MBES data were acquired using the EM 1002 echo-sounding system. The Simrad EM 1002 is a phase interpolated beam-forming MBES with 128 transducer elements forming 111 beams in a semicircular transducer array of 45 cm radius. The echo-sounder was calibrated following a patch test to minimize navigational and motion errors as described in the Simrad EM 1002 installation manual. The line spacing was around 3–4 times water depth to provide sufficient overlap between adjacent lines. An Applied Microsystems SV Plus velocimeter was

used to carry out sound speed calibration profiles of the water column during the survey.

During the time of data acquisition, the Simrad EM 1002 system primarily measures the time average of the received backscattered signal envelope (EL) in each of its 111 beams. The received signal envelopes are corrected for time variable gain (TVG), predicted beam patterns, and the insonified area. The data gets recorded online in a packet format called “datagram” and stored for every ping as representative of the seafloor’s backscatter strength (Hammerstad, 2000). However, the raw data recorded by the MBES is not directly suitable to compute the angular dependence of seafloor backscattering. Therefore, post processing steps have to be carried out essentially for the removal of Lambert’s law¹, corrections for actual bottom slope and the insonified area (Hammerstad, 2000). Moreover, if the sonar is not routinely calibrated, the backscatter values obtained after the post processing are probably not accurate (i.e., the reference level is effectively arbitrary), nevertheless they are likely to be sufficiently reliable in a relative sense to record differences between the sediment types. Consequently, even after post processing, prior to model-data comparison, there is a lack of absolute calibration and a depth-dependent offset (scaling parameter in dB) is required to be added with each of the processed data sets.

The corrections applied by the MBES to the echo level (EL) of the backscatter signal can be derived from the sonar equation as:

$$EL = SL - 2TL + TS \quad (2.2)$$

where SL is the MBES source level, $2TL$ is the two-way transmission loss, and TS is the target strength that includes the local backscattering strength, the insonified area and Lambert’s law to normalize the acoustic image of the seafloor (Lurton *et al.*, 1994).

In normal operation mode, the MBES applies a time variable gain (TVG) to the received signals to compensate beam spreading and absorption losses. The purpose

¹ The angular variation is given by Lambert’s law as: $BS = BS_0 + 20\log(\cos\varphi)$, where BS_0 is the mean backscattering coefficient and φ is the incidence angle.

of *TVG* is to maintain a constant sensitivity for the observation of a given target at any range. The *TVG* must be predicted before the reception (based on previous pings), and must be applied online so that the average signal level in the receiver is at an optimum level to avoid saturation or clipping of the echo envelope. An additional reason for implementing *TVG* is to flatten the beam sample amplitudes. The technique is advantageous for bottom detection and also important for the proper display of the seabed image.

The PROBASI-II (PROcessing BAcKscatter SIGnal) algorithm (Fernandes and Chakraborty, 2009) was utilized to apply necessary corrections related to the position, heading, bathymetry slope, seafloor insonified area, and Lambert's law corrections (Fig. 2.3). The program reads the raw data as a batch file and extracts the specified parameters including backscatter strength, bathymetry, heading, position, and beam angle required during the processing.

2.3.1 Heading and position correction

The recorded data is normally corrected for ship motion during the time of acquisition. However, the data is not compensated accurately for heading, likely due to latency problem during ship turning. By comparing the preceding and succeeding pings, the PROBASI-II algorithm calculated the heading offsets and appropriately applied to the data. Often, due to the unavailability of GPS satellites, the raw data record erroneous position information indicating inappropriate locations. The heading corrected data was monitored for any position jump and corrected suitably using preceding and succeeding ping data.

2.3.2 Bathymetry slope and seafloor insonified area correction

The bathymetry slope has significant influence on seafloor backscattering as the seabed slope varies across and along the swath. The MBES records data with a simplifying assumption of a flat seafloor, and bathymetry slope related position deviation of the beams on the seabed are not accounted during data acquisition. The insonified beam area incorporated in Eq. (2.2) is not accurate and re-calculation of

the insonified area is required if the seafloor is not flat. The insonified beam area was re-computed to obtain better accuracy for each beam, following the formula given in Hammerstad (2000).

2.3.3 Lambert's law removal and corrected angular backscatter data

After applying appropriate corrections related to the position, heading, bathymetry slope, and insonified area, the influence of Lambert's law was removed from the measured echo level. The Lambert's law correction within MBES was introduced for normalizing the sonar image. Prior to inversion modeling, the processed multi-beam angular backscatter data (varying between the incidence angles of -75° to $+75^\circ$) were binned in equal angular bins of 1° intervals, utilizing 20 consecutive pings at each of the sampling locations. The data were subsequently averaged over the available number of samples within each bin. The resulting data was folded with respect to the normal incidence angle to represent backscatter values corresponding to incidence angles 0° to 75° (Fig. 2.3) (Jackson *et al.*, 1986; de Moustier and Alexandrou, 1991; Matsumoto *et al.*, 1993; Chakraborty *et al.*, 2000; Chakraborty *et al.*, 2003).

2.3.4 Backscatter image data processing

The application of the PROBASI-II algorithm was further utilized to generate backscatter image data. The algorithm has been developed with 4 modules, and module 1 is primarily used for generating angular backscatter data to carry out inversion modeling. The other modules 2, 3, and 4 are intended for backscatter image data generation. The modules 2 and 3 comprise normalization of backscatter strengths with respect to 10° incidence angle, angle wise averaging of backscatter strength, and removal of the beam pattern artifact as coarse and fine methods. In module 4, the noise in the backscatter image was removed with the combination of low and high pass filters. The representative raw and processed backscatter images are illustrated in Figure 2.3.

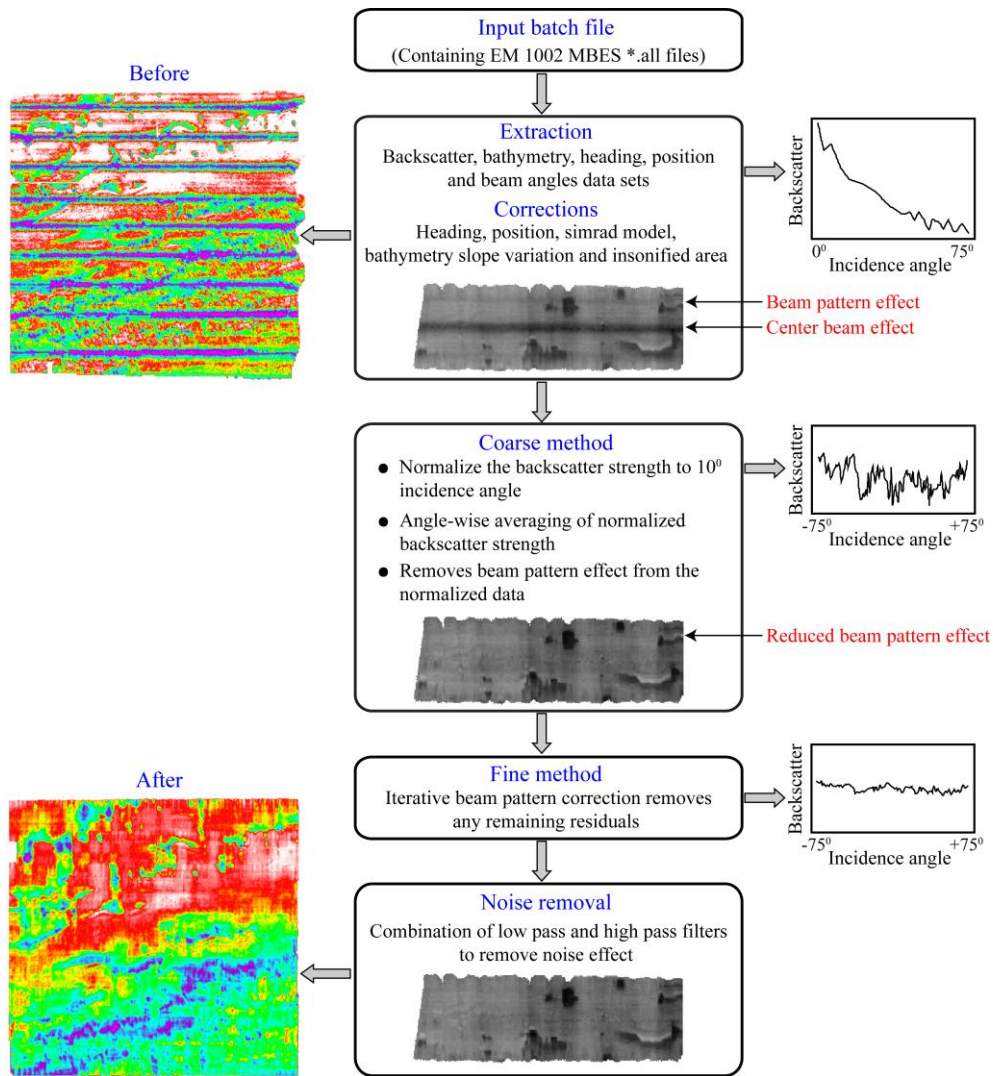


Fig. 2.3 Graphical abstract of the MBES data processing methodology.

2.4 Sediment sampling

The sediment data were collected using a Van-Veen grab, covering an area of 0.04 m^2 and penetration of 10 cm, following a standard protocol. About 20 g sediment was taken from each grab sample to carry out the textural analyses using a 4.0 cm diameter core tube. The sediment was repeatedly washed in distilled water until all the chloride ions detectable with 4 % silver nitrate were removed. These samples were treated with 10 % sodium hexametaphosphate and kept overnight for

dispersion before being subjected to the grain size analyses (Ingole *et al.*, 2002). The acquired sediment samples were subjected to wet sieving using a 62 μm sieve to separate the sand from the mud fraction. The size distribution of the mud fraction ($< 62 \mu\text{m}$) was measured with a Malvern laser particle size analyzer (MASTERSIZER 2000). The size distribution of the sand fraction was determined using standard dry sieving method as it was difficult to maintain uniform suspension of sandy material within the laser particle analyzer. The shelf sediments normally contain shelly material, which had to be sieved prior to measurement by laser diffraction. The mean grain size $M_\phi = -\log_2 U_g / U_0$ (where $U_0 = 1 \text{ mm}$) was then calculated for each of the sediment data locations (Table 2.1).

The sediment samples for benthos identification were washed through a 0.5 mm mesh sieve, and all organisms retained on the sieve were collected and preserved in 10% seawater formalin Rose Bengal solution for subsequent identification. These samples were again washed through 0.5 mm mesh in running water in the laboratory to clear adhering sediments. All organisms were sorted into major groups, preserved in 90% alcohol for further identification and counted group-wise. Specimens were identified to the lowest possible taxon. The average number of organisms from the samples was converted to number per square meter (no. m^{-2}). Biomass was determined by using the wet weight method after blotting. The biomass obtained (shell included) was converted to g m^{-2} (wet weight). The species identification was based on the work by Ingole *et al.* (2010). We have grouped benthic macro-fauna into two communities: (i) soft body organisms, referred to as “deposit feeders”, which include majority of polychaete worms and related soft body species like nematode, oligochaetes, nemertinea, echurids and (ii) hard body organisms, referred to as “filter feeders”, which include mainly bivalves and gastropods (Table 2.1). Total organic carbon analyses were carried out on the freeze-dried sediments using a NCS 2500 (Model EA/NA1110) CNS analyzer after removing inorganic carbon from the total sample.

Table 2.1 Location wise distribution of sediment type, biomass and benthic macro-fauna.

Station	Sand (%)	Silt (%)	Clay (%)	Laboratory measured M_{ϕ}	Sediment type	Water depth (m)	Biomass (g m^{-2})	Soft body organisms (no. m^{-2})	Hard body organisms (no. m^{-2})
1	0.78	70.95	28.27	6.66	Clayey Silt	29	0.35	271	00
2	0.54	75.86	23.60	6.42	Silt	39	2.18	132	66
3	0.64	75.91	23.45	6.50	Silt	47	2.21	308	44
4	57.42	32.30	10.28	4.02	Silty Sand	54	0.78	396	88
5	91.26	6.87	1.87	2.03	Sand	60	4.97	220	176
6	0.13	70.66	29.21	6.79	Clayey Silt	42	1.78	484	00
7	0.92	79.05	20.03	6.20	Silt	53	0.49	264	00
8	80.90	14.24	4.86	2.42	Sand	60	1.42	264	252
9	89.05	8.65	2.30	1.16	Sand	66	1.85	110	154
10	70.31	24.45	5.24	2.40	Silty Sand	74	2.18	176	221
11	73.64	22.29	4.07	1.99	Silty Sand	87	2.49	198	121
12	54.58	38.52	6.90	3.32	Silty Sand	100	0.57	00	44
13	83.77	14.01	2.23	2.07	Sand	109	1.20	78	226
14	1.49	65.28	33.23	6.71	Clayey Silt	22	–	–	–
15	0.41	71.59	27.99	6.68	Clayey Silt	32	–	–	–
16	1.78	70.06	28.16	6.67	Clayey Silt	37	–	–	–
17	3.17	71.93	24.90	6.32	Clayey Silt	48	–	–	–
18	8.03	71.52	20.45	5.83	Clayey Silt	56	–	–	–
19	95.33	3.08	1.59	1.69	Sand	60	–	–	–
20	91.26	6.13	2.61	2.31	Sand	63	–	–	–
21	1.2	40	58.8	7.716	Silty Clay	27	0.062	796	00
22	0.7	15	84.3	8.501	Clay	33	3.875	576	00
23	2.7	40	57.3	7.611	Silty Clay	42	–	–	–
24	2.2	45	52.8	7.496	Silty Clay	52	1.593	155	44
25	77	15	8	3.16	Silty Sand	67	7.492	99	298
26	68.7	17.5	13.7	3.657	Sand	76	7.962	796	1393
27	94	0	6	2.42	Sand	84	–	–	–

Chapter 3

Model-based seafloor characterization

3.1 Introduction

The use of high-frequency SBES and MBES operable within the frequencies 300 kHz is well established for remote acoustic seafloor characterization. The acoustic backscatter data obtained from such echo-sounding systems can be matched with theoretical scattering models to interpret the information embedded in the data. The numerical approach employed for extracting information from the data is commonly referred to as “inversion modeling”. The inversion modeling primarily involves physics based model for inversion of echo-sounding data to obtain the seafloor roughness parameters, namely the sediment mean grain size (M_ϕ); spectral parameters at the water-seafloor interface (γ_2, w_2); and sediment volume parameter (σ), that can be further used to examine fine scale seafloor processes (APL Handbook, 1994). The composite roughness model developed by Jackson *et al.* (1986), using the shape of the angular backscatter data has been extensively applied in this context (de Moustier and Alexandrou, 1991; Matsumoto *et al.*, 1993; Chakraborty *et al.*, 2003). In this chapter, a model-based seafloor characterization technique based on the composite-roughness theory has been developed and demonstrated utilizing the data acquired using a MBES operable at 95 kHz. The MBES angular backscatter data acquired over the substrates ranging from clayey silt

to sand (at 12 locations) in the central part of the WCMI are subject to inversion modeling (Fig. 3.1).

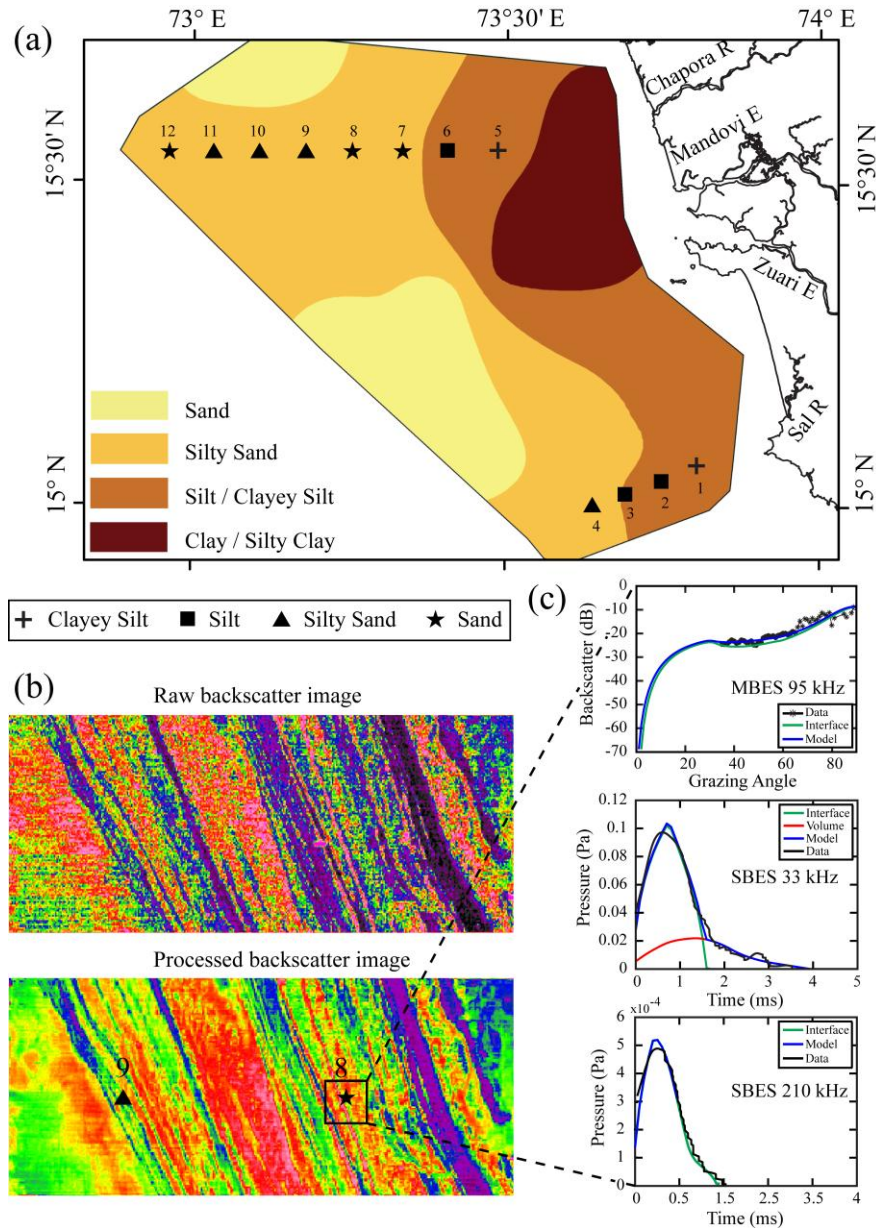


Fig. 3.1 Panel (a) illustrates the acoustic and sediment sample data acquisition locations with respective sediment types. The panel (b) demonstrates the effectiveness of the PROBASI-II algorithm to generate spatial image of the backscatter data. Presented in panel (c) are the processed MBES and SBES (angular backscatter and echo envelope) data used to carry out the inversion modeling.

Moving beyond the techniques that employ MBES angular backscatter data, Pouliquen and Lurton (1992) initiated a modeling method for seabed identification using the shape of the echosounder signals. Sternlicht and de Moustier (1997, 2003a, b) also developed a robust time-dependent seafloor acoustic backscatter model within the frequency range 10–100 kHz, that has been effectively demonstrated for seafloor characterization using the normal-incidence SBES (De and Chakraborty, 2011). The use of multiple acoustic frequencies (van Walree *et al.*, 2006) highlighted in this work improves seafloor characterization, because the roughness spectrum and the sediment volume heterogeneities cause backscatter variation that can be conveniently substantiated using multi-frequency inversion results. In this chapter, the seafloor parameters computed using 95 kHz MBES data are compared with the ground-truth data as well as with the inversion results obtained using 33 and 210 kHz SBES data at the same locations (De and Chakraborty, 2011).

3.2 Model-data comparison

The composite roughness model¹ using the shape of the angular backscatter data developed by Jackson *et al.* (1986) requires few geoacoustic parameters as the model input. In the absence of measured geoacoustic parameters in the study area, these parameters are computed in terms of the mean grain size (M_ϕ). The equations relating geoacoustic model parameters to the mean grain size (M_ϕ) are adapted from the APL-UW High-Frequency Ocean Environmental Acoustics Models Handbook (APL Handbook, 1994).

3.2.1 Computation of scaling parameter to calibrate the data

Even after implementing the pre- and post-processing procedures discussed in the preceding chapter, prior to the model-data comparison, there was an unfulfillment of absolute calibration, and a depth-dependent offset (scaling parameter in dB) was required to correct each of the processed data sets. The scaling

¹ The basic equations formulating the composite roughness model is detailed in Jackson *et al.* (1986).

parameters (calibration offsets) were computed by comparing the model derived backscatter values with the measured data. The seabed scattering model combines the most dominant dimensionless scattering mechanism of the surface roughness coefficient $S_s(\theta_g)$ and volume scattering coefficient $S_v(\theta_g)$, as a superposition of the incoherent scatter to estimate the total seabed backscattering strength $BS_{model}(\theta_g)$ as:

$$BS_{model}(\theta_g) = 10 \log_{10}[S_s(\theta_g) + S_v(\theta_g)] \text{ dB} \quad (3.1)$$

where θ_g is the grazing angle (90°–incidence angle). The scaling difference between the APL-UW model predicted backscatter values and the processed MBES data is apparent for the fine and coarse sediment regions (as can be seen in Fig. 3.2). These differences may be due to instrument calibration, model accuracy or erroneous TVG applied online (de Moustier and Matsumoto, 1993; Dziak *et al.*, 1993; Kloser *et al.*, 2010). Therefore, it would be convenient to treat the level of measured backscatter values as relative for appropriate model-data comparison.

The error-to-signal (E/S) ratio has been used as a merit function to evaluate the model-data matching procedure with the goal of minimizing the value. The E/S is expressed as (Haris *et al.*, 2011):

$$E/S = \frac{\sum_{\theta_g=35}^{\theta_g=65} [BS_{data}(\theta_g) - BS_{model}(\theta_g)]^2}{\sum_{\theta_g=35}^{\theta_g=65} BS_{data}^2(\theta_g)}, \quad (3.2)$$

where the terms $BS_{data}(\theta_g)$ and $BS_{model}(\theta_g)$ represent the data and model predicted backscatter values. This method is independent of the backscatter angular range, and provides a convenient numerical evaluation of the model-data comparison. The resulting scaling parameter (difference between model and data), which minimizes the E/S ratio is used as the representative scaling factor to calibrate the data. Accordingly, the scaling parameters at 12 locations from the study area have been computed. The scatter diagram among the derived scaling parameter and water depth of the study depicts a linear relationship with a correlation coefficient of 0.85 (Fig.

3.2). For model-data comparison and subsequent inversion modeling, the processed backscatter data for all the grazing angles were calibrated with the corresponding scaling parameter obtained from the linear trend line of the scatter diagram.

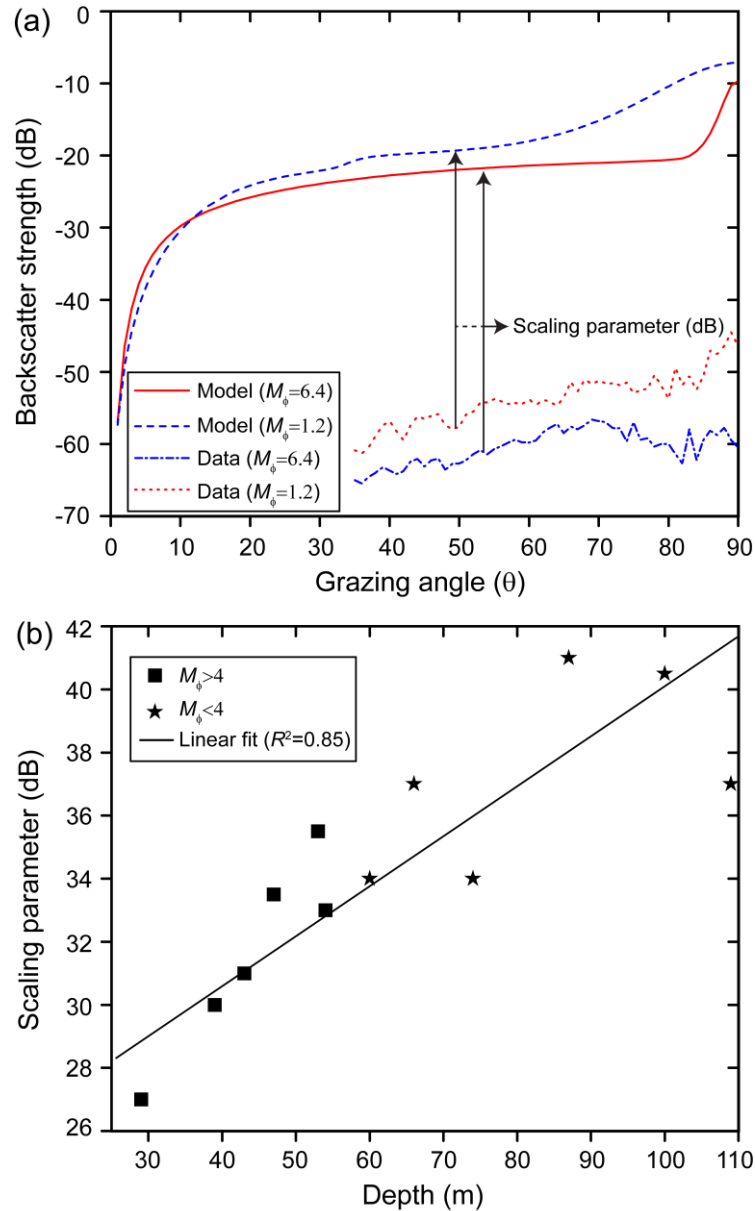


Fig. 3.2 (a) The differences between the model predicted backscatter values and the corresponding processed MBES data are significant for representative sediment types. Panel (b) depicts the linear relationship among the scaling parameter (in dB) and water depth (m) of the study area.

3.2.2 Two-stage parametric optimization

The computation of the correct set of geoacoustic parameters gets convoluted by the large number of good fits existing in the multidimensional search space. It is possible to obtain convincing model-data fits in the search space that do not necessarily represent correct set of seafloor parameters. Accordingly, we have parsed the problem into a two stage parametric optimization method (Sternlicht and de Moustier, 2003b) by constraining the search space (Fig. 3.3). Several options are available to quantify the corresponding results involving the data and model. Here, we have designated the cost-function the error to signal ratio (E/S) as the suitable parameter to evaluate the model-data matching procedure (with the goal of minimizing the value). A low value of E/S signifies a finer model-data comparison. In the frame work of a 3D global search based echo envelope matching procedure, Sternlicht and de Moustier (2003b) have applied simulated annealing with the downhill simplex method to compute the parameters M_ϕ , w_2 , and σ_v . In the present study, we have developed a 4D global search technique including γ_2 , and have substituted the sediment volume scattering coefficient (σ_v) with the sediment volume scattering parameter (σ_2). The first stage of the model-data matching procedure employs a 1D search to estimate the general values of the sediment mean grain size (M_ϕ). The output of the 1D search process provides the input M_ϕ value for the subsequent 4D global search method to calculate the precise mean grain size (M_ϕ); the roughness spectral exponent (γ_2) and strength (w_2); and the sediment volume parameter (σ_2) (Fig. 3.3).

3.3 Inversion results and discussion

The following sections describe the analyses of the computed sediment geoacoustic inversion results (at 33, 95 and 210 kHz) along with the ground truth values of the mean grain size of the seabed sediment. The analyses provide a comparison among the computed seafloor parameters at three acoustic frequencies to evaluate and assess the modeling performance and bottom characterization

potentialities. The end results (given in Table 3.1) have been statistically analyzed and compared with the ground truth data and published information available in the literature. Figure 3.4 shows the model-data comparison in three geologically distinct sediment provinces².

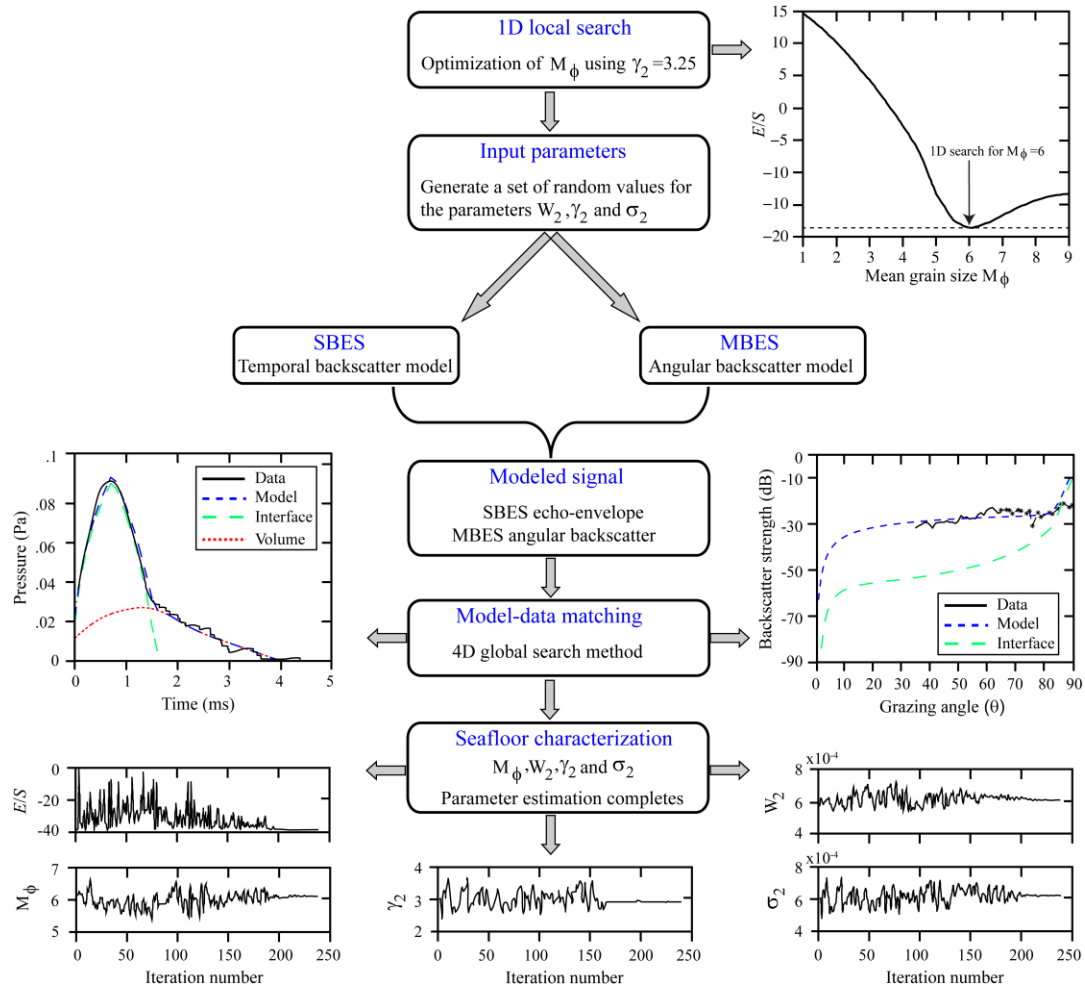


Fig. 3.3 Flow chart representing 4D inversion procedure for seafloor parameter computation.

² For simplicity, throughout the thesis, silty-sand and sand sediments will be referred to as coarse sediments (with $M_\phi < 4$); and clayey-silt and silt sediments will be referred to as fine sediments (with $M_\phi > 4$).

Table 3.1 Summary of the seafloor parameters derived from three acoustic frequencies, 33 and 210 kHz (SBES) and 95 kHz (MBES).

Station	Measured M_ϕ (phi)	Computed seafloor parameters at 33 kHz				Computed seafloor parameters at 95 kHz				E/S at 95 kHz dB	Computed seafloor parameters at 210 kHz			
		M_ϕ (phi)	γ_2	w_2 (cm ⁴)	σ_2	M_ϕ (phi)	γ_2	w_2 (cm ⁴)	σ_2		M_ϕ (phi)	γ_2	w_2 (cm ⁴)	σ_2
1	6.66	6.96	3.32	0.000527	0.0037	6.67	3.26	0.000503	0.0045	-22	5.00	3.22	0.000524	0.0040
2	6.42	6.59	3.29	0.000561	0.0049	6.74	3.23	0.000512	0.0043	-26	4.75	3.27	0.000625	0.0040
3	6.50	6.29	3.10	0.000643	0.0049	6.53	3.21	0.000601	0.0044	-23	5.02	3.29	0.000670	0.0045
4	4.02	2.79	3.29	0.002370	0.0045	4.54	3.27	0.000917	0.0046	-24	3.08	3.12	0.001530	0.0041
5	6.79	6.71	3.21	0.000593	0.0050	6.75	3.21	0.000498	0.0048	-24	5.01	3.34	0.000582	0.0044
6	6.20	6.08	3.24	0.000516	0.0050	6.47	3.23	0.000510	0.0047	-26	4.21	3.28	0.000603	0.0045
7	2.42	1.97	3.12	0.00343	0.0046	1.99	3.15	0.00365	0.0041	-27	1.40	3.10	0.00401	0.0029
8	1.16	2.10	3.25	0.00365	0.0042	1.21	3.24	0.00375	0.0039	-23	1.31	3.14	0.00438	0.0040
9	2.40	2.37	3.24	0.00366	0.0043	2.10	3.21	0.00343	0.0038	-28	2.05	3.11	0.00255	0.0029
10	1.99	1.86	3.20	0.00419	0.0039	1.78	3.21	0.00428	0.0031	-29	1.10	3.10	0.00439	0.0027
11	3.32	2.33	3.19	0.00346	0.0038	2.17	3.18	0.00347	0.0034	-26	1.03	3.20	0.00452	0.0032
12	2.07	1.75	3.10	0.00388	0.0029	1.80	3.17	0.00397	0.0024	-24	1.51	3.20	0.00424	0.0028

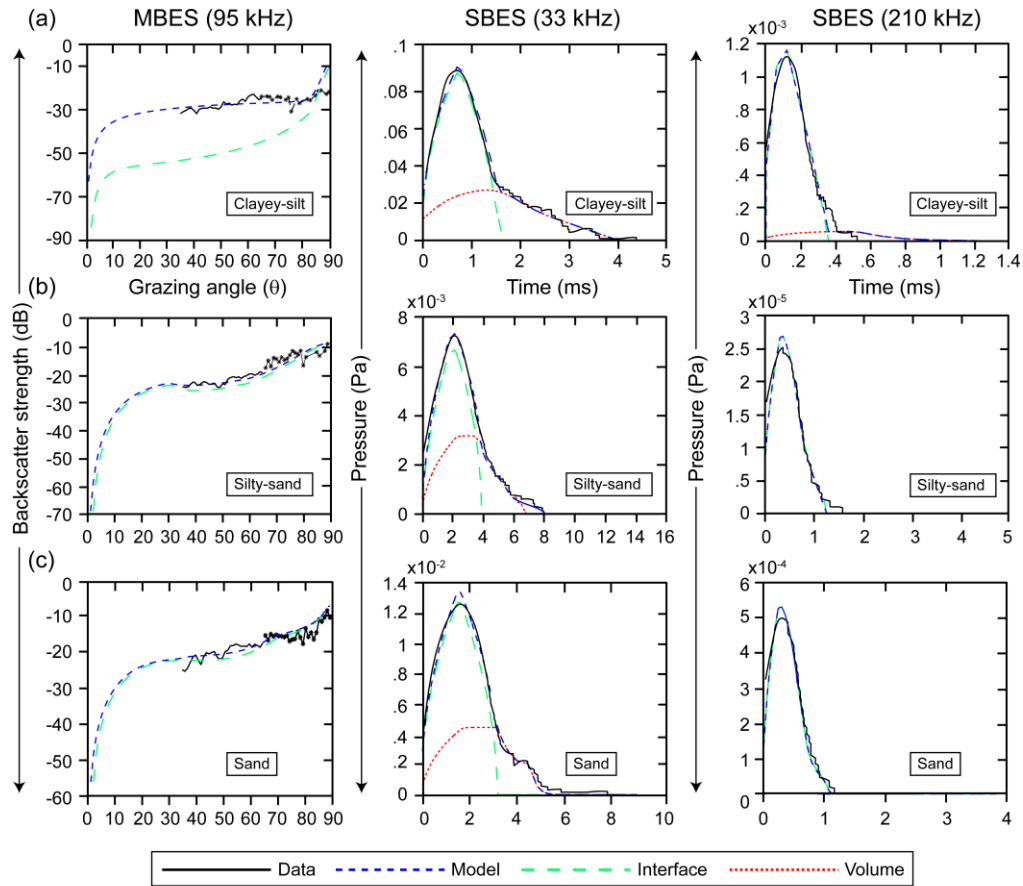


Fig. 3.4 Panels (a), (b) and (c) represent the model-data comparison for three geologically distinct sediment provinces: clayey-silt (location 1), silty-sand (location 10) and sand (location 8) with respective 33-, 210-(SBES) and 95-kHz (MBES) frequencies. The model-data matching procedure for the 95 kHz angular MBES data was carried out within the grazing angles 35° to 65°. The excluded data (star) between 65° and 90° is also plotted to depict the relationship with the data.

3.3.1 Mean grain size (M_ϕ)

The peak amplitudes of the echo envelopes fundamentally depend on the impedance contrast between the water-sediment interfaces. The impedance contrast is often correlated with the mean grain size of sediments (Sternlicht and de Moustier, 2003a). With reference to the inversion modeling study carried out by De and Chakraborty (2011), the computed M_ϕ values of the surficial sediments obtained employing SBES inversions were found to be correlated well with the measurements

(having 95% of confidence limit). Similarly, the M_ϕ values derived from the inversion of MBES data is expected to exhibit correlation with the measurements (based on the sediment ground truth) or information available in De and Chakraborty (2011). Accordingly, the computed M_ϕ values at the three acoustic frequencies are analyzed with respect to the measured M_ϕ values (Fig. 3.5). The computed M_ϕ values are in good corroboration with the measured M_ϕ , indicating statistically significant correlation coefficients of 0.97, 0.98, and 0.96, respectively, at 33, 95, and 210 kHz.

The linear regression analyses carried out to validate the SBES inversion results indicate marginally better computation of M_ϕ at 33 kHz as compared with 210 kHz. The correlation analyses have been carried out including the published SBES inversion results to substantiate the estimated M_ϕ values at 95 kHz. Statistically significant correlation coefficients of 0.97, 0.97 and 0.98 is evident among the model derived M_ϕ values at 33 and 210 kHz, 33 and 95 kHz, and 95 and 210 kHz respectively, indicating the suitability of MBES data for inversion modeling.

The model derived M_ϕ values are in good corroboration with the ground-truth measurements (laboratory derived M_ϕ values). However, variations are noticeable among the computed M_ϕ values at three acoustic frequencies. The backscattering from the seabed can be generally ascribed to two contributing factors, namely interface and volume scattering. The strength of the backscatter signal is primarily controlled by the acoustic frequency, the acoustic impedance contrast between water and sediment, the contributions from seafloor interface roughness, as well as the sediment volume heterogeneity. In fine sediment region, a part of the transmitted acoustic energy penetrates the sediment and is scattered back by the buried inhomogeneities including coarse sand particles and mollusk shells (De and Chakraborty, 2011). The buried heterogeneities can cause local impedance contrast resulting in deviation of the geoaoustic parameters (values correlated with M_ϕ) calculated in the model-data matching procedure (Sternlicht and de Moustier, 2003a). The input geoaoustic parameters are sensitive to the acoustic impedance contrast (the product of density and sound speed in the sediment), and the variation

of density within the sediment layers can contribute to disparity between the model derived and the ground-truth M_ϕ values.

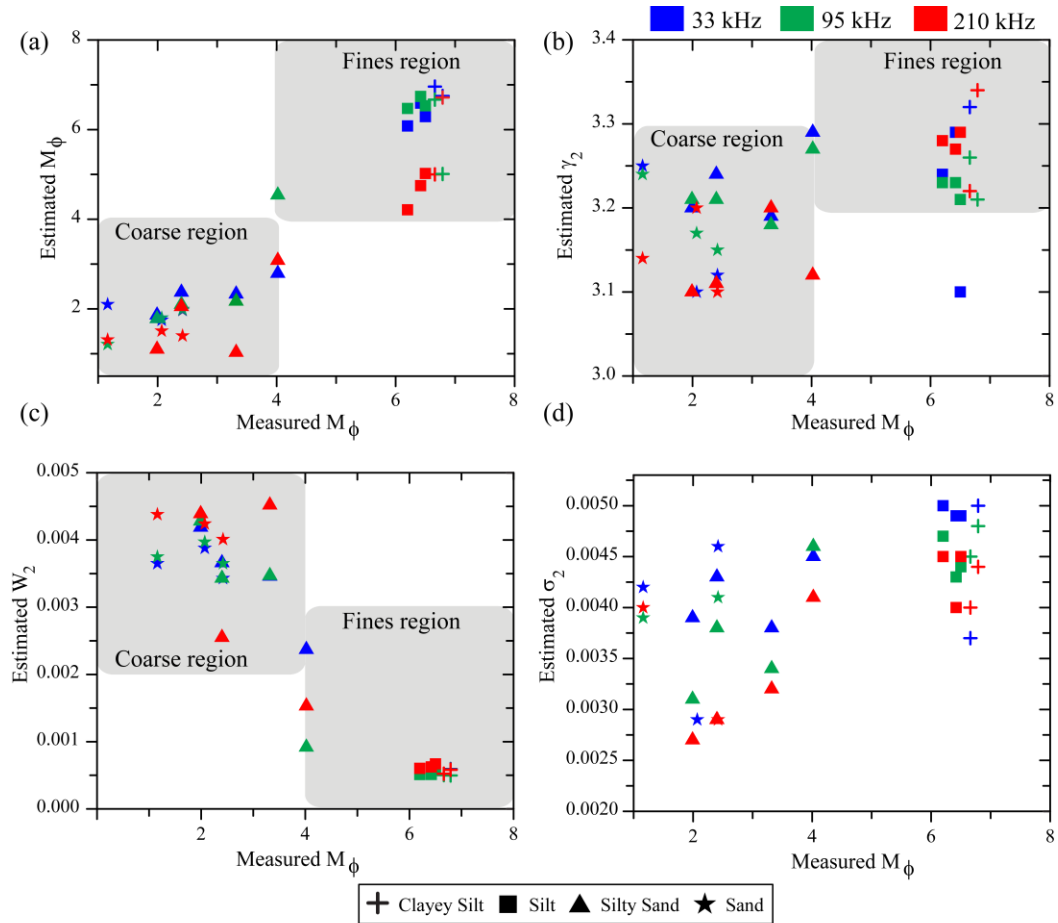


Fig. 3.5 The scatter plot showing multi-frequency inversion results.

3.3.2 Seafloor roughness parameters (γ_2 and w_2)

The computed seafloor roughness parameters (γ_2 and w_2) at 95 kHz along with the SBES inversion results have been analyzed to evaluate the relationship between the backscatter and relief spectral parameters (Fig. 3.5). The scatter diagram between the measured M_ϕ and estimated γ_2 reveals that, in the coarse sediment region, the γ_2 values are confined within the limits of 3.10–3.25, 3.15–3.24, and 3.10–3.20, respectively, at 33, 95, and 210 kHz, but that in fine sediments, the γ_2 values are found to vary between 3.21–3.32, 3.21–3.27, 3.22–3.34, respectively, at 33, 95, and

210 kHz. Moreover, in the coarse sediment region, the average γ_2 values are restricted to values around 3.18 ± 0.061 , 3.19 ± 0.032 , and 3.14 ± 0.047 , respectively, at 33, 95, and 210 kHz. In the fine sediment region, the average γ_2 values are found to be within 3.23 ± 0.085 , 3.22 ± 0.020 , and 3.28 ± 0.043 , respectively, for 33, 95, and 210 kHz. It is observed that the relatively higher values of γ_2 are associated with fine sediments, while the lower values of γ_2 are the characteristics of coarse sediments (Fig. 3.5).

The seafloor “roughness power spectrum” estimated from the SBES and MBES data characterizes the size and periodicity of the seafloor height fluctuations as a function of the spatial frequency (Briggs *et al.*, 2005). The roughness power spectrum is often parameterized using a power law by slope and intercept of a linear regression line through the points of the periodogram estimate in log–log space. The parameters γ_2 and w_2 used in the scattering model of Jackson *et al.* (1986) are the slope and intercept, respectively, of the 2D roughness power spectrum, which are calculated from the 1D power-law values. A wide range of 2D roughness power spectrum parameters can be gleaned from the literature (Briggs, 1989; Stanic *et al.*, 1989; Jackson *et al.*, 1996a; Briggs *et al.*, 2005), and indicate that the majority of the 2D spectral exponent values are confined within 2.90–3.30 in coarse sediments and 3.20–3.50 in fine sediments. In the present study, the computed γ_2 values are corroborated well with the published data, but have a narrower range of values.

Several studies (Jackson *et al.*, 1986; Stanic *et al.*, 1989) have concluded that the majority of measured 2D spectral strength (w_2) values are greater than 0.002 cm^4 in coarse sediments and restricted to values around 0.003 cm^4 in fine sediments (Sternlicht and de Moustier, 2003a). The scatter diagram between the measured M_ϕ and estimated w_2 (Fig. 3.5) reveals that the w_2 values are less than 0.001 cm^4 in fine sediments and confined within the limit $0.002\text{--}0.005 \text{ cm}^4$ in coarse sediments. Moreover, in the coarse sediment region, the average w_2 values are restricted to values around 0.0037 ± 0.00028 , 0.0037 ± 0.00032 and 0.0040 ± 0.00074 , respectively, at 33, 95, and 210 kHz. In the fine sediment region, the average w_2 values are found to be within 0.00057 ± 0.000052 , 0.00052 ± 0.000043 , and 0.00060 ± 0.000054 ,

respectively, for 33, 95, and 210 kHz. The computed w_2 values were validated with the published data. The w_2 values are well clustered at the three acoustic frequencies, having fewer fluctuations for the fine sediment as compared with the coarse sediment region (Fig. 3.5). It is also observed that the relatively higher values of w_2 and lower values of γ_2 are associated with coarse sediments, while the lower values w_2 and higher values of γ_2 are the characteristics of fine sediments.

Briggs *et al.* (2005) and Jackson and Richardson (2007) have reported that the computed w_2 and γ_2 values can cluster depending on the sediment type with distinct trends in coarse and fine sediment regions. Similar clustering patterns of roughness parameters are conspicuous in the present study, demarcating the coarse and sediment provinces (Fig. 3.5). Briggs (1989) also reported that the parameters derived from a roughness power spectrum can vary with respect to the sediment type, such that the roughness spectra characteristic of coarse sediments have a less-steep decay (i.e., lower value of γ_2) in the power-law relationship. The less-steep decay (i.e., less-steep slope of the regression line) in the power spectrum can be attributed to relatively high intercept energy of the spectrum at a unit spatial frequency (1 cm). Therefore, it is likely to have higher values of w_2 and lower values of γ_2 for coarse sediments and comparatively lower values w_2 and higher values of γ_2 characteristics in fine sediments. Apparently, these aspects are evident in the presented analyses (Fig. 3.5).

3.3.3 Sediment volume scattering parameter (σ_2)

The shape of the SBES echo envelope has two distinct parts, the initial part and the tail part. The initial part of the data represents the reflection from the water-sediment interface (interface scattering and the related γ_2 and w_2), and the tail portion corresponds to the backscatter from the sediment volume (volume scattering and the associated parameter σ_2). The σ_2 values are generally related to the sediment type (fine or coarse) and seafloor inhomogeneities (Jackson *et al.*, 1986). Jackson and Briggs (1992) have demonstrated dominant sediment volume backscatter in finer sediments, and Jackson *et al.* (1986) used σ_2 as a variable parameter with a

maximum range up to 0.004 in soft sediments. However, Stewart and Chotiros (1992) have experimentally demonstrated that the limit of σ_2 designated in soft sediment is low, and the sediment volume scattering coefficient is usually much higher than the predicted value. Nonetheless, it is convenient to use σ_2 as a variable parameter in the model-data matching procedure. The sensitivity analyses carried out on the shape of the SBES data³ indicates significant contribution of sub-bottom scattering conspicuous near the tail of the echo-envelope with relatively higher σ_2 value. The higher σ_2 has marginal effect on the peak amplitude of the echo-envelope. With reference to the recent study carried out by De and Chakraborty (2011), the selection of low σ_2 values (<0.004) resulted in higher values of E/S ratio during the inversion modeling. Improved model-data comparisons (with low values of E/S ratio) were achieved by increasing the σ_2 values (>0.004). The variation of the computed σ_2 among the coarse and fine sediments was subtle because it has been chosen as a variable parameter that varies with the locations. In the absence of measured σ_2 parameters in the study area, based on the published SBES inversion results (De and Chakraborty, 2011), the input value of σ_2 is assigned as 0.004 for MBES inversion modeling irrespective of the sediment type.

In the coarse sediment region, the average σ_2 values are restricted to values around 0.0039 ± 0.00059 , 0.0034 ± 0.00063 , and 0.0031 ± 0.00048 , respectively, at 33, 95, and 210 kHz. In the fine sediment region, the average σ_2 values are found to be within 0.0047 ± 0.00056 , 0.0045 ± 0.00021 , and 0.0043 ± 0.00026 , respectively, for 33, 95, and 210 kHz. The computed σ_2 are important to provide convincing model-data comparison at the three acoustic frequencies (Fig. 3.5). Jackson and Briggs (1992) have reported dominant volume scattering in fine sediments. The experiment carried out by Jackson and Briggs (1992) demonstrated improved model-data comparison in the fine sediment region with relatively higher values of σ_2 (0.004–0.006). In the present study, the σ_2 values computed in the fine sediments have been found to be

³ The method used to examine relative importance of input parameters to the model output is commonly termed as sensitivity analyses. The readers are referred to the PhD thesis of De. (2010), for more information on the sensitivity analyses of SBES model.

relatively higher as compared with the coarse sediment region. An appropriate assessment on the accurateness of the estimated σ_2 values is difficult due to lack of supporting data and further studies are required to draw better conclusion.

3.4 Concluding remarks

The composite roughness scattering model (Jackson *et al.*, 1986) derived seafloor parameters (M_ϕ , γ_2 and w_2) using the 95 kHz MBES data are compared with the ground-truth data as well as with the inversion results obtained using 33 and 210 kHz SBES data at the same locations. The resulting geoacoustic parameters provide important information that can be utilized for acoustic seafloor characterization. Statistically significant correlations are noticeable between the model derived M_ϕ values and the ground truth sediment information, substantiating the multi-frequency inversion results. The M_ϕ values estimated at 33 and 95 kHz appears to be marginally better as compared with 210 kHz⁴. In the absence of measured roughness data, the computed roughness spectrum parameters (γ_2 and w_2) are compared with the published information available in the literature. The computed γ_2 and w_2 values are corroborated well with the published data, displaying subtle variations among 33, 95, and 210 kHz.

Williams *et al.* (2002) have postulated transition of the scattering theory in the critical frequency range of 150–300 kHz. Utilizing the backscatter data of the experiments SAX99 and SAX04, Williams *et al.* (2009) have reported the emergence of a new scattering mechanism at 200 kHz or higher frequencies. Significant difference in scattering strength from the surrounding medium and the embedded

⁴ The analyses of multi-frequency inversion results and related geoacoustic parameters for different combination of sediment substrate, operating frequency, and transducer orientation suggests that the moderate frequencies (33 and 95 kHz) are more appropriate for model-based seafloor characterization. The subtle difference among the roughness parameters computed at 33, 95, and 210 kHz is possibly due to limitations of Helmholtz-Kirchhoff theory implemented in the SBES temporal backscatter model. The Helmholtz-Kirchhoff theory basically computes the seafloor interface roughness (and the resulting model) with the assumption of isotropic Gaussian distribution of the surface relief. The assumption restricts the application of Helmholtz-Kirchhoff theory to extremely rough (rocky) seafloor and higher operating frequencies (>100 kHz), where the Kirchhoff's criterion fails (Sternlicht and de Moustier, 2003b). However, De. (2010) computed the Kirchhoff's criterion for 210 kHz and demonstrated its suitability for seafloor characterization.

coarse material in the controlled laboratory experiments is also obvious at higher frequencies between 150 kHz to 2 MHz (Ivakin and Sessarego, 2007). Besides, it has been reported that at higher frequencies (> 200 kHz), even a small portion of the embedded shell fragments can significantly alter the seafloor scattering characteristics, resulting in the subtle difference among the roughness parameters computed at 33, 95, and 210 kHz. In the context of multi-frequency inversion, the results derived using the 95 kHz MBES data are more correlated with the seafloor parameters corresponding to 33 kHz as compared with 210 kHz SBES data.

Chapter 4

Seabed habitat mapping

4.1 Introduction

The application of acoustic remote sensing using high-frequency SBES and MBES sonar imageries can generate significant data for ocean multidisciplinary studies including seafloor characterization and benthic habitat studies (Kloser *et al.*, 2001; Tegowski, 2005; Brown and Blondel, 2009a). The technological innovations in SBES and MBES for acoustic seabed classification and benthic habitat mapping are currently an active area of research, and have become an imperative tool in ecosystem based management of marine environment.

Considering the ecological aspects of benthic habitats on the seafloor, cost-effective methods to study the seabed at large spatial scales are desirable. Studies investigating the distribution of seafloor sediments and benthic habitat usually involve collection of samples using sediment grabs or diving methods for characterizing the sediment substrate and the associated benthic species, and assessment of benthic density. Such methodologies provide precise representation, however they are time consuming and are rather preferred for assessment of relatively small areas of the seafloor (Quintino *et al.*, 2009). Alternatively, the acoustic remote sensing techniques are widely used to study the seafloor and the benthic habitat environment with the purpose of delineating sediment substrates and the associated species communities. Amongst the acoustic systems the normal

incidence SBES provides backscatter data over relatively small areas of the seafloor. Several studies have been carried out in the past to characterize the seafloor and benthic habitats using SBES data (Anderson *et al.*, 2002; Freitas *et al.*, 2003; Chakraborty *et al.*, 2007; Quintino *et al.*, 2009). There has been significant improvement in swath sounding system resulting in the technological development of MBES for studying the seafloor (Chakraborty *et al.*, 2004; van Walree *et al.*, 2005; Brown *et al.*, 2011; Hamilton and Parnum, 2011) and the related habitat environment (Brown and Blondel, 2009b; McGonigle *et al.*, 2009; De Falco *et al.*, 2010; Kloser *et al.*, 2010; Ierodiaconou *et al.*, 2011). In this chapter, the multi-frequency acoustic backscatter computed from MBES and SBES operable at 95 kHz and 33/210 kHz, respectively, have been used to demarcate the distribution of sediment texture and benthic macro-fauna abundance along the central part of the WCMI (Fig. 4.1).

Marine benthos present on the seafloor can be broadly categorized as micro and macro organisms. In this study, only the macro benthos is considered. Its presence on the seafloor can affect the backscatter in many ways: (i) due to the movement of the hard body fauna such as bivalves and gastropods that scatters the sound signal due to strong impedance mismatch between the sediments or their body parts (Jumars *et al.*, 1996), and (ii) by altering the local density of sediment-water interface, including displacements responsible for producing or erasing the small scale features. Such changes are caused by burrowing and tube building of soft body fauna, mainly dominated by polychaete worms (Kogure and Wada, 2005). Besides, the micro benthic organisms commonly produce gas. The gas in the form of bubbles are trapped in the top layer of sediments, scattering the acoustic wave (Pouliquen and Lyons, 2002; Holliday *et al.*, 2004). Then scattering strength is expected to be high when the spatial scale of the scattering animal or the modifications in the sediment substrates becomes comparable to the transmitting acoustic wavelength (De and Chakraborty, 2011). In the present study, the backscatters at three acoustic frequencies (33, 95, and 210 kHz) are analyzed to demonstrate the interrelationship among acoustic backscatter, grain size, and benthic macro-fauna abundance.

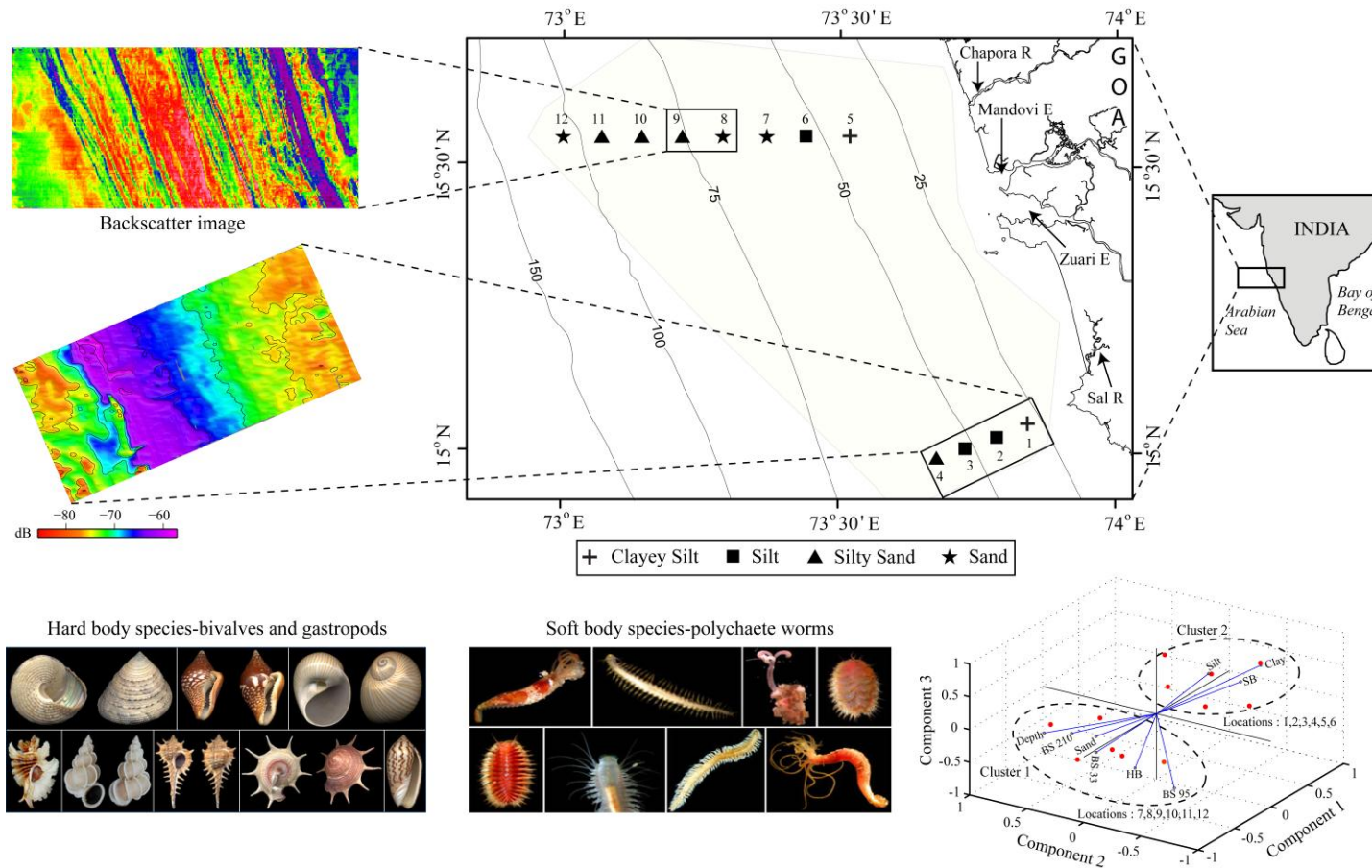


Fig. 4.1 Study area shows the acoustic and sediment sample data acquisition locations with respective sediment types. The depth contours are expressed in meters. The geographic locations of the two estuaries (Mandovi and Zuari) and rivers (Chapora and Sal) have also indicated.

4.2 Results and discussion

The comprehensive application of GIS has been implemented (Mortensen *et al.*, 2009) to generate spatial map of the ground truth and derived backscatter data. The spatial maps were generated incorporating available data sets from the study area (the type of data collected has been illustrated in Fig. 2.1). However, in the statistical analyses we have examined the data corresponding to 12 locations along with acoustical, physical, and biological information. ArcGIS “Kriging” technique was used for image generation. The technique involves an interactive investigation of the spatial behavior of the phenomenon or data. Kriging is an advanced geostatistical procedure that generates an estimated surface from a scattered set of points with z-values. Unlike other interpolation methods supported by ArcGIS Spatial Analyst, Kriging account for the spatial behavior of the phenomenon represented by the z-values. It is based on the regionalized variable theory that assumes that the spatial variation in the phenomenon represented by the z-values is statistically homogeneous throughout the surface. This hypothesis of spatial homogeneity is fundamental to the regionalized variable theory.

The following sections compare the computed backscatter strengths of SBES and MBES with weight percentage of the sediment fraction and the number density of benthic macro-fauna present on the seafloor. The use of traditional statistical techniques to examine spatial and temporal dependence of benthic habitat on the acoustic backscatter has been proposed in the past (Jackson *et al.*, 1996b). Similarly, in the present analyses we have employed PCA to better understand shelf seafloor processes along the WCMI. PCA is a mathematical procedure that uses an orthogonal transformation to convert a set of observations of possibly correlated variables into a set of values of linearly uncorrelated variables called principal components (PCs). This technique has three features: it orthogonalizes the components of the input vectors (so that they are uncorrelated with each other), it orders the resulting orthogonal PCs such that those with the largest variation come first, and it eliminates the PCs that contribute least variation in the data set. The first several PCs account for cumulatively 80–90% of the variances in the data. The

insignificant data variances are also included in the PCs with higher indexes (Manly, 1994).

4.2.1 Ground-truth data

The percentage distribution of sediment compositions based on Shepard's classification (Shepard 1954) indicates the presence of four sediment types: clayey-silt, silt, silty-sand and sand with varied levels of mixing of three textural grades, namely, sand, silt, and clay. The sediment texture was relatively coarse ($M_{\phi} < 4$) in the deeper depths (60–109 m), whereas fine-grained sediment ($M_{\phi} > 4$) was found in the shallow depth region (29–54 m). Table (2.1) in Chapter 2 provides location wise details of the sediment type, biomass, and population density of benthic macrofauna.

4.2.2 Backscatter and grain size

The computed backscatter data (using Eq. 2.1 in Chapter 2) at three acoustic frequencies are compared with weight percentage of the individual grain size classes namely, sand, silt, and clay. The correlation coefficient (R^2) between backscatter intensity and grain size classes is displayed in Figure 4.2. The backscatter intensity is directly correlated with coarse fractions (sand within the range 62–2000 μm) and inversely correlated with finer fractions, namely silt (2–62 μm) and clay (<2 μm) at three acoustic frequencies. The relationship between backscatter intensity and the weight percentage of the sand fraction is depicted in Figure 4.2. The acoustic backscatter shows a linear relationship with the percentage of the sand fraction. Conversely, the relationship between backscatter intensity and the weight percentage of the silt and clay indicates that the backscatter intensity decreases with increasing weight percentage of both silt and clay fraction (Fig. 4.2).

Several studies while comparing the acoustic backscatter responses with the ground-truth sediment information have concluded the suitability of different acoustic technologies to classify seafloor types (e.g. Goff *et al.*, 2004; Ferrini and Flood, 2006; Simons and Snellen, 2009; De Falco *et al.*, 2010). The backscatter

intensity from a muddy seafloor has been reported to be inversely related to the percentage content of silt and clay (Goff *et al.*, 2004; Sutherland *et al.*, 2007). Fine sediments generally exhibit low backscatter intensity due to low density and sound velocity (De Falco *et al.*, 2010). The spatial variability of backscatter intensity in coarse sediments is mainly driven by the weight percent of coarse grains (sand) (Goff *et al.*, 2004; De Falco *et al.*, 2010). Coarse sediments are more likely to result in higher backscatter intensity due to scattering from coarse particles, lower porosity, higher density and sound velocity, and greater roughness of the water-sediment interface. The results obtained in the present study are in corroboration with De Falco *et al.* (2010), establishing a linear relationship between weight percentage of sand and backscatter intensity. An inverse relationship revealed between backscatter intensity and percentage content of silt and clay in fine sediments validates the previous studies (Goff *et al.*, 2004; Sutherland *et al.*, 2007).

The benthic macro-fauna present on the seafloor can affect backscatter in several ways. The hard body fauna as an individual and group can scatter acoustic energy. The benthic macro-fauna can compact and dilate the sediment, resulting in modification of seafloor roughness, sediment density and fluctuations in the sound speed. They can also destroy layers created by sedimentary events (Diaz *et al.*, 1994). The collective mixing processes of sediment substrates by the benthic macro-fauna are termed as bioturbation. Besides bioturbation, the acoustic energy transmitted by the echosounder penetrates the sediment and is scattered back by the buried inhomogeneities including coarse sand particles, shell hash, mollusk shells, and layers of coarse materials. The intensity of the scattered energy depends on the sizes of the buried heterogeneities relative to the impinging acoustic wavelength (De and Chakraborty, 2011). The collective processes might be controlling higher backscatter strength observed in the coarse sediment region with substantial occupancy of hard body organisms.

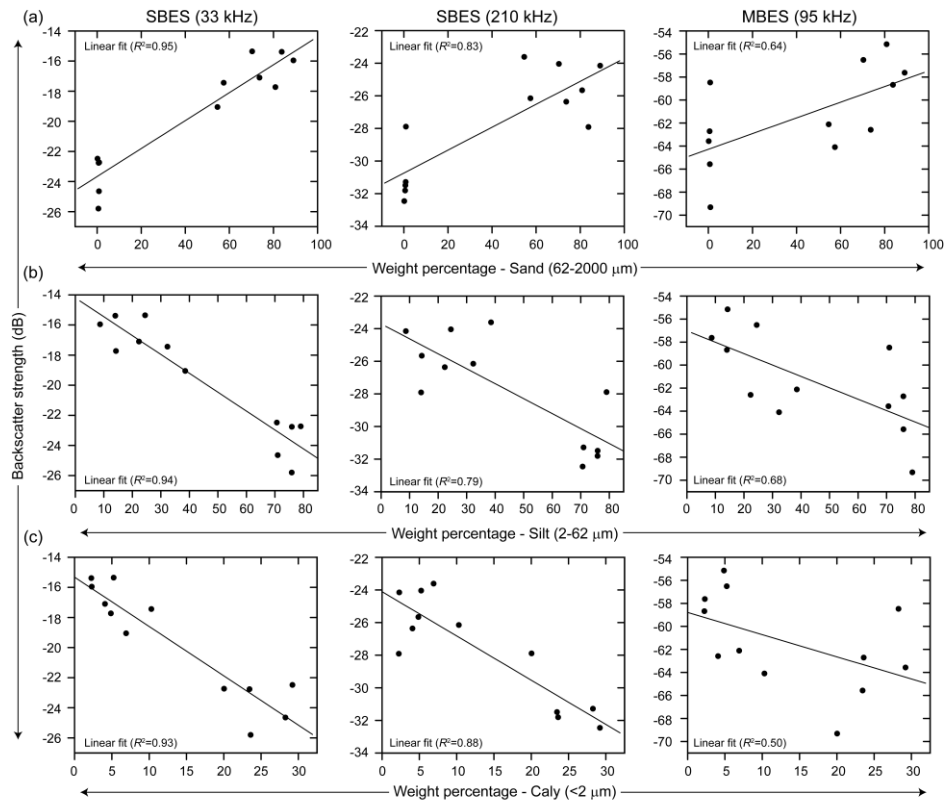


Fig. 4.2 Scatter diagram demonstrating the relationship between the backscatter at three frequencies and weight percentage of sediment types sand (Panel a), silt (Panel b), and clay (Panel c).

Relatively significant correlations between the backscatter intensity and grain size are evident for SBES as compared to MBES measurements. The difference in correlation coefficient (R^2) is not directly related to the acoustic frequency because the SBES measurements were performed at 33 and 210 kHz. The low correlation coefficients attributed to 95 kHz MBES measurements may possibly due to the selection of reference angle used for backscatter computation. In the present study, to compute representative backscatter values for statistical analysis, it was necessary to designate a reference angle that is minimally sensitive to slope correction and absorption errors. Accordingly, the backscatter values corresponding to 40° incidence angles were chosen for the analysis carried out (Kloser *et al.*, 2010). A generic representation of backscatter strength versus incidence angle is illustrated in

Figure 4.3 with the description of physical processes involved in the seafloor backscattering. At higher frequencies used by seafloor mapping sonar, the backscattering from the seabed can be generally ascribed to two contributing factors (Fig. 4.3). Part of the energy is scattered by the interface relief, either by the subhorizontal facets at incidence angle close to the vertical or by microscale roughness at grazing incidence. The other part of the energy penetrates the sediments and is scattered back by the volume heterogeneities. The volume scattering can become predominant at oblique incidence (Lurton, 2002).

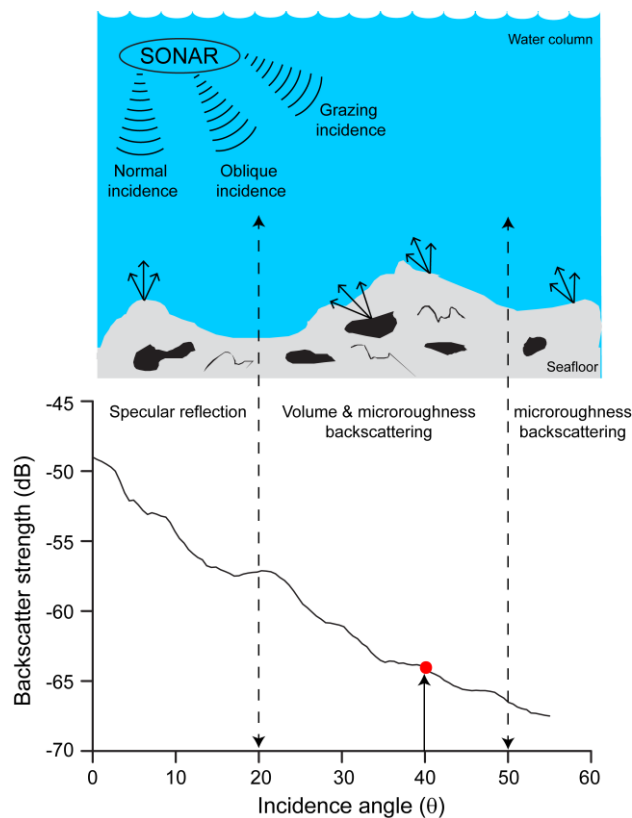


Fig. 4.3 Generic representation of backscatter strength versus incidence angle (after Lurton, 2002) illustrating the physical processes involved in seafloor backscattering. The angular backscatter data presented here corresponds to the location 11 (silty-sand). The marked backscatter value at reference angle 40° was chosen for the statistical analysis carried out in this study. This particular reference angle is minimally sensitive to slope correction and absorption errors as compared to other values in the angular profile.

4.2.3 Grain size and benthic habitat

The number density of both hard and soft body organisms are compared with weight percentage of the individual grain size classes. The correlation coefficient R^2 to determine the animal-sediment relationship is depicted (Fig. 4.4). The number density of hard body organism is directly correlated with coarse fractions (sand within the range 62–2000 μm) and inversely correlated with finer fractions, namely silt (2–62 μm) and clay (<2 μm). The number density of hard body organisms shows a linear relationship with the percentage of the sand fraction. In fine region, the number density of hard body organism indicate an inverse relationship with weight percentage of both silt and clay fraction (Fig. 4.4). Conversely, the number density of soft body organisms is linearly correlated with both silt and clay fractions and inversely correlated with coarse fractions. The meager correlations are suggestive of unquantified factors influencing the distribution of benthic macro-fauna.

Two distinct feeding groups are observed in the study area: namely, deposit feeders (majority of polychaete worms and related soft body species like nematode, oligochaetes, nemertinea, and echurids) mainly in shallow region and filter feeders (hard body bivalves and gastropods) in deeper depths. Besides, a coexistence of deposit feeder along with filter feeder in the deeper regions is also observed. The dominance of deposit feeders in the fine-grained sediment has been previously reported from Indian waters (Jayaraj *et al.*, 2007, 2008). Ansari *et al.* (1977) and Jayaraj *et al.* (2007, 2008) have concluded that fine-sediment including clayey regions are not a favorable substratum for filter feeders. Sanders (1958) had suggested that the coarse region (sand sediment), with filter feeder dominance, reflects the environment with pronounced under water current activity providing sufficient food source to filter feeding organisms. Conversely, the fine sediment region towards the shallow depth reflects the environment with weaker currents, allowing the fine particles to settle down. This can cause inadequate amount of organic matter in suspension as the food source for filter feeders and inhibits them from inhabiting in such environments (Jayaraj *et al.*, 2008). The dominance of deposit feeders in the fine sediment regions and filter feeders in the coarse sediment

regions suggests the influence of sediment texture on the feeding behavior of the organisms (Fig. 4.5).

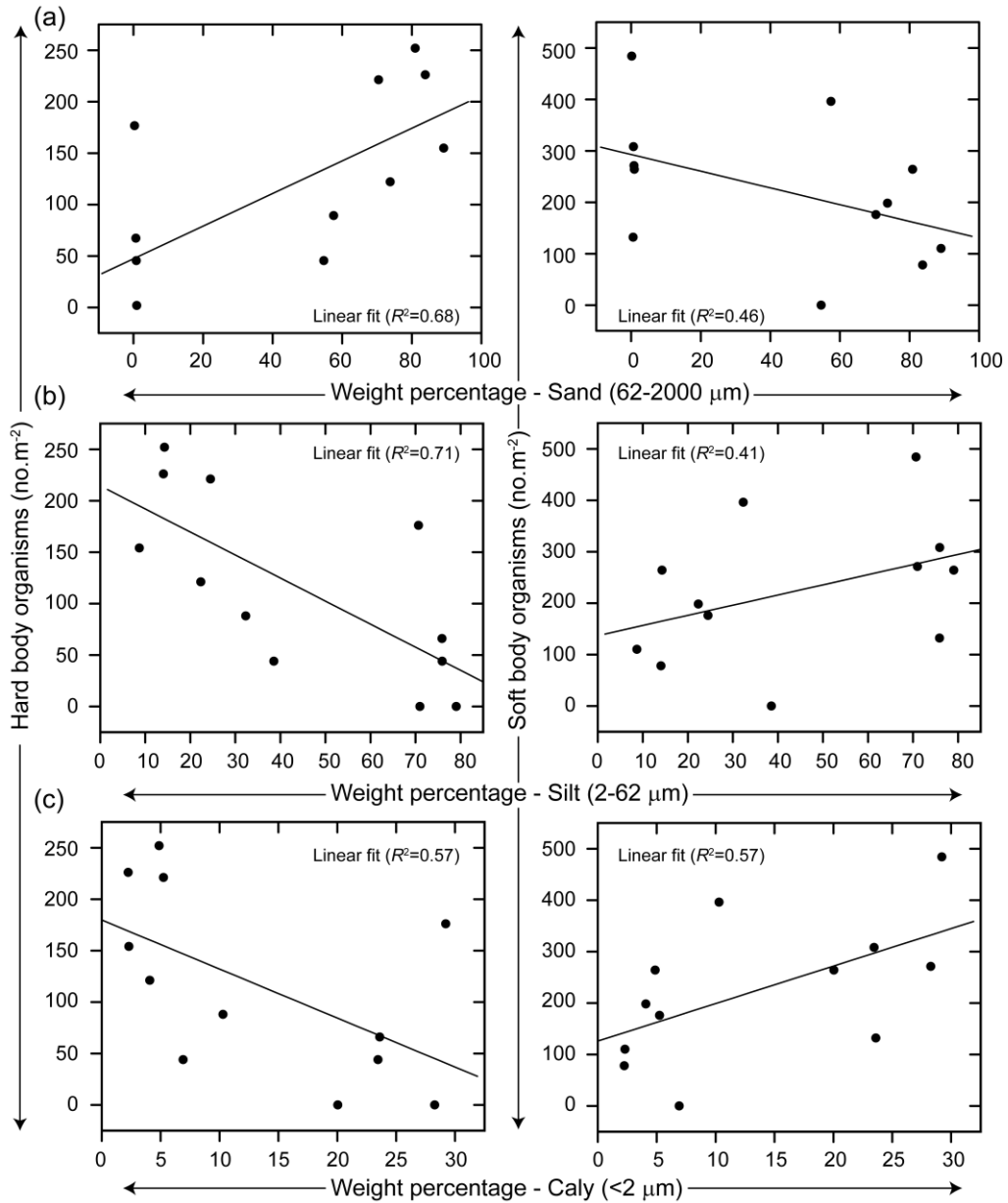


Fig. 4.4 Scatter diagram depicting correlation between the benthic macrofauna and weight percentage of sediment types sand (Panel a), silt (Panel b), and clay (Panel c).

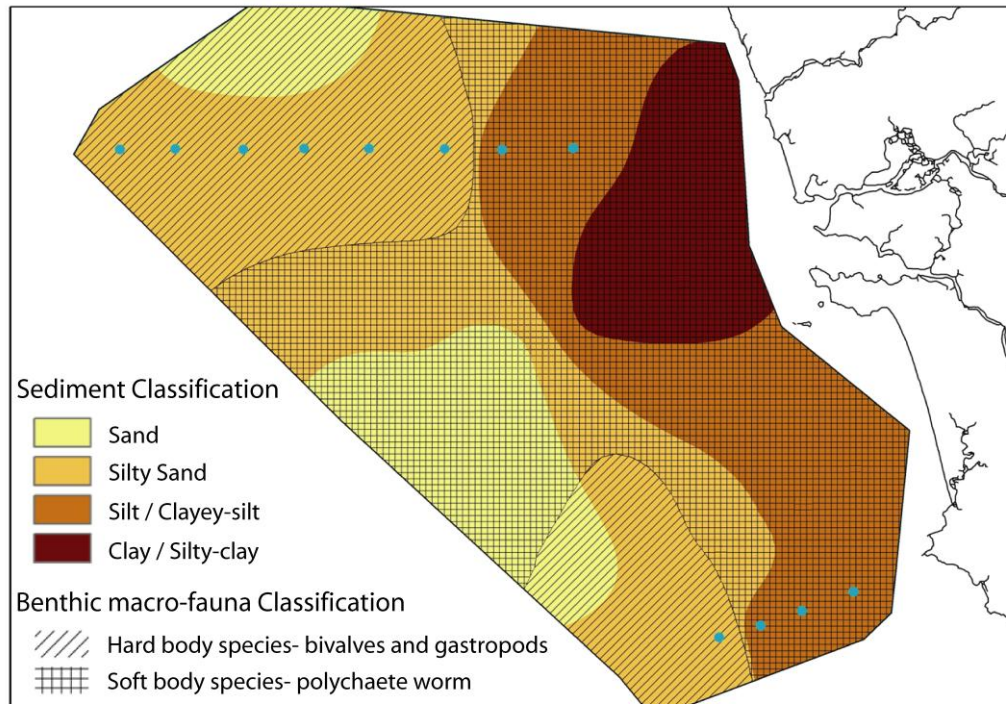


Fig. 4.5 GIS-based classification representing the animal-sediment relationship. The distribution of benthic macro-fauna in relation to the sediment types is clearly distinguished.

4.2.4 Interrelationship between backscatter, grain size, and benthic macro-fauna abundance

The correlation among the acoustic backscatter strength, grain size, and benthic macro-fauna abundance are validated by applying PCA. The associated dendrogram incorporating 8 variables delineates two major clustering patterns from the study area (Fig. 4.6). The dendrogram involves many U-shaped lines connecting the variables in a hierarchical tree. The height of each U represents the distance between the two objects being connected. The cluster 1 consists of coarse sediment texture (with higher sand percentage) and high backscatter intensity values at three acoustic frequencies with substantial occupancy of hard body benthos. The sediments in cluster 2 are characterized by relatively low backscatter values and fine sediment texture (high percentage content of both silt and clay) with significant occupancy of soft body organisms. Briefly, high backscatter intensity values, coarse

sediments, and hard body organisms are the major components contributing to cluster 1. Conversely, low backscatter intensity values, fine sediments, and soft body organisms are the major components associated with cluster 2. The location wise clustering of the input variables is shown as a biplot of PCA in 3D view (Fig. 4.6). In PCA, each variable is represented by a vector, and the direction and length of the vector indicates how the variable contributes to each of the clusters formed. The related variances are found to be 74.74, 10.83, and 9.38 %, respectively, for PC1, PC2, and PC3. The other variances of the data are also included in the PCs with higher indexes, but they are insignificant to be represented. The dominance of deposit feeders in the fine-sediment regions (locations: 1–6) and filter feeders in the coarse sediment regions (locations: 7–12) are substantiated by applying PCA. The clustering analysis also reveals the suitability of acoustic backscatter and sediment texture data to demarcate the distribution of the benthos present on the seafloor (Fig. 4.7 and Fig. 4.8).

The benthos inhabiting on the seafloor have diverse population and complex community dynamics (Kloser *et al.*, 2010) that are often affected by factors other than the substrate type. In this context, we have mapped the variations of total organic carbon in the study area and correlated with the distribution of biomass and benthic density. The overall variation of biomass displays a peak at 54 m water depth, with decreasing trend towards both shallow (<54 m) and deeper (>54 m) depths (Fig. 4.9). Noticeably, the low biomass was apparent at 29 m depth. The distribution of benthic density is relatively significant at water depths 43, 54, and 60 m (Fig. 4.9). Beyond 60 m, the benthic density exhibits a decreasing trend with increasing water depth. The present findings are in good corroboration with the earlier studies from Indian waters (Jayaraj *et al.*, 2007, 2008).

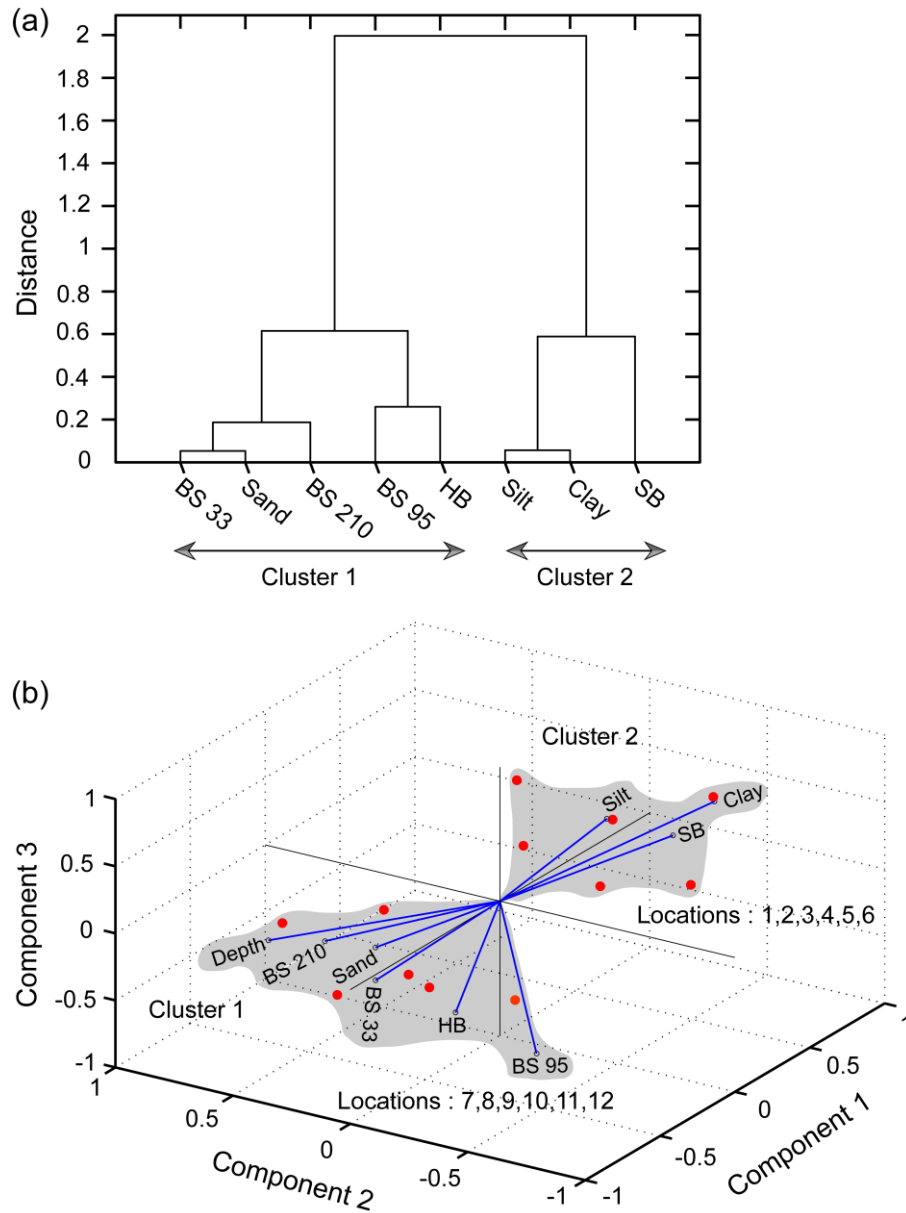


Fig. 4.6 Panel (a) represents the dendrogram and clustering of benthic macrofauna, multi-frequency backscatter, and sediment types. The acronym BS, SB and HB denotes backscatter, soft body and hard body benthic macro-fauna respectively. Panel (b) represents the location wise clustering of the 8 variables in 3D view. The first three PCs representing 94.95% variance in the data sets are presented. Each variable in the data set is represented by a vector, and the direction and length of the vector indicates how the variable contributes to each of the clusters formed.

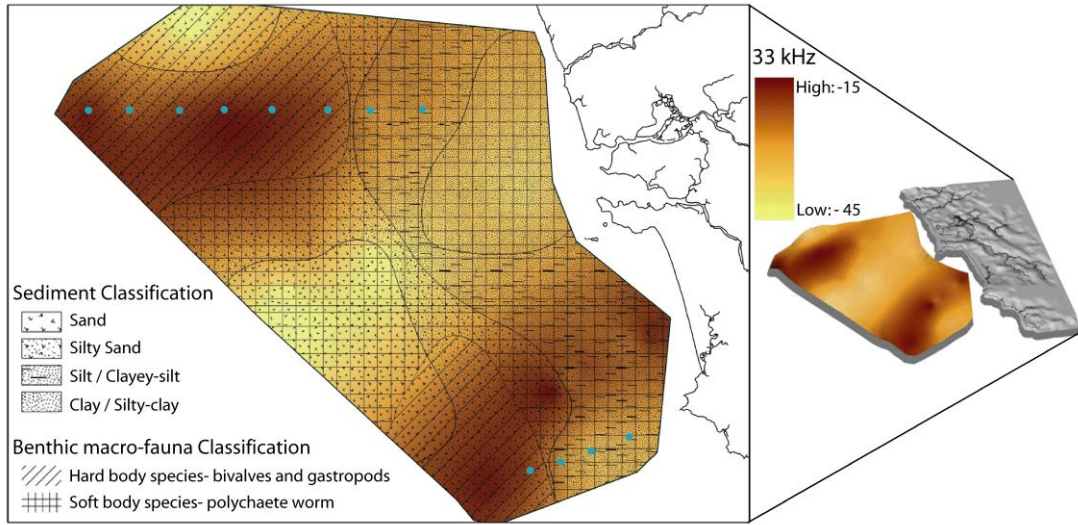


Fig. 4.7 GIS-based classification representing the backscatter-animal-sediment interrelationship at 33 kHz.

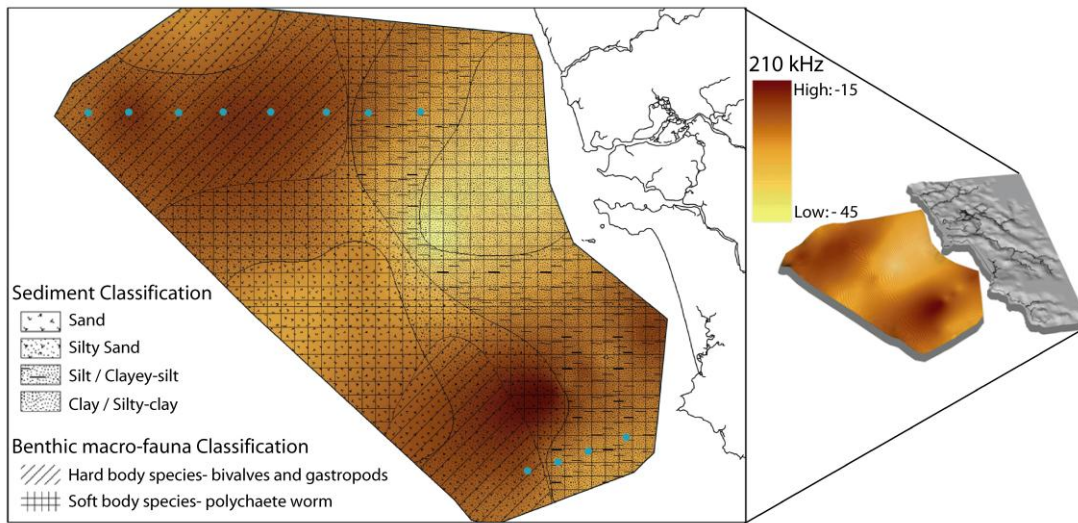


Fig. 4.8 GIS-based classification representing the backscatter-animal-sediment interrelationship at 210 kHz.

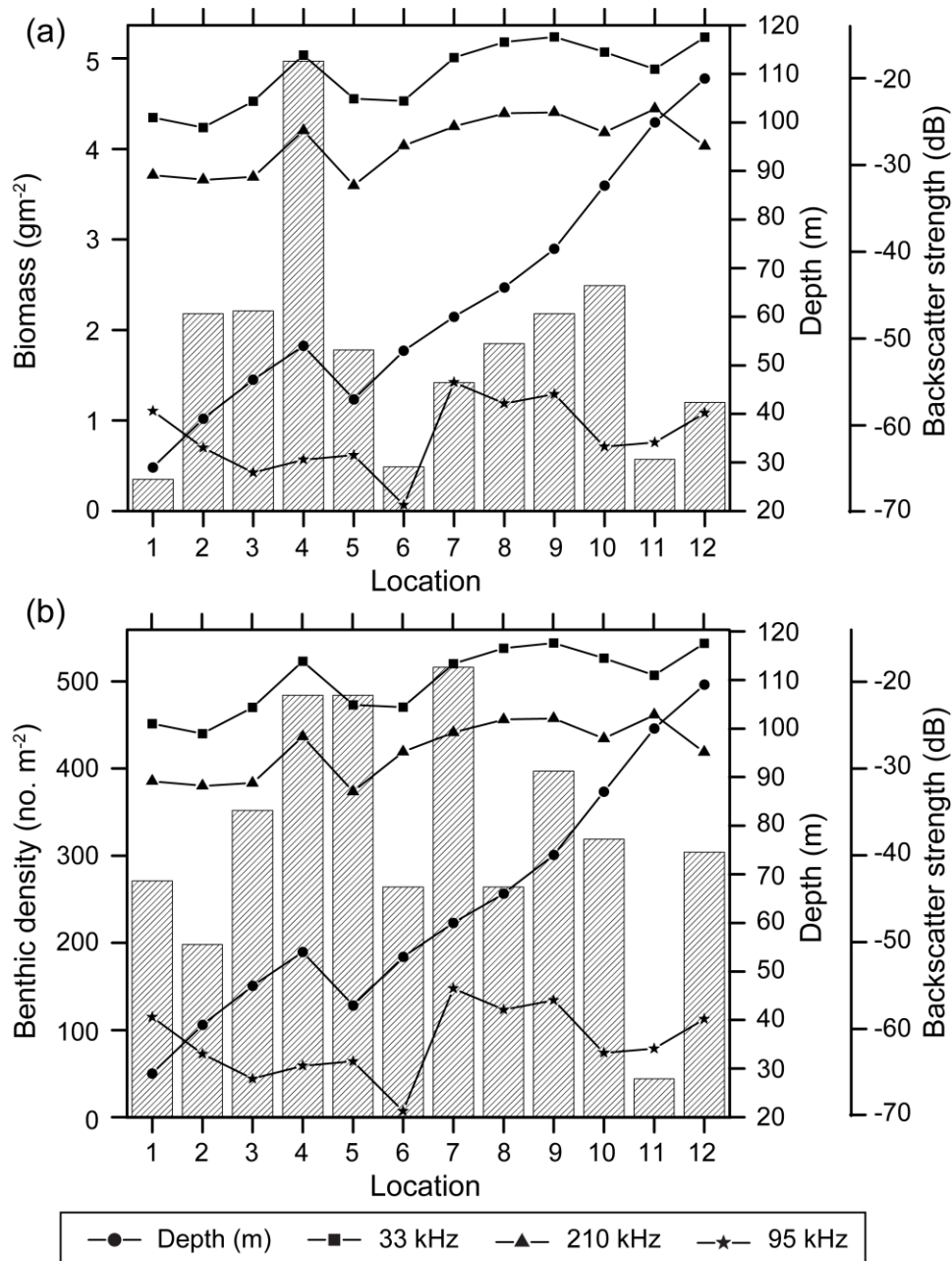


Fig. 4.9 Panels (a) and (b) exemplifies the depth wise spatial variations of biomass, backscatter, and benthic density.

Relatively high species richness and diversity apparent in the coastal region (<100 m) of the study area could be ascribed to the enrichment of coastal waters caused by riverine flow and land runoff (Parulekar, 1973). The high percentage distribution of fine grained sediments with relatively abundant organic carbon is

noticeable in the shallow region (Fig. 4.10). The distribution of organic carbon is governed by a set of physico-chemical, sedimentological and hydrographic factors (Jayaraj *et al.*, 2007). The study area receives relatively high annual rainfall that can transport organic matter through the rivers and discharges to the shallow water regions. This process might have resulted in significant amount of both fine sediment and organic carbon in the shallow region. The present study indicates comparatively low benthic density at shallow region (29 and 39 m) as compared to deeper depths (43, 54, and 60 m). The low biomass evident at 29 m water depth (with clayey-silt substrate and abundant organic carbon) further suggests that the fine sediment and organic carbon enrichment in the shallow region can adversely affect the benthic density (Jayaraj *et al.*, 2007).

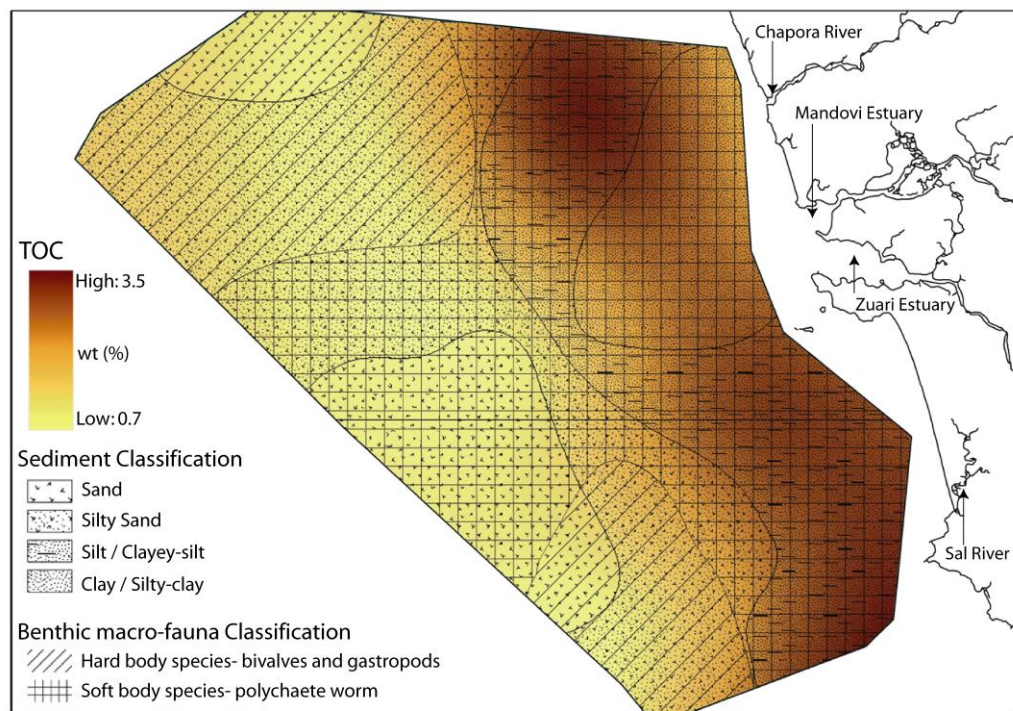


Fig. 4.10 GIS-based classification representing the distribution of total organic carbon in relation to the benthic macro-fauna and sediment types. The geographic locations of the two estuaries (Mandovi and Zuari) and rivers (Chapora and Sal) transporting organic matter to the shallow water regions of the study area are also indicated.

4.3 Concluding remarks

The backscatter data from dual-frequency SBES and MBES operable at 33/210 kHz and 95 kHz, respectively, have been utilized to demonstrate the correlation among the derived backscatter, grain size, and benthic macro-fauna abundance. The resulting benthic habitat maps illustrate the nature, distribution and extent of the distinct sedimentary environment and the associated species communities along the central part of the WCMI. The preferences of deposit feeders (soft body benthic macro-fauna) in the fine-sediment regions and filter feeders (hard body benthic macro-fauna) in coarse sediment regions indicate the influence of sediment texture and total organic carbon on the feeding behavior of the organisms. The correlation among the derived acoustical (multi-frequency backscatter intensity) and biological parameters (number density of benthic macro-fauna) was identified from the spatial map generated using GIS and validated by applying PCA. The acoustic backscatter data presented here accentuates the versatility of SBES and MBES to conveniently map seafloor sediment distribution and associated benthic habitat across large areas of seafloor.

Chapter 5

Benthic habitat characterization using geoacoustic inversion results

5.1 Introduction

Acoustic remote sensing technique using high-frequency SBES and MBES has been recognized as an effective tool for studying the seafloor over a wide area (Jackson and Richardson, 2007). The backscatter data acquired using the echosounding systems can be matched with the theoretical scattering models to interpret the fine scale seafloor information embedded in data (Jackson *et al.*, 1986; Sternlicht and de Moustier, 2003a, b). The numerical approach employed for extracting information from the data is commonly referred to as inversion modeling (detailed in Chapter 3). Inversion modeling primarily involves physics based approach to calculate seafloor roughness parameters, namely, the sediment mean grain size (M_ϕ); spectral parameters at the water-seafloor interface (γ_2, w_2); and sediment volume parameter (σ_2) (De and Chakraborty, 2011; Haris *et al.*, 2011). However, the study of the interaction of sound with the seafloor and the application of inversion modeling can provide new insights if the physical structure of the seafloor and the associated benthic communities with its diversity coexists (Thorsos *et al.*, 2001).

The bottom dwelling benthic organisms often modify the physical properties of the sediment and create fine scale seabed structures (Jones and Jackson, 1998). The multiple processes that are continually occurring at the water-sediment interface and within the sediment volume significantly causes fluctuation in acoustic backscattering. The collective displacement and mixing processes of sediment substrates by the benthic macro-fauna are termed as bioturbation. The bioturbation can affect the sediment properties including derived parameters as follows: a) due to the movement of the hard body fauna such as bivalves and gastropods that scatters the sound signal due to strong impedance mismatch between the sediments or their body parts (Jumars *et al.*, 1996), and b) by altering the local density of sediment-water interface, including displacements responsible for producing or erasing the small-scale features. Such changes are caused by burrowing and tube building of soft body fauna, mainly dominated by polychaete worms (Kogure and Wada, 2005; Haris *et al.*, 2012).

Relatively high backscattering is expected when the spatial scale of the scattering animal or its modifications in the sediment substrates become comparable to the transmitting acoustic wavelength. Besides, the SBES echo-envelope shape parameters such as peak along with its width, rise, fall time, and the tail part gets modified due to the bioturbation. Therefore, it is important to examine the role of bioturbation on the acoustic backscatter using high-frequency echo-sounding systems. In the present study, the spatial variability of the previously estimated sediment geoacoustic inversion results (De and Chakraborty, 2011; Haris *et al.*, 2011), using MBES and dual-frequency SBES operable at 95 kHz and 33/210 kHz, respectively, were analyzed along with the sediment texture and benthic macro-faunal information obtained at the same locations (Fig. 5.1).

The analyzed results demonstrate the interrelationship among seafloor micro-roughness parameters, grain size, and benthic macro-faunal abundance (Haris *et al.*, 2012) along the central part of the western continental shelf of India (WCSI).

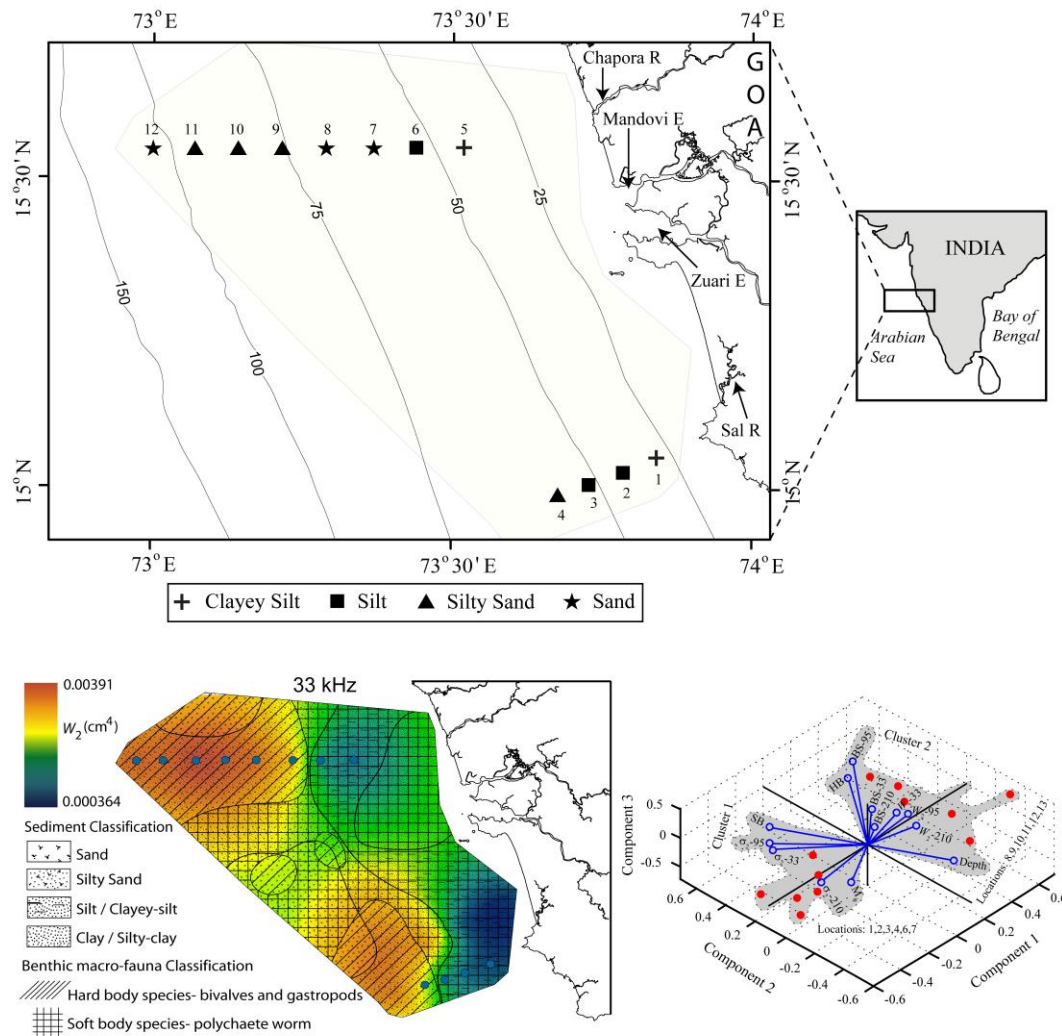


Fig. 5.1 The figure shows the study area with respective sediment types: clayey-silt (cross), silt (square), silty-sand (closed-triangle) and sand (star). The depth contours are expressed in meters. The acoustic data was acquired with EM 1002 MBES and RESON-NS 420 SBES along the two tracks. The sediment samples for textural and benthic studies were acquired using a Van-Veen grab. The inversion results (described in Chapter 3) are analyzed here with the sediment texture and benthic macro-faunal abundance obtained at the same locations.

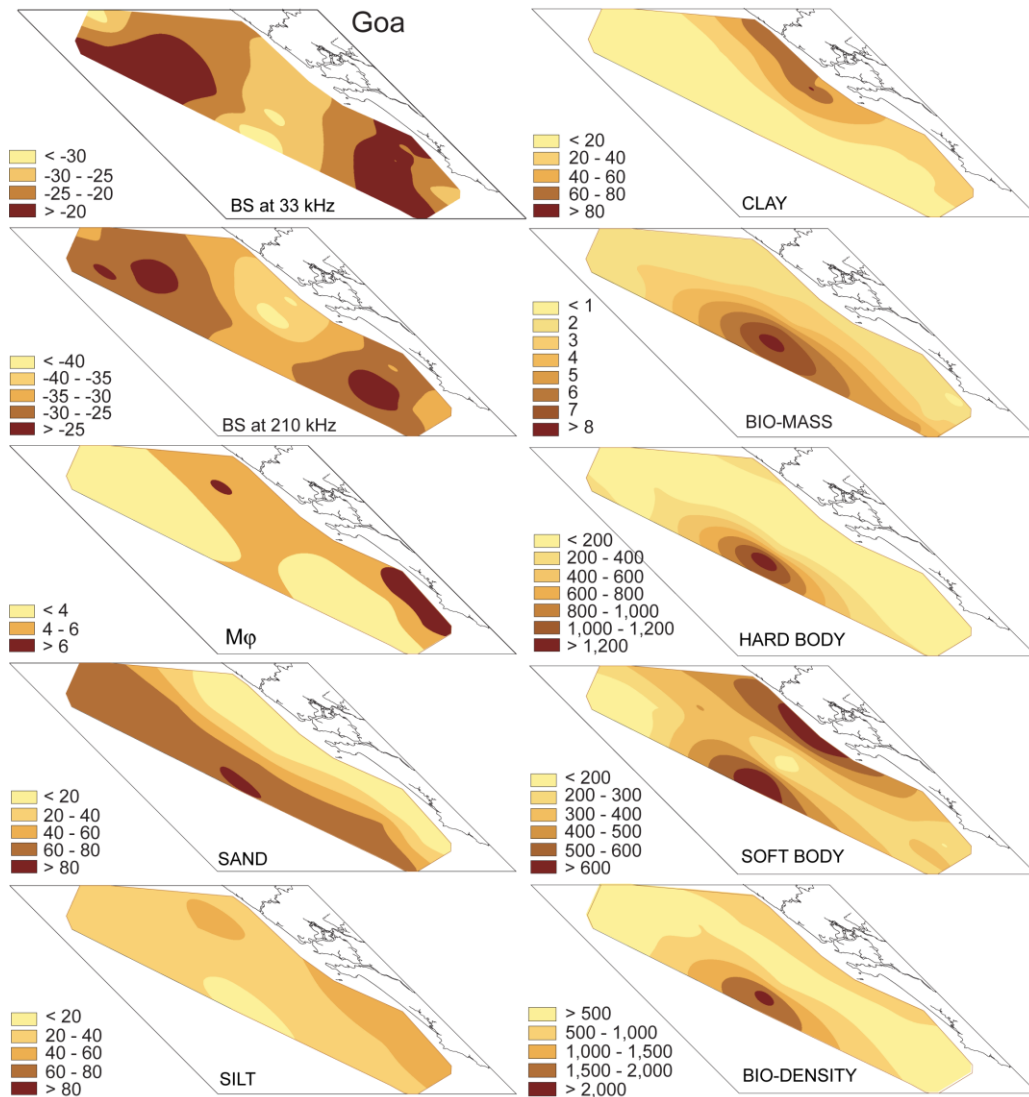


Fig. 5.2 GIS-based sediment distribution and benthic macro-faunal abundance map of the study area. The maps illustrate general environmental scenarios of the study region, including acoustical, physical, and biological properties.

5.2 Results and discussion

In the following sections, the geoacoustic inversion results derived from the MBES and SBES data (Chapter 3) have been compared with the sediment texture and benthic macro-faunal information.

5.2.1 Backscatter and mean grain size

The percentage distribution of sediment compositions indicates the presence of four seafloor sediment types: clayey-silt, silt, silty-sand and sand. The sediment texture was relatively coarse ($M_\phi < 4$) in the deeper depths (60–109 m), and fine-grained sediment ($M_\phi > 4$) was found in the shallow depth region (29–54 m) (Fig. 5.2). Statistically significant correlations observed among the measured and computed M_ϕ values demonstrates the success of inversion modeling carried out (Fig. 5.3). The multi-frequency inversion is advantageous because the studies (Williams *et al.*, 2002) assessing the scattering models with the data acquired are rare so as to provide an evaluation of the model over a broader range of sediment types and frequency.

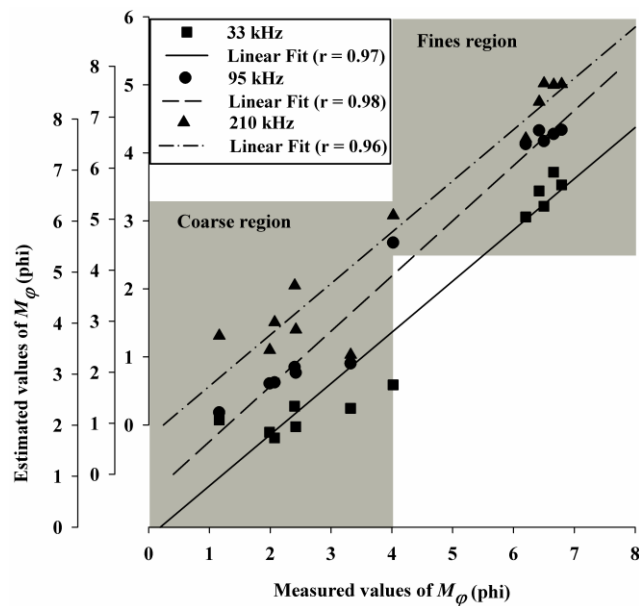


Fig. 5.3 Scatter plot demonstrating the success of inversion modeling carried out.

The backscatter strength from the seafloor is primarily controlled by the acoustic frequency, the acoustic impedance contrast between water and sediment, and the contributions from seafloor interface roughness as well as sediment volume inhomogeneity. Several studies (Goff *et al.*, 2004; De Falco *et al.*, 2010; Haris *et al.*,

2012) while comparing the backscatter response with the ground truth sediment data have concluded that the acoustically soft fine sediments ($M_\phi > 4$) generally exhibit low backscatter intensity due to low density and sound velocity. On the flip side, the acoustically hard coarse sediments ($M_\phi < 4$) results relatively higher backscatter intensity due to scattering from coarse particles, lower porosity, higher density and sound velocity, and greater roughness of the water-sediment interface (Fig. 5.4).

The benthic macro-fauna can compact and dilate the sediment, resulting modification in seafloor roughness, sediment density and fluctuations in the sound speed (Diaz *et al.*, 1994). Besides, the hard body epifauna as an individual and group can scatter acoustic energy (Stanton *et al.*, 2000). The collective biological processes might be controlling higher backscatter strength observed in the coarse sediment region with substantial occupancy of hard body organisms (Fig. 5.4).

5.2.2 Macrobenthos-sediment relationship

PCA indicates two major clustering patterns (Fig. 5.4). The number density of hard body organism is inversely correlated with the computed M_ϕ . Whereas, the soft body abundance is linearly correlated with the estimated M_ϕ . Two distinct feeding groups are observed from the study area: the deposit feeders in the shallow region (including polychaete worms and related soft body species like nematode, oligochaetes, nemertinea, and echurids) and filter feeders (hard body bivalves and gastropods) in deeper depths.

Studies (Jayaraj *et al.*, 2008; Ingole *et al.*, 2010) have been conducted in past to report animal-sediment relationship along the Indian coast. Sanders (1958) and Jayaraj *et al.* (2008) suggested that the coarse sediment region reflects the environment with pronounced under water current activity (with filter feeder dominance). In contrast, the fine sediment region towards the shallow depth reflects the environment with feeble current. The weaker current allows the fine particles to settle down and provides an adequate source of nutrition for deposit feeders. Therefore, only a limited amount of organic matter would be available in suspension as the food source for filter feeders and inhibits them from inhabiting in such

environments. The dominance of deposit feeders in the fine-sediment regions and filter feeders in the coarse sediment regions are well corroborated by the distinct trends observed in the computed backscatter and M_ϕ values (Fig. 5.4).

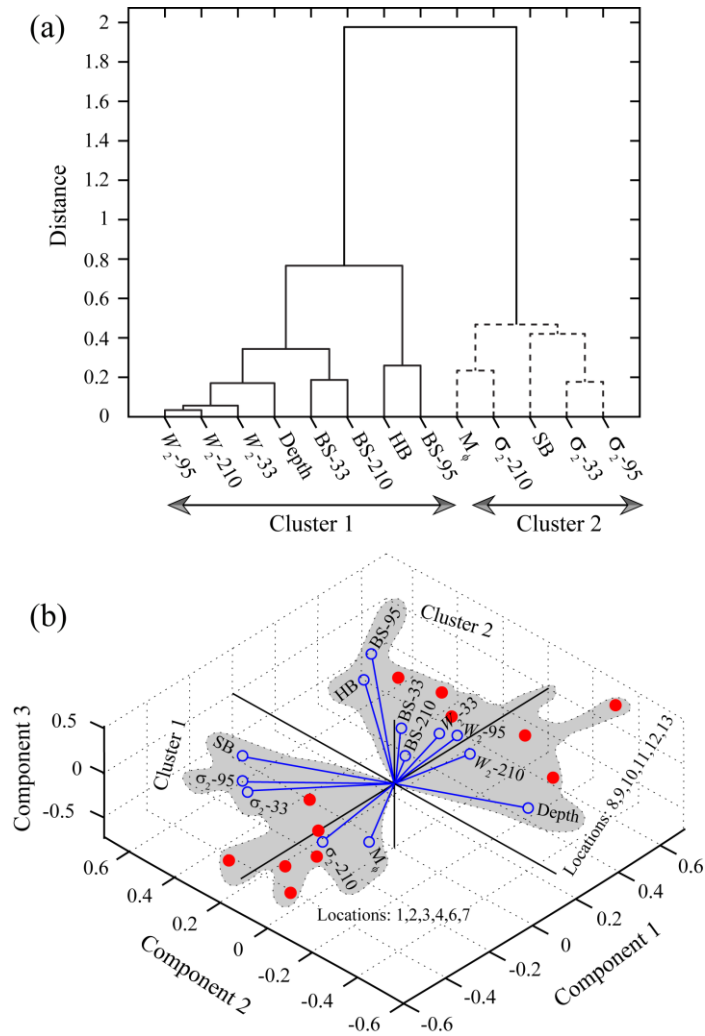


Fig. 5.4 The dendrogram in panel (a) and biplot of PCA (b) illustrates the location wise clustering of measured and derived parameters. The acronym BS, SB, HB denotes backscatter, soft body and hard body benthic macro-fauna respectively.

5.2.3 Macrobenthos-roughness relationship

The computed geoaoustic parameters (Haris *et al.*, 2011) w_2 and σ_2 , that account for the interplay of sediment interface and volume scattering have been analyzed with the macrobenthos abundance. The variation of geoaoustic parameters conforms to the shape of the SBES echo-envelope and MBES angular backscatter data (e.g., peak of the echo-envelope along with the width, rise, fall time, and tail part). The bioturbation occurring at the seafloor interface and sediment volume can modify the shape parameters, and the extend of bioturbation gets reflected in the computed parameters (w_2 and σ_2). The sensitivity analyses carried out on the shape of the echo-envelope data indicates lees-steep slope and reduced amplitude of the response curve with higher value of w_2 . The higher w_2 has significant influence on the interface scattering and marginal effect on the tail part. The contribution of sub-bottom scattering is conspicuous near the tail of the echo-envelope with relatively higher σ_2 value. The fine sediment provinces are penetrated more deeply by the acoustic signal, consequently the sediment volume scattering increases in comparison with the interface scattering.

With reference to the multi-frequency inversion modeling study carried out by Haris *et al.* (2011), in the coarse sediment region, the w_2 values were restricted within the range 0.002 to 0.005 cm^4 . In the fine sediment region, the w_2 values were found to be less than 0.001 cm^4 . The corresponding GIS generated roughness map (Fig. 5.5) reveals relatively higher values of w_2 in the coarse sediment region with substantial occupancy of hard body organisms (Fig. 5.4). Likewise, the lower w_2 values are apparent in the fine sediment provinces with dominant soft body abundance. The average value of σ_2 computed at three acoustic frequencies (Chapter 3) were found to be relatively higher in the fine sediment region as compared to the coarse sediment provinces. Correspondingly, GIS generated volume scattering map (Fig. 5.6) indicates comparatively lower σ_2 values in the coarse sediment region with significant occupancy of hard body organisms (Fig. 5.4). Conversely, the higher σ_2 values are evident in the fine sediment provinces with dominant soft body abundance.

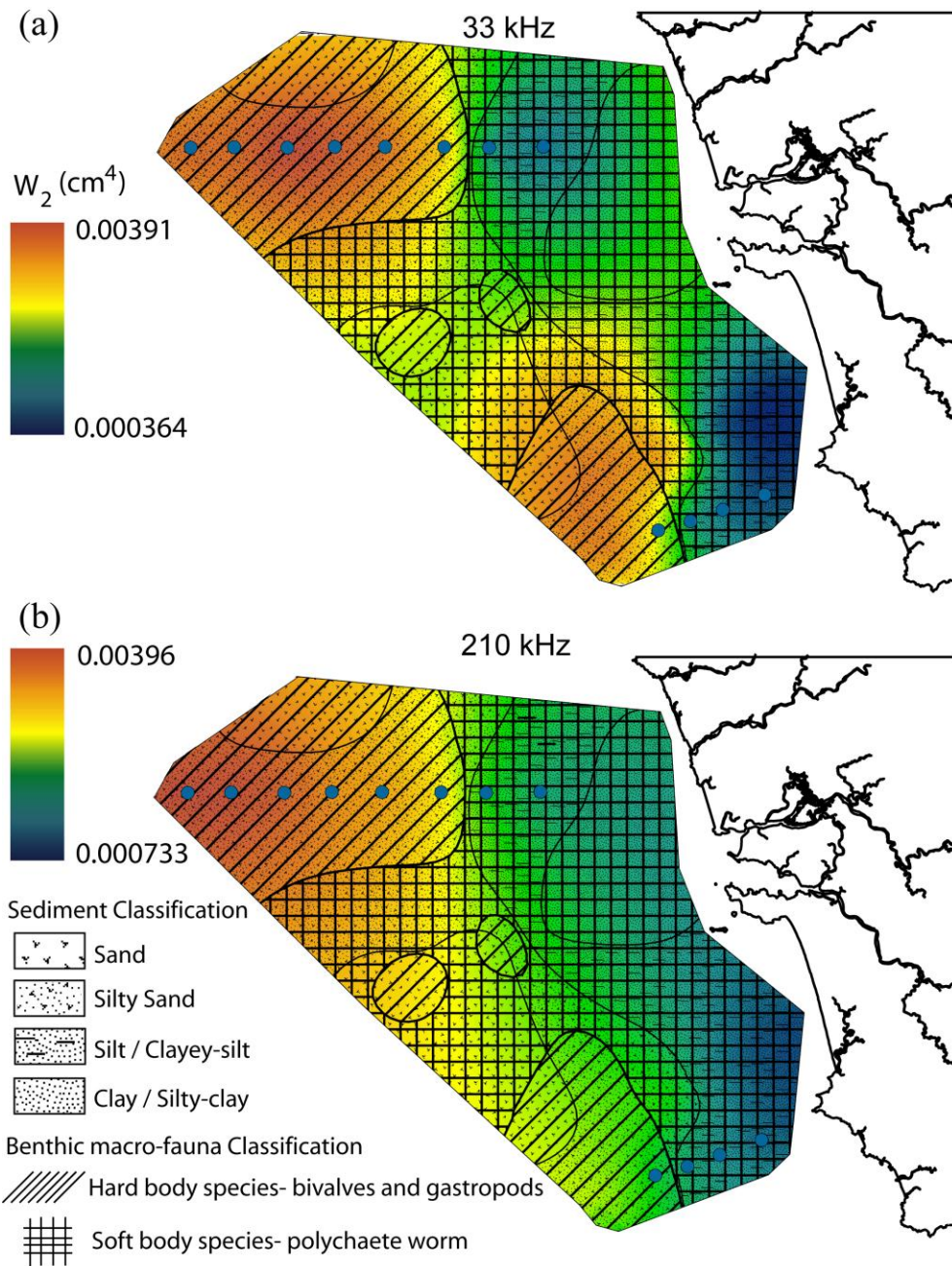


Fig. 5.5 GIS-based image classification representing the variation of interface roughness spectral parameter w_2 in relation to the benthic macro-fauna and sediment types at 33 (a) and 210 kHz (b).

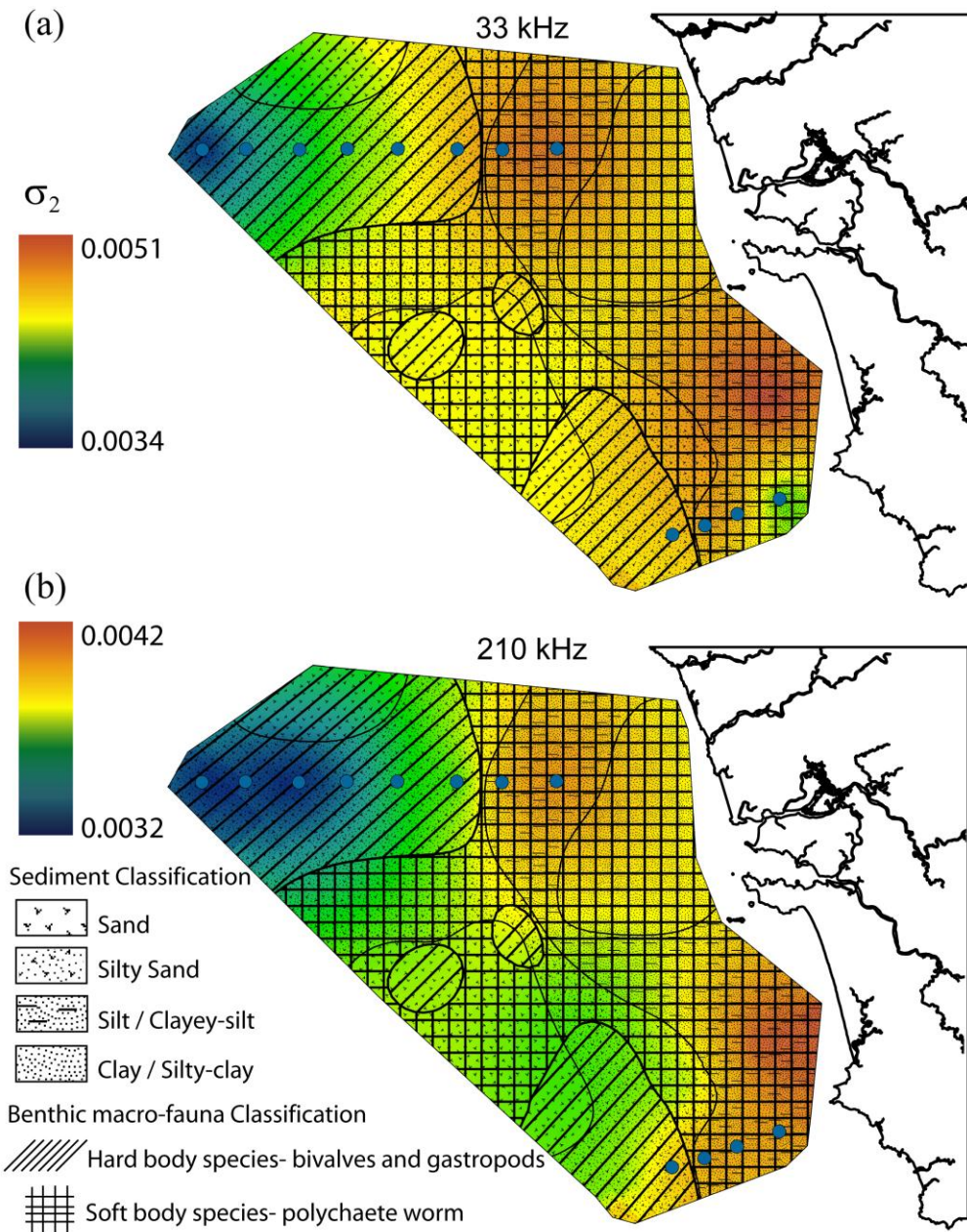


Fig. 5.6 GIS-based image classification representing the variation of sediment volume scattering parameter σ_2 in relation to the benthic macro-fauna and sediment types at 33 (a) and 210 kHz (b).

The biologically active marine sediments get continually modified due to the collective activities of epifauna (hard body organisms that live on the sediment surface) and infauna (soft body organisms living within the sediment). The epifaunal

activities basically include locomotion and home building that creates additional roughness at the sediment-water interface, causing relatively high interface scattering. On the other hand, the infaunal activity, including tube building is responsible for the vertical and the horizontal redistribution of solid material within the sediment volume. The process can create spatial and temporal inhomogeneities in sediment bulk properties (density, porosity, and compressibility). Such changes are mainly driven by burrowing and tube building by soft body infauna including polychaete worms. Accordingly, strong volume scattering is inevitable from the corresponding habitat region. In the present study, the high values of w_2 and σ_2 are attributed to the coarse and the fine sediment region, with the dominance of hard body epifauna and the soft body infauna respectively (Fig. 5.4).

5.3 Concluding remarks

The multi-frequency sediment geoacoustic inversion results, derived from the MBES (Haris *et al.*, 2011) and SBES (De and Chakraborty, 2011) data have been analyzed to demonstrate the interrelationship among the sediment texture and benthic macro-faunal abundance. Two distinct feeding groups were observed in the coarse and fine sediment regions. The preference of hard body organisms to coarse sediment region causes the relatively high interface scattering due to the collective epifaunal activities including locomotion and home building. In the fine sediment region, the tube building infaunal activity generated by the soft body organisms creates spatial and temporal inhomogeneities in the sediment bulk properties, evidencing dominant sediment volume scattering as compared to the interface scattering.

Chapter 6

Multifractal approach for seafloor characterization: Part 1. Application to multi-beam image data

6.1 Introduction

The seafloor bathymetry and the associated backscattering data of submerged objects have an extremely wide range of spatio-temporal scales necessitating application of “power law” to carry out the analyses. The power law behavior in such instances requires multifractal analyses (Mandelbrot¹, 1967, 1989) in order to determine if both (seafloor backscatter and bathymetry image data) follow “fractal” statistics. It is imperative to treat such data as a scale invariant field requiring multifractal measures and exponent functions, rather than a unique scaling exponent (such as fractal dimension) (Hentschel and Procaccia, 1983). An infinite number of fractal dimensions would be needed to completely characterize the scaling, as evident in other fields like: satellite radiance data (Lovejoy *et al.*, 2009b), medicine (Ivanov *et al.*, 1999), and ecology (Seuront, 2010).

¹ Benoit B. Mandelbrot is widely regarded as the “father of fractal geometry”. Mandelbrot was a mathematical genius who advanced the concept of power law scaling as the fundamental property of a broad range of natural processes and patterns in geophysics, mathematics, economics, and virtually all the branches of science. Mandelbrot died on 14 October 2010 in Cambridge, Mass., at the age of 85.

The two important formalisms of multifractal analyses such as: (i) “strange chaotic attractors” (Halsey *et al.*, 1986) and (ii) “stochastic” multifractal fields (Schertzer and Lovejoy, 1987) have been used in this study. The first formalism is based on the “box counting” method. It involves analyses of multifractal distribution pattern using the correlation dimension $D(q)$, and multifractal spectrum $f(\alpha)$ related shape parameters [i.e., width of the spectrum W , degree of asymmetry B , and stability of spectrum $\Delta f(\alpha)$]. The properties of these functions at different statistical moments are used to characterize the spatial distribution of seafloor backscatter and bathymetry seepage² blocks used in this study. The other formalism allows quantification of the seepage blocks with three fundamental parameters namely, degree of multifractality α , sparseness C_1 , and degree of smoothness H (Gagnon *et al.*, 2006).

Dandapath *et al.* (2010) had reported seafloor seepages in the WCMI using MBES backscatter and bathymetry data (Fig. 6.1). The investigations were related to underlying geology, pockmark occurrences, overlying sediment texture, and sediment movements due to strong influences of monsoonal bottom currents. Thereafter, utilizing the method proposed by Seuront and Spilmont (2002), Dandapath *et al.* (2012) had noted the possible multifractal behavior of the MBES backscatter and bathymetry image data. Therefore, the present study involves quantitative estimation of the multifractal parameters from seafloor seepage to improve the understanding of the processes in the WCMI.

The application of inversion modeling for seafloor roughness characterization impose a challenging task as most of the models presume the input data in stationary form. Therefore, the application of segmentation techniques (Malinverno, 1989) is indispensable and facilitates in achieving stationary profile data sets suitable for inversion modeling. The application of online segmentation techniques can also

² Seafloor seepages offer important proxy for shallow or deep water hydrocarbon accumulations. Pockmark associated seepages (Hovland and Judd, 1988) are prevalent from sub-arctic to tropical seas, continental shelf to deep ocean basins, even in shallow and deep lakes under different geological environments. Pockmarks are craters in the seabed caused by fluids (gas and liquids) erupting and streaming through the sediments. The presence of fluid escape features like seafloor pockmarks was first discovered by King and MacLean (1970) over the Nova Scotian shelf.

significantly reduce the frequency of time consuming ground-truth measurements required for the validation of model parameters. The use of soft-computing technique (Alexandrou and Pantzartzis, 1993; Michalopoulou *et al.*, 1995) including artificial neural networks (ANNs) were effectively demonstrated for hydroacoustic data classification (Chakraborty *et al.*, 2015) to segment the data into stationary form.

The application of the multifractal techniques could substantiate the hitherto applied numerical inversion based characterization (De and Chakraborty, 2011; Haris *et al.*, 2011), and the soft computational technique based classification (Chakraborty *et al.*, 2001, 2004; De and Chakraborty, 2009) of the seafloor sediments employing the backscatter data.

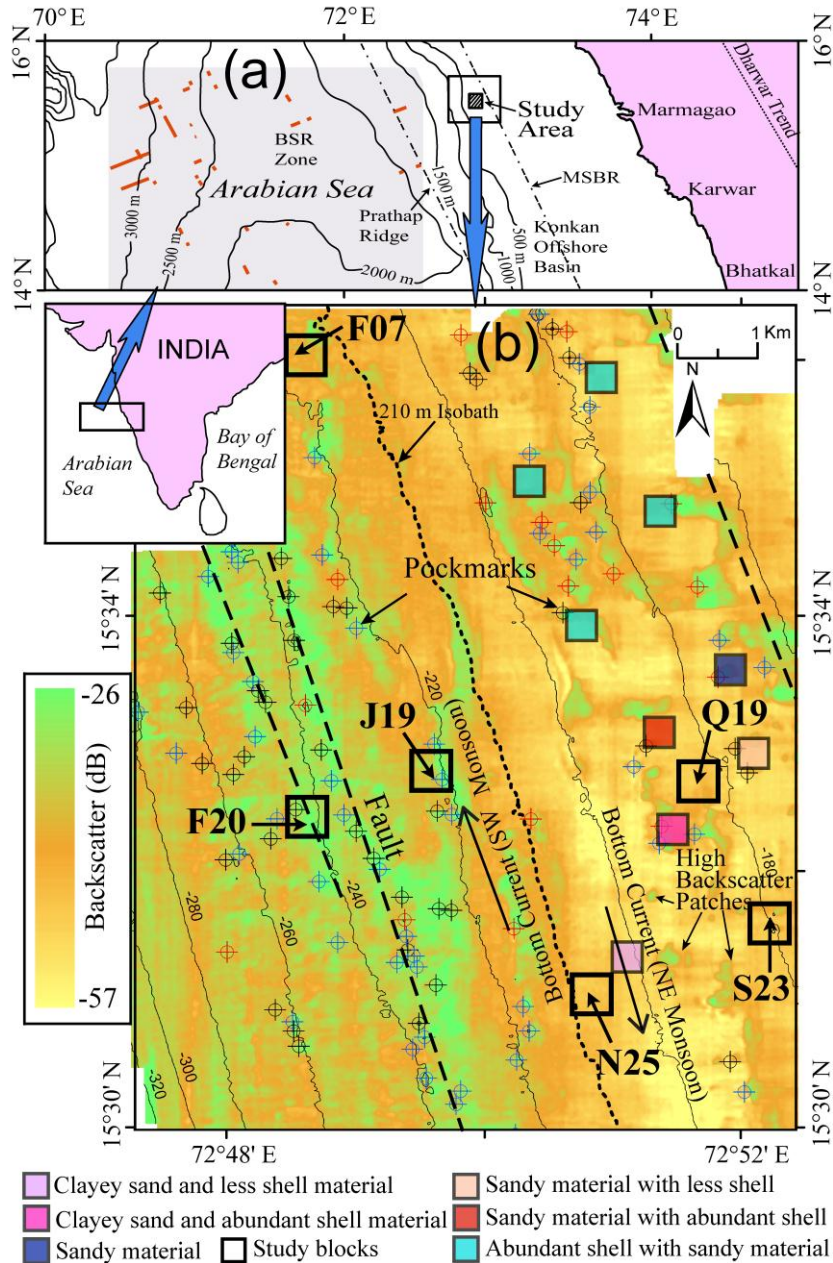


Fig. 6.1 (a) Study blocks including some of the main structural features of the region of the WCMI. (b) Backscatter map of the study area showing 160–320 m isobaths with 20 m interval. Pockmarks are indicated by crossed circles. Black, blue and red color mark represents circular, elliptical and elongated pockmarks respectively. The dashed lines indicate location of the identified faults. The black arrows show bottom current directions. Solid colored squares represent the sediment types (modified after Dandapath *et al.* 2010).

6.2 Data sets

The backscatter and bathymetry data used in the present study were acquired from the central part of WCMI, where the water depth varies between 145–330m (Fig. 6.1). Simrad EM 1002 MBES operating at 95 kHz was used to acquire the data. The important morphological aspects of the study area have been investigated in detail, and 112 pockmarks related to the seepages were identified from the seafloor maps generated using ArcGIS (Dandapath *et al.*, 2010). The backscatter and bathymetry image blocks having 400×400 pixels, were classified according to the degree of seepage based on the backscatter strength as well as fractal dimension (determined using box-dimension technique) (Dandapath *et al.*, 2012). The analyses carried over each gray tone image blocks (with digital numbers ranging 0 to 255) suggest that the area with very high seepage has higher fractal dimension and lower dimension with very low seepage. In this study, six representative seepage blocks i.e., F20, J19, F07, Q19, S23 and N25 having very high, high, moderate, low, very low, and no evidence of seafloor seepages respectively (Fig. 6.2) have been considered for analyses.

Sample blocks	F20	J19	F07	Q19	S23	N25
Seepage type	Very high	High	Moderate	Low	Very low	No evidence
Mean backscatter (dB) (max to min)	-31.58 (-27.46 to -35.71)	-34.40 (-27.50 to -42.62)	-38.99 (-33.84 to -42.84)	-38.96 (-36.18 to -46.78)	-43.28 (-37.24 to -45.11)	-42.62 (-41.36 to -44.19)
Backscatter image						
Bathymetry image						

Fig. 6.2 Backscatter (in digital number: 0–255) and bathymetry seafloor seepage blocks selected from the Figure 6.1 for the present investigation.

6.3 Strange attractors

Self-similar fractals are scale invariant, i.e. possessing a structure with a basic characteristic of nonscaling. They can be divided into two categories. The first one is the monofractal, having strict geometric self-similarity that can be described with a single fractal dimension. The other is the multifractal that requires a series of fractal spectrum rather than a unique fractal dimension. Highly intermittent multifractal fields common in nature are the generic outcome of multiplicative cascade processes dominated by scaling non-linear interactions.

The multifractal formalism based on the strange chaotic attractors followed here identifies a set of parameters derived from the shape of such a fractal spectrum. As a part of the image analyses, the variation of these shape parameters among the seafloor seepage blocks is examined to measure the “complexity” of the field. In view of this, a probability distribution is estimated using the box counting method (Chhabra and Jensen, 1989). The partition function $\chi(q, \varepsilon)$ that describes the probability of “containing the object” (i.e., the values of backscatter and bathymetry in this application), within each box i , can be calculated for different moments of q using:

$$\chi(q, \varepsilon) = \sum_{i=1}^{n(\varepsilon)} m_i^q \quad (6.1)$$

where m is the mass of the measure, ε is the length of the box and $n(\varepsilon)$ is the number of boxes. Based on this, the mass exponent function $\tau(q)$ shows how the moments of the measure scales with the box size and is given as:

$$\tau(q) = \lim_{\varepsilon \rightarrow 0} \frac{\log \chi(q, \varepsilon)}{\log(\varepsilon)} = \lim_{\varepsilon \rightarrow 0} \frac{\log \langle \sum_{i=1}^{n(\varepsilon)} m_i^q \rangle}{\log(\varepsilon)}. \quad (6.2)$$

The generalized fractal dimension function $D(q)$ can be calculated from $\tau(q)$ as $D(q) = \tau(q)/(q-1)$ (where $q \neq 1$). The singularity index (α) is subsequently determined to calculate the singularity spectrum $f(\alpha)$ by Legendre transformation of the $\tau(q)$ curve as $\alpha(q) = d\tau(q)/dq$. Finally the $f(\alpha)$, which represents the fractal dimension of the subset with the same singularity strength (α) is determined to

describe the characteristic of the different hierarchy of fractal as $f(\alpha) = q\alpha(q) - \tau(q)$.

An image can be realized as multifractal when the graph of α vs. $f(\alpha)$ (i.e., multifractal spectrum), exists and has the shape of an inverted parabola. If the curve $f(\alpha)$ converges to a single point, it can be termed as monofractal wherein $D(q)$ is constant for all values of q . The width of the generalized dimension i.e., $\Delta D(q) = D(q_{max}) - D(q_{min})$, is a measure of multifractality and indicates the deviation from monofractal behavior. The particulars of the shape parameters used to describe the multifractality (based on the said formalism) are shown in Figure 6.3.

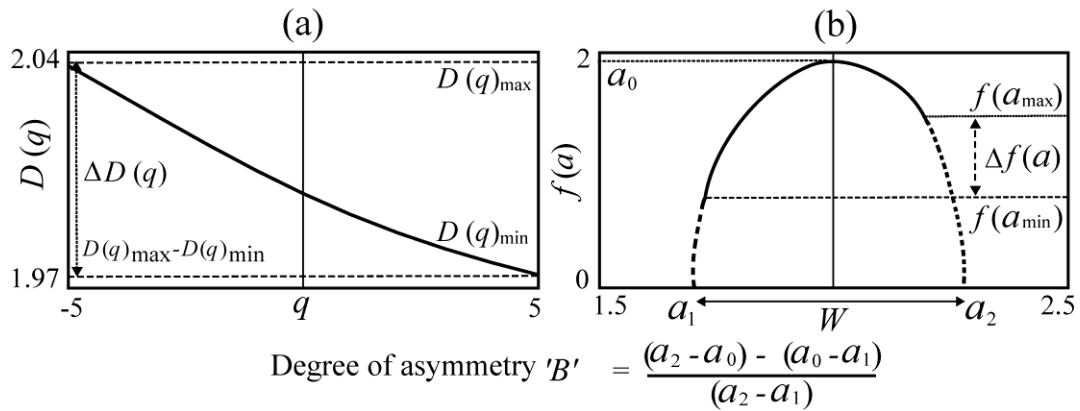


Fig. 6.3 Schematic representation of (a) generalized correlation dimension function $D(q)$ for estimation of the parameter $\Delta D(q)$ and (b) multifractal spectrum $f(\alpha)$ for assessment of the three multifractal parameters i.e., width of the spectrum W , degree of asymmetry B and stability of the spectrum $\Delta f(\alpha)$ based on strange attractor formalism.

In order to distinguish the multifractal spectrum $f(\alpha)$ quantitatively, it is convenient to calculate the width of the spectrum W so as to measure the overall variability (Fig. 6.3). A wider $f(\alpha)$ spectrum is indicative of larger W , denoting multifractality. Such a situation reveals a “heterogeneous” seafloor. In the case of a monofractal set, W would be small and tending to “zero”. The spectrum will converge to a single point signifying a “homogeneous” seafloor. The other parameter B measures the asymmetry of the curve and shows the dominance of low or high fractal exponents (Szczepaniak and Macek, 2008). The value of B is zero for

symmetric shapes and positive or negative for right or left-skewed shapes respectively. A left-skewed spectrum denotes low fractal exponents dominating the distribution, while a right-skewed spectrum implies dominance of high fractal exponents (Telesca *et al.*, 2003). Thereafter, the values of α_{min} and α_{max} are estimated to obtain the parameter $\Delta f(\alpha)$ as $\Delta f(\alpha) = f(\alpha_{min}) - f(\alpha_{max})$. $|\Delta f(\alpha)|$ defines the undulation or instability of the system under study. The degree of undulation or instability is minimum for the smallest $\Delta f(\alpha)$ (≈ 0).

6.4 Stochastic multifractal formalism

6.4.1 Moment scaling function and universal multifractals

The seafloor bathymetry and the related backscatter data can be modeled taking into consideration a small number of (generally deterministic) or many (stochastic) degrees of freedom. In order to incorporate high degree of freedom and variability over a wide range of scales, stochastic approaches are preferred as they have infinite dimensional probability space³ (Lovejoy *et al.*, 2009a). One way to characterize the statistics of stochastic processes is to use its statistical moments. When a multifractal cascade has proceeded over a scale ratio $\lambda=L/l$ (L and l representing largest and smallest scale⁴ in the data), the statistical moments of the conserved multifractal flux (the field values of the MBES bathymetry\backscatter image and the pressure values of the SBES echo envelope⁵) measured at scale λ , follow a power law that can be expressed as (Schertzer and Lovejoy, 1987, 1991):

$$\langle \phi_\lambda^q \rangle = \lambda^{K(q)} \quad (6.3)$$

where ϕ_λ is the scale by scale conserved multifractal flux, q is the order of the moment, and $K(q)$ is a nonlinear convex function. $K(q)$ characterizes the scaling of

³ See Figure 1.2 in Chapter 1.

⁴ Two types of data are utilized in this chapter. In Part 1, the MBES bathymetry and backscatter image data have been analyzed in the frame work of stochastic multifractal formalism. In Part 2, the same formalism has been applied to the time dependent SBES echo envelope data. Note that the term “scale” mentioned here is different for MBES and SBES data. The spatial scale in “meter” is applicable to MBES image data and the temporal scale in “millisecond” is ascribed to SBES echo envelope.

⁵ See Part 2.

the moments of the ϕ_λ , hence it is called the “moment scaling function”. With reference to the existence of stable attractive multifractal processes called universal multifractals (Schertzer and Lovejoy, 1987, 1991, 1997; Lovejoy and Schertzer, 1990), $K(q)$ can be expressed as:

$$K(q) = \frac{C_1}{\alpha - 1} (q^\alpha - q) \quad (6.4)$$

where α^6 and C_1 are the basic parameters characterizing the scaling properties of the multifractal flux ϕ_λ . The parameter α is the degree of multifractality and varies from 0 to 2, where $\alpha=0$ is the monofractal case and $\alpha=2$ is the log normal case. This parameter describes how rapidly the fractal dimensions of the sets at different thresholds vary as they leave the mean singularity. C_1 is the codimension parameter of the set. Low value of C_1 (≈ 0), implies that the field values are close to the mean. C_1 (> 0) indicates that the region making the dominant contribution to the mean is a sparse fractal set such that the vast majority of the field doesn't contribute (Gagnon *et al.*, 2006). The function $K(q)$ is related to the generalized dimension $D(q)$ as:

$$D(q) = d - \frac{K(q)}{q - 1} \quad (6.5)$$

where d is the dimension of the space (=2 here) (Seuront, 2010).

6.4.2 Fractionally Integrated Flux model

The multiplicative process (the cascade) discussed above generates a scale by scale conserved multifractal flux ϕ_λ characterized by a moment scaling function $K(q)$. The spectrum of such a conserved flux has an exponent $\beta = 1 - K(2) < 1$. In order to discriminate the seafloor echo-envelopes (having $\beta \approx 2$), FIF model (Gagnon *et al.*, 2006) has been utilized. The FIF model of the multifractal flux provides the following statistics in relation to the intensity field⁷ I_λ at scale ratio λ as (Schertzer and Lovejoy, 1987, 1991):

$$I_\lambda = \phi_\lambda \lambda^{-H}. \quad (6.6)$$

⁶ The symbol α used in the strange attractor formalism represents the singularity index.

⁷ For MBES image data the intensity field represents the values of bathymetry and backscatter within each bock. Whereas, in SBES echo envelope data the intensity field signifies the pressure values.

Here the linear scaling λ^{-H} corresponds to a fractional integral of order H . The parameter H can be designated as a degree of smoothness where higher H signifies smoother fields. Characterization of seafloor backscattering using FIF model is difficult to distinguish the underlying cascade dynamics as it involves a convolution due to the exponent H . Therefore resorting to the use of “trace moments” (that directly characterizes the conserved multifractal flux ϕ_λ), is necessary so that the differentiation is possible⁸ (Gagnon *et al.*, 2006; Chakraborty *et al.*, 2014).

The first step to obtain ϕ_λ from the intensity field involved the removal of λ^{-H} in the Eq. (6.6). This is equivalent to a filtering as in Fourier space with “power law”, which is a scale invariant smoothing. On elimination of λ^{-H} , only the underlying conserved multifractal flux ϕ_λ is retained. The next step was to examine the scaling of the statistical moments of ϕ_λ and compare them with Eq. (6.3). To this end, we normalized ϕ_λ so that the ensemble average of all the samples is $\langle \phi_\lambda \rangle = 1$. Thereafter, the q^{th} power of the samples (bathymetry\backscatter and pressure values) over the sets of size (or time interval) $l = L/\lambda$ was determined. It gives the moments of the normalized multifractal flux for a given value of q . This procedure was performed with different values of q and $K(q)$ was evaluated from the logarithmic slopes (Fig. 6.4⁹). The multifractality of the intensity field has been validated with nonlinear $K(q)$. Using the values of $K(q)$ the parameters C_1 and α were estimated as $C_1 = K'(1)$ and $\alpha = K''(1)/C_1$ (Stolle *et al.*, 2009; Gires *et al.*, 2013). The values of α and C_1 combined with spectral slope β were utilized to estimate values of H , using the relationship $\beta = 1 + 2H - K(2)$. The three universal multifractal parameters (α , C_1 , and H) computed here, determine the statistics of the data at all scales and moments.

⁸ The trace moment algorithm accessible on the website: <http://www.physics.mcgill.ca/~elias/> has been used in this study.

⁹ The corresponding figure for SBES data is illustrated in Part 2.

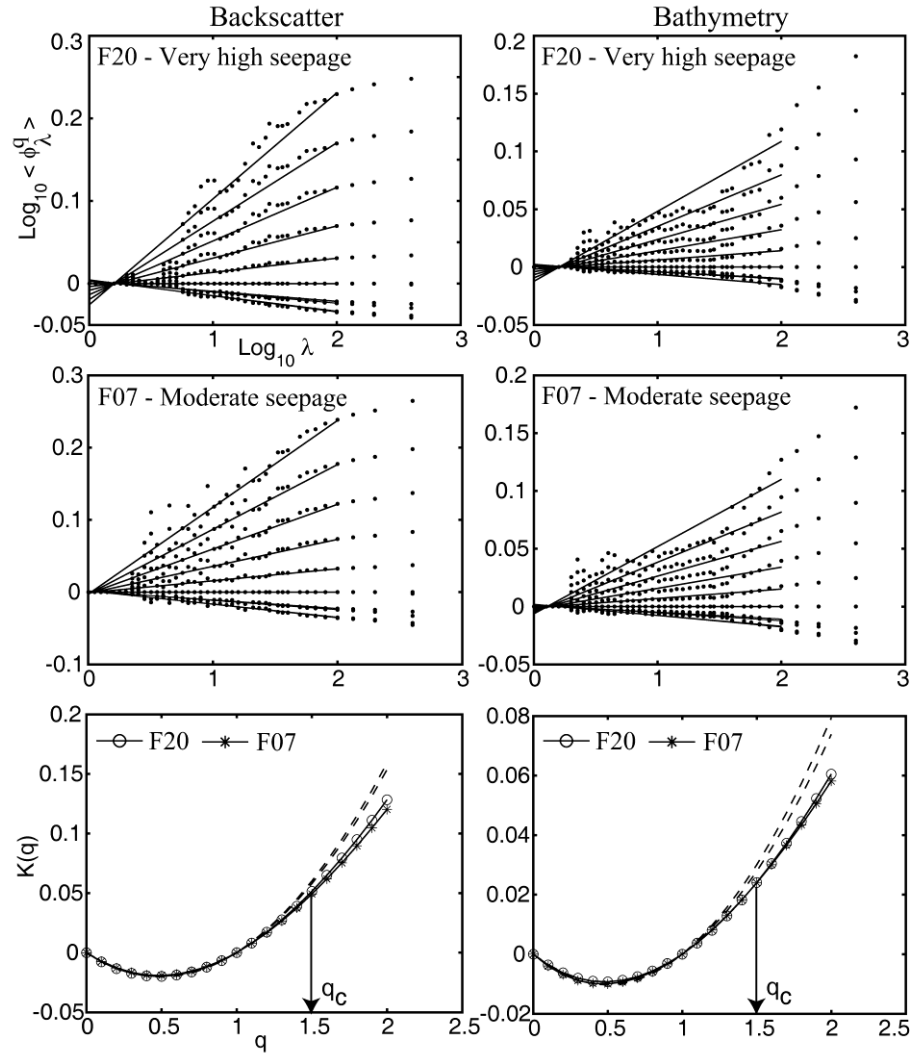


Fig. 6.4 The scaling behavior of the statistical moments of the two representative backscatter and bathymetry image data is illustrated here by the straightness of the Log/log curves of the normalized trace moment (M) as functions of the scale ratio $\lambda=L/l$. The values of the exponent q of each trace moments are varied between 0-2. The linear deviation of dashed curves for $q \geq q_c > 1.5$ is indicative of a multifractal phase transition.

6.5 Results and discussion

6.5.1 Strange attractors based technique

As mentioned earlier, the degree of multifractality can be easily related to the width of the generalized dimension $\Delta D(q)$ and the $f(\alpha)$ spectrum. The computed $\Delta D(q)$ values get successively reduced from maximum to minimum, in the case of the backscatter blocks: Q19, J19, S23, F07, N25 and F20, associated with low, high, very low, moderate, nil, and very high seepages respectively (Fig. 6.5). Such reductions in $\Delta D(q)$ values indicate decrease in the degree of multifractality. Generally, low $\Delta D(q)$ values of bathymetry data blocks indicate comparatively reduced multifractality than the corresponding backscatter block (Fig. 6.5). However, gradual reduction of $\Delta D(q)$ values among the bathymetry data blocks show successive reduction in the degree of multifractality or monofractality (particularly in Q19 and S23 blocks) as $D(q)$ vs. q curves are unvarying. Interestingly, the overall observation of the $D(q)$ vs. q plots of backscatter as well as bathymetry data blocks imply similar construal for $f(\alpha)$ spectrum. The Q19 and S23 bathymetry blocks show single data point in the $f(\alpha)$ spectrum i.e., monofractality (Fig. 6.5).

It is further observed that the shape parameters estimated from the $f(\alpha)$ spectrum also provide information about the multifractality (Telesca *et al.*, 2003). The W values of the four backscatter blocks, Q19, S23, J19 and F07, show gradual decrease in the degree of multifractality (heterogeneity) in a decreasing order. Though, Q19 and S23 blocks are located at a relatively shallower depth ($\approx 180\text{m}$), they have low to very low backscatter strength indicating dominant multifractality (heterogeneity) (Fig. 6.6). Intriguingly, bathymetry blocks with negligible W values display relatively reduced degree of multifractality as compared to the corresponding backscatter blocks. This may be due to the presence of shell materials along with coarse sediments and the changes in the seafloor roughness at the textural level caused by bottom currents (Fig. 6.1) (Dandapath *et al.*, 2010, 2012). Such changes at the textural level can only be notably detected in the backscatter data as compared to the bathymetry data.

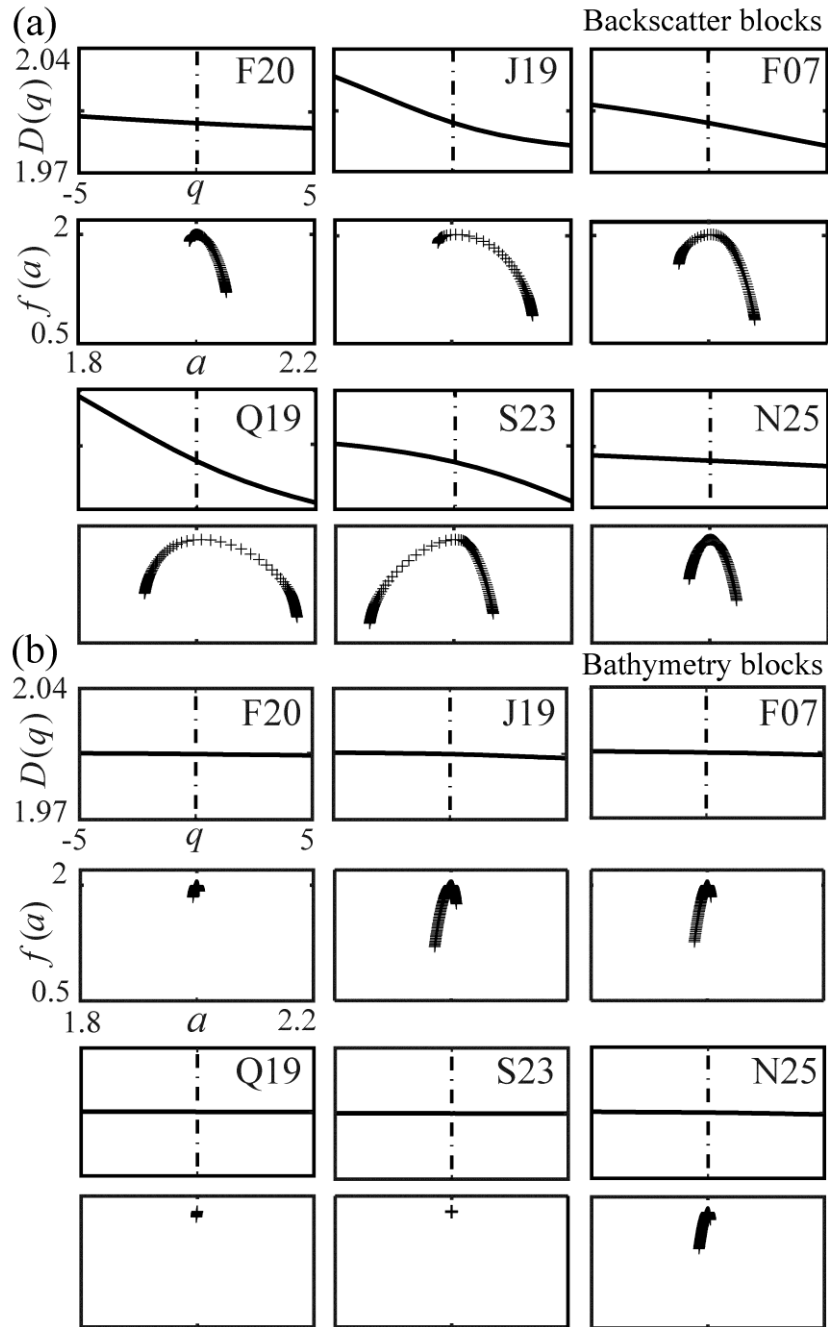


Fig. 6.5 Block wise generalized correlation dimension $D(q)$ and multifractal spectrum $f(\alpha)$ plots for (a) backscatter strength, and (b) bathymetry data of the study blocks.

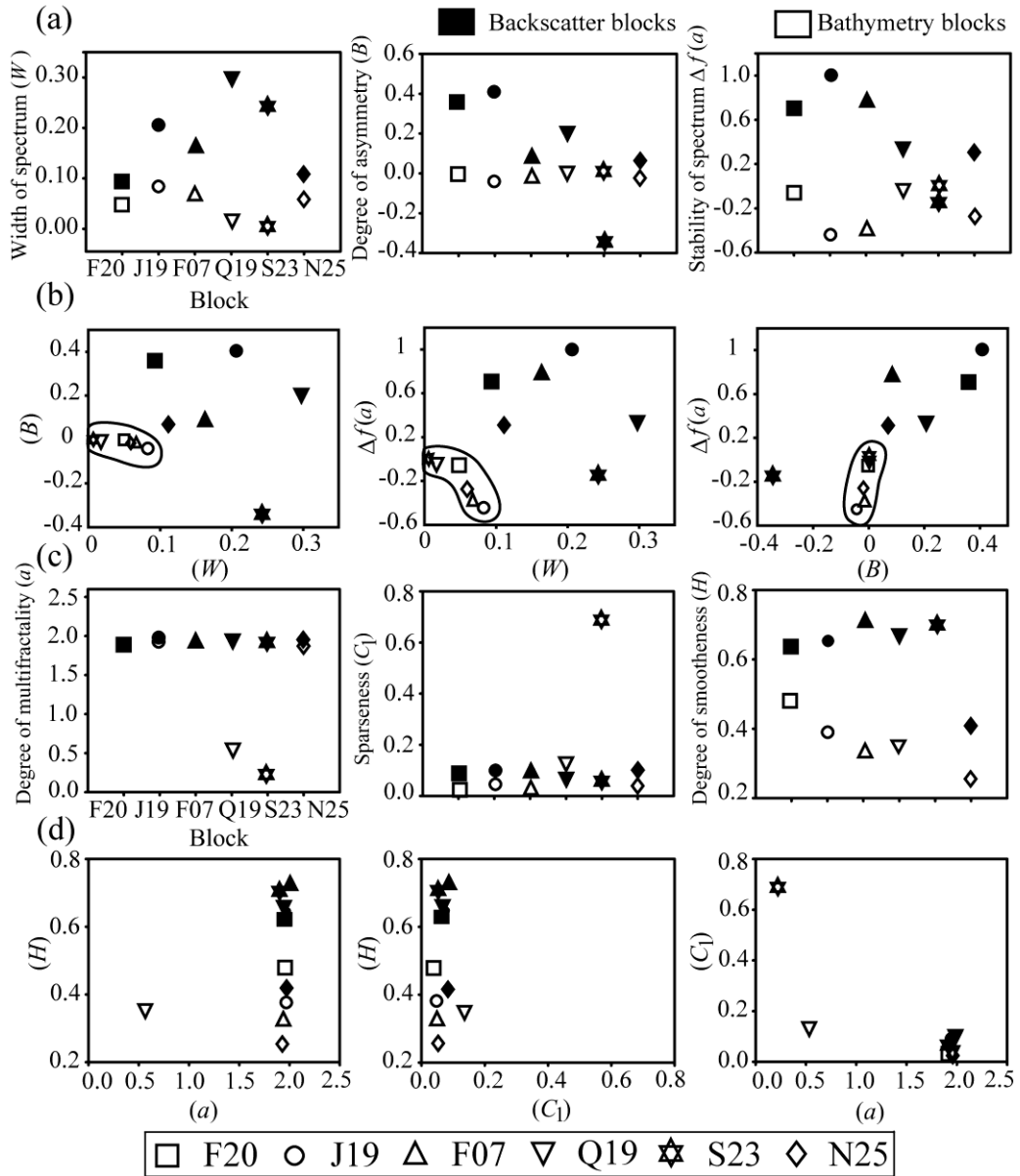


Fig. 6.6 Results obtained using the two multifractal formalisms. (a) Block wise multifractal spectrum $f(\alpha)$ related shape parameters estimated using strange attractor formalism. (b) Scatter plots of the three multifractal parameters [W , B , and $\Delta f(\alpha)$]. The bathymetry blocks are encircled. (c) Block wise multifractal parameters estimated using stochastic multifractal formalism. (d) Scatter plots of the three multifractal parameters (α , C_1 and H). The solid and hollow shapes represent different study blocks as shown in the legend.

The estimated B values using backscatter image blocks reveal that all the blocks are positive or right skewed except S23. Among them, the blocks J19 and F20, located away from fault regime (Fig. 6.1), possess higher B values indicating dominance of higher fractal exponents (Fig. 6.6). Whereas S23 block possess a negative value of B showing left skewed spectrum i.e., the dominance of lower fractal exponents. The estimated B parameters of all the bathymetry blocks are significantly low and negative (left skewed), indicating that the distributions are dominated with lower fractal exponent.

The positive values of the parameter $\Delta f(\alpha)$, are seen successively diminishing in the case of backscatter image blocks J19, F07, F20, Q19, N25 and S23, suggesting reduction in the undulations or instability at the textural level (Fig. 6.6). However in the case of bathymetry image blocks, low negative values of $\Delta f(\alpha)$ are observed in all the six blocks. The variability of the three parameters [W , B , and $\Delta f(\alpha)$] of the backscatter blocks is more conspicuous than their corresponding parameters of the bathymetry blocks, indicating dominant fine scale undulations in the backscatter as compared to the depth data. The scatter plots (Fig. 6.6) of the three parameters affirm the location wise study results using the strange attractor technique.

6.5.2 Stochastic multifractal field based technique

In our analyses, the universal form [determined from Eq. (6.4) based on the estimated α and C_1] fits the empirical $K(q)$ (determined from the logarithmic slopes of trace moments) quite well. A “multifractal phase transition” (Schertzer and Lovejoy, 1992) is observable in the plot (Fig. 6.4) of empirical and theoretical $K(q)$ curves, indicating that the measured moments will only have the theoretical $K(q)$ for q below a critical moment q_c . Beyond q_c there is a multifractal phase transition where $K(q)$ becomes asymptotically linear for $q \geq q_c > 1.5$ (a sample size-dependent effect corresponding to the domination of the statistics by the largest flux values present). Indeed, for $q < 1.5$, the deviations from the universal form are negligible.

The α values of the bathymetry and backscatter blocks show identical trend (≈ 2) expressing similar degree of multifractality excluding Q19 and S23 of the bathymetry blocks (Fig. 6.6). The low α values of the two blocks are well

corroborated with the results of the other formalism signifying monofractality. The C_1 values of the backscatter and bathymetry blocks are found to be varying between 0.058 and 0.091 and between 0.038 and 0.690 respectively. Excluding the S23 bathymetry block ($C_1= 0.690$), the lower values of C_1 attributed to the remaining blocks, indicate that the field values are close to the mean values. Fluctuations in higher values of H between 0.636 and 0.706 are observed in the backscatter image blocks, except in the N25 block (0.412) having no evidence of seepages. Whereas, lower H values (0.255–0.480) are observed in the bathymetry as compared to the backscatter blocks at the same location. The estimated H value of N25 bathymetry block is the lowest.

Cluster analyses output (Fig. 6.6) of H vs. α reveals a uniform α in the backscatter and bathymetry blocks except in the Q19 bathymetry block. However, the H value of the bathymetry block S23, does not subsist owing to the isotropic field condition as mentioned in p. 549 of Gagnon *et al.* (2006). Remarkably the clustering tendency around the high α (≈ 2) and low C_1 of the bathymetry and backscatter data, show extremely close relationship among, the six backscatter and four bathymetry blocks (Fig. 6.6). However both Q19 and S23 bathymetry blocks possess comparable α values and relatively higher C_1 values. The C_1 (0.690) value of the S23 bathymetry block espouse the setting wherein the depths at specific locations (i.e., center of the pockmark) are higher as compared to the rest of the locations within the block. In this study, the stochastic multifractal based technique show no significant variation in α and C_1 of the backscatter field data, except parameter H .

6.6 Concluding remarks

Two multifractal formalisms (strange attractor and stochastic) were applied to the backscatter and corresponding bathymetry blocks to characterize the pockmark seepage associated seafloor in the WCMI. The outcome of the application of the strange attractor technique, $\Delta D(q)$ and the $f(\alpha)$ spectrum related shape parameters [W , B and $\Delta f(\alpha)$] reveal multifractal character of the six backscatter blocks. The variability of the estimated shape parameters is more apparent in the backscatter as

compared to the corresponding bathymetry blocks. This can be related to the interpretation of $\Delta D(q)$, and $f(\alpha)$ parameters of the ECG signal of a healthy and a diseased heart (Stanley *et al.*, 1999). The above referred multifractality aspects support the fact that greater the data heterogeneity, higher would be the system stability. Characteristically, higher stability can be realized when $|\Delta f(\alpha)|$ is low. Appropriately Q19 and S23 backscatter blocks reveal low $|\Delta f(\alpha)|$ values. The stability attributed to the blocks could be ascribed to their location in shallow depth ($\approx 180\text{m}$) as compared to the rest of the blocks. Moreover, the above blocks possess coarse seafloor sediments having dominant shell materials, and are influenced by the monsoonal bottom currents, resulting in greater heterogeneity (Dandapath *et al.*, 2010).

The three computed parameters (α , C_1 , and H) from bathymetry and backscatter blocks using stochastic multifractal formalism show almost similar degree of multifractality with the exception of Q19 and S23 bathymetry blocks. The low values of the two blocks are in sound corroboration as they show monofractality. Generally the level of the C_1 values of backscatter data blocks are found to be higher (0.058–0.091) than the bathymetry (0.038–0.690). In the case of backscatter image blocks, higher H values (0.636–0.706) are observed except in N25 block (0.412) having no seepages. On the other hand, lower H values (0.255–0.480) are observed in the bathymetry blocks in relation to the backscatter. The advantage of the stochastic multifractal technique is that it provides three distinct parameters, with which it is easier to comprehend the multifractality aspects of the seafloor than the strange attractor based $f(\alpha)$ spectrum related shape parameters. Cheng and Agterberg (1996) had made assessment between the interrelationships of the two methods (akin to the ones we have used here) and had suggested the aptness of the multifractal spectrum $f(\alpha)$ over the codimension function C_1 . The two multifractal techniques utilized in our work is a first-time attempt to analyze the high resolution MBES backscatter and bathymetry data. The present investigation employing both the methods ascertain an important finding, however further interest is required to expound the techniques.

Chapter 6

Multifractal approach for seafloor characterization: Part 2: Application to single-beam echo envelope data

6.7 Introduction

Acoustic remote sensing methods using the normal-incidence SBES and MBES are mainly concern with identifying, classifying and mapping surficial geological features of the seafloor. These methods are well recognized as a useful tool in oceanography to characterize the seafloor over a wide area and facilitate preliminary geological analyses (Anderson *et al.*, 2008). The seafloor characterization and classification methodologies available in the literature using SBES and MBES can be traditionally grouped into two categories namely, model based techniques and empirical methods. The model-based techniques often utilize physics-based acoustic backscatter models to characterize the seafloor sediments by optimizing the match between the measured and the modeled signals (Sternlicht and de Moustier, 2003a, b; van Walree *et al.*, 2006; De and Chakraborty, 2011; Snellen *et al.*, 2011; Williams *et al.*, 2012; Snellen *et al.*, 2013). The empirical methods however rely on the statistical and artificial neural network based approaches to correlate the features of echo signals with the sediment type (Chakraborty *et al.*, 2004; van Walree *et al.*,

2005; De and Chakraborty, 2009; Amiri-Simkooei *et al.*, 2011; Madricardo *et al.*, 2012; Chakraborty *et al.*, 2015).

The success of the model-based inversion procedure depends on the scattering theory employed in the forward backscatter model and requires detailed understanding of the scattering mechanism. The study of sound interaction with the seafloor and the corresponding inversion modeling impose a challenging task, particularly with the existence of diversity in the benthic habitat of the area (Holliday, 2007). The scattering process of acoustic wave is influenced by the presence of benthic fauna responsible for modifying the small-scale morphological features and the density fluctuations within the sediment volume (in addition to the hydrodynamic processes). Incorporation of the number density of biological organisms and their collective activities (i.e. burrowing and home building) in the forward backscatter model complicate the inverse modeling even further. The continuous form of seafloor heterogeneity (due to bioturbation, sediment deposition, or hydrodynamic processes) therefore necessitates the development of versatile and robust statistical techniques to determine the seafloor roughness statistics (Jackson and Richardson, 2007). Accordingly, to further improve the seafloor feature discrimination we introduce an empirical method that uses the scaling and multifractality of the dual frequency SBES echo-envelopes at 33 and 210 kHz (Fig. 6.7).

The “stochastic” multifractal formalism followed herein discriminates the SBES echo-envelopes with three fundamental parameters namely, degree of multifractality α , sparseness C_1 , and degree of smoothness H (related mathematical equations are described in Part 1 of Chapter 6¹). In the specific framework of stochastic based “universal multifractals” (Schertzer and Lovejoy, 1987, 1991, 1997; Lovejoy and Schertzer, 1990), the statistics of the underlying cascade process is completely characterized by the aforementioned scale invariant fundamental parameters (Gagnon *et al.*, 2006). The reason for using multifractal framework is to build on the fact that the layers of seafloor imprints a fractal signature on the echo signal along

¹ See Eq. (6.4) and related explanation.

with the self-similarity of sediment ripples of various sizes. Moreover, acoustically soft sediments are penetrated more deeply by acoustic signals and produce longer and corrugated echoes than hard sediments, evidencing fractal structures. Therefore, the estimated multifractal parameters of echo-envelopes as a measure of complexity and roughness proffer useful information to improve seafloor feature discrimination.

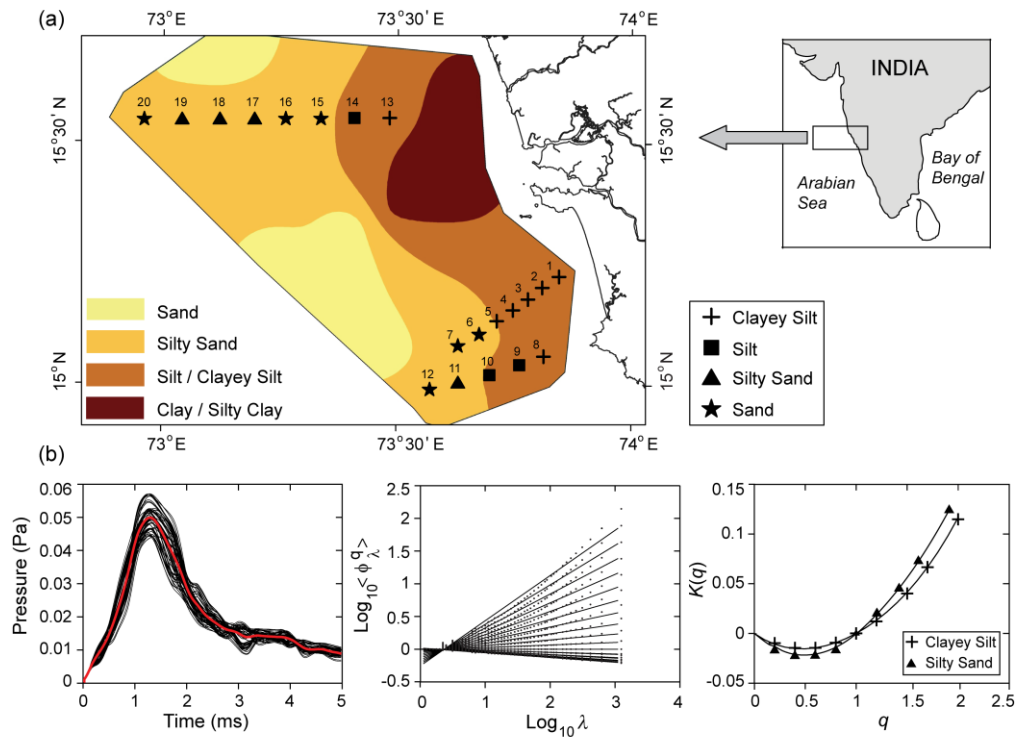


Fig. 6.7 Panel (a) represents GIS-based sediment distribution map of the study area indicating the acoustic and sediment data acquisition locations. The acoustic data were sampled with RESON-NS 420 dual-frequency SBES along the three tracks. The ground truth sediment information (given Table 2.1) was collected using a Van-Veen grab. Panel (b) represents the graphical abstract of the methodology implemented in the study. The dual frequency echo-envelopes from 20 locations are subject to stochastic based universal multifractal analyses to verify the existence of multiscaling.

6.8 Multiscaling

Many geophysical fields have been shown to be multifractal over various ranges (Lovejoy and Schertzer, 2007a). However, in the specific case of SBES echo envelopes, the power law behaviour of the data calls for stochastic multifractal analyses to verify the existence of multiscaling. When a multifractal cascade proceed over a scale ratio $\lambda=L/l$ (L and l representing largest and smallest time scale in the data), the statistical moments of the conserved multifractal flux ϕ_λ (the pressure values of the echo envelope data) measured at scale λ , follow a power law that can be expressed using Eq. (6.3). The multiplicative process (the cascade) mentioned here generates a scale by scale conserved multifractal flux characterized by a moment scaling function $K(q)^2$. The $K(q)$ characterizes the scaling of the moments of the ϕ_λ and can be termed as the “moment scaling function”. Generally, the spectrum of such a conserved flux has an exponent $\beta=1-K(2)<1$. In order to discriminate the SBES echo envelope data (having $\beta \approx 2$), FIF model (Gagnon *et al.*, 2006) has been utilized (the theoretical formalism and the related equations are described in the Part 1 of Chapter 6). However, the characterization of SBES echo envelopes using FIF model is difficult to distinguish the underlying cascade dynamics, because it involves a convolution due to the exponent H (see Eq. 6.6). Therefore, resorting to the use of “trace moments” (that directly characterizes the conserved multifractal flux ϕ_λ), is necessary so that convenient differentiation is possible. The multiscaling of the statistical moments corresponding to the SBES echo envelopes can be verified by the straightness of the curves fitted in the resulting Log/log plot between the normalized trace moments and the scale ratio λ (Fig 6.8)³.

² See Eq. (6.4).

³ The multiscaling of trace moments generally holds quite well up to $q<1.6$. The deviation of trace moments (dots) from the fitted linear curve is indicative of “break” in the multiscaling. The break is less apparent for low q (<1.6) values, but becomes conspicuous for large q (>1.6) values. The break associated with the time dependent seafloor backscattering is possibly due to the collective effect of inherent heterogeneities present in the seafloor (mainly because of the coarse sand particles, shells, gas bubbles, benthic organisms and sediment layers). Depending on acoustic wavelength/frequency the individual features such as shells and other roughness elements at the sediment-water interface may be more appropriately characterized as discrete scatters than as micro topography (Jackson and

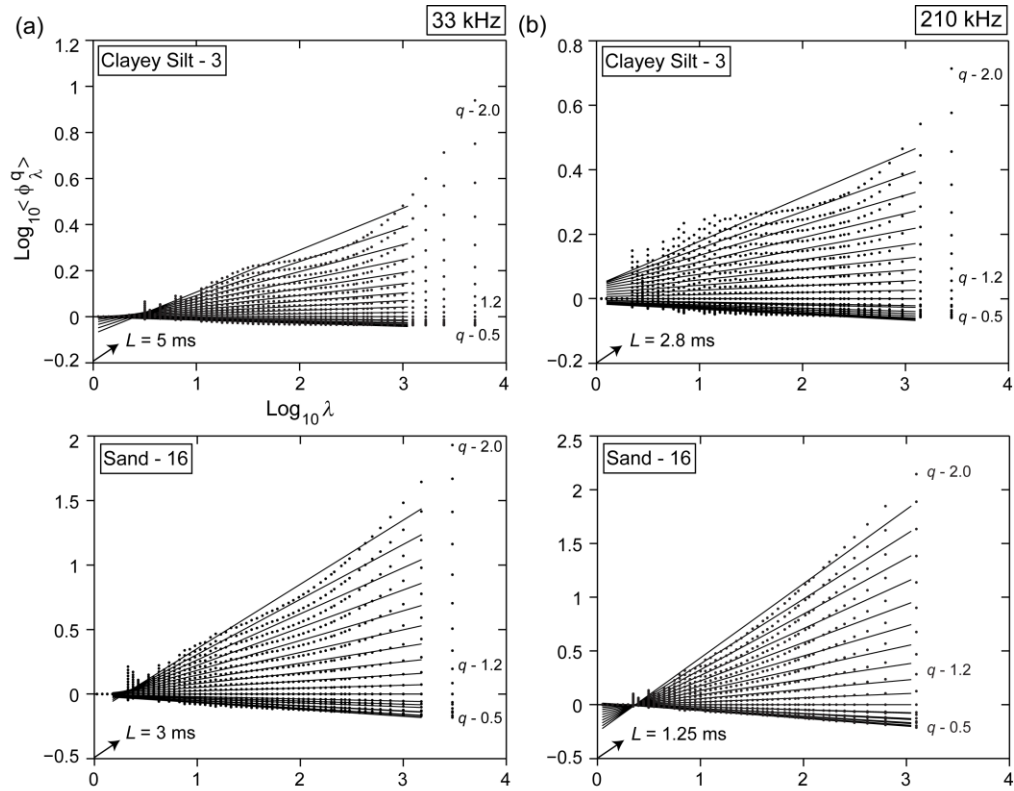


Fig. 6.8 Panels (a) and (b) shows the Log/log plot of the normalized trace moments as a function of the scale ratio $\lambda=L/l$ at 33 and 210 kHz. The multiscaling of the statistical moments of the representative clayey silt and sand substrate is verified by the straightness of the curves. The q values of the each trace moments are varied between 0 and 2, in intervals of 0.1 (from top to bottom, $q=2-1, 0.1, 0.9, 0.2, 0.8, 0.3, 0.7, 0.4, 0.6$ and 0.5).

Richardson, 2007). An appropriate assessment in this regard is difficult due to lack of supporting data [Similar results were also reported earlier by Gagnon *et al.* (2006) and Lovejoy and Schertzer (2007a) while analyzing the high resolution Lower Saxony DEM data over Germany. The break observed in their analyses was due to the effect of “trees” evident in the high resolution topography data].

6.9 Results and discussion

The following sections describe the analyses of the estimated universal multifractal parameters (at 33 and 210 kHz) along with ground truth values of the mean grain size of the seabed sediment. The end results are statistically analyzed and compared to the ground truth data as well as with the previously estimated sediment geoacoustic inversion results (De and Chakraborty, 2011) obtained at the same locations.

6.9.1 Sediment distribution

The percentage distribution of sediment composition indicates the presence of four sediment types: clayey-silt, silt, silty-sand and sand with varied levels of mixing of three textural grades namely sand, silt, and clay. The important substrate characteristics of the study area have been investigated in detail (Haris *et al.*, 2012), and four distinct sediment provinces were identified from the map generated using GIS (Fig. 6.7). The sediment texture was relatively coarse in the deeper depths (60–109 m) whereas fine-grained sediment was found in the shallow depth region (29–54 m). The high percentage distribution of fine-grained sediment in the shallow depth region is being governed by a set of sedimentological and hydrodynamic conditions. The study area receives relatively high annual rainfall, which can bring the sediment load through the rivers and discharges to the shallow water regions of the study area. Besides, the shallow region is influenced by an environment with a feeble current that allows fine particles to settle down as compared to the regions of higher depth. These processes might have resulted in the accretion of fine sediment in the shallow depth region.

6.9.2 Multifractal phase transition

Self-Organized Criticality (SOC) was first introduced by Bak *et al.* (1987) as an explanation to the $1/f$ noise detected in various dynamical systems. The SOC is generally evident in multifractal processes along with a multifractal phase transition (Schertzer and Lovejoy, 1992; Schertzer *et al.*, 1993; Hooge *et al.*, 1994; Schmitt *et al.*, 1994; Garrido *et al.*, 1996; Stolle *et al.*, 2009). In our analyses, the universal form (determined from Eq. 6.4 based on the estimated α and C_1) fits the empirical $K(q)$ (determined from the logarithmic slopes of trace moments) quite well. A multifractal phase transition is observable in the plot (Fig. 6.9) of empirical and theoretical $K(q)$ curves, indicating that the measured moments will only have the theoretical $K(q)$ for q below a critical moment q_c . Beyond q_c there is a multifractal phase transition where $K(q)$ becomes asymptotically linear. The linear behaviour of the empirical moment scaling function is either due to sampling limitations (i.e. second-order multifractal phase transition; Schertzer and Lovejoy, 1992) or its association with a divergence of statistical moments (i.e. first-order multifractal phase transition; Schertzer and Lovejoy, 1992). In the first-order multifractal phase transition, q_c corresponds specifically to maximum singularity measured and is associated with the occurrence of very rare and violent singularities, whereas in the case of a second-order multifractal phase transition, q_c corresponds to the maximum singularity effectively measurable from a finite sampling (Seuront *et al.*, 1999).

In order to differentiate between first and second order multifractal phase transitions, we compare the theoretical value of the critical moment q_s with the empirical critical moment q_c calculated from the $K(q)$ curve. The theoretical value of the critical moment q_s can be computed as (Schertzer and Lovejoy, 1992):

$$q_s = \left(\frac{1}{C_1} \right)^{1/\alpha}. \quad (6.7)$$

If $q_c \approx q_s$, the phase transition can be termed as a second-order multifractal phase transition wherein the critical moments are only related to sampling limitations. Also, if $q_c < q_s$ the critical moments q_c are independent of the sampling and characterizes the occurrence of very rare and violent singularities present in the

dataset (i.e. first-order multifractal phase transition) (Seuront *et al.*, 1999). Using the values of C_1 and α , the average q_s values computed for coarse sediment region are found to be 2.32 and 2.16, respectively at 33 and 210 kHz, whereas in fine sediment region, the average q_s values are observed to be 4.22 and 3.97, respectively at 33 and 210 kHz. The estimated q_s values indicate a first-order multifractal phase transition ($q_c < q_s$) in the dual frequency echo-envelopes with the occurrence of rare and violent singularities in the dataset. The detection of the presence of a first-order multifractal phase transition possibly suggests that the time dependent dual frequency seafloor backscattering could be a SOC process.

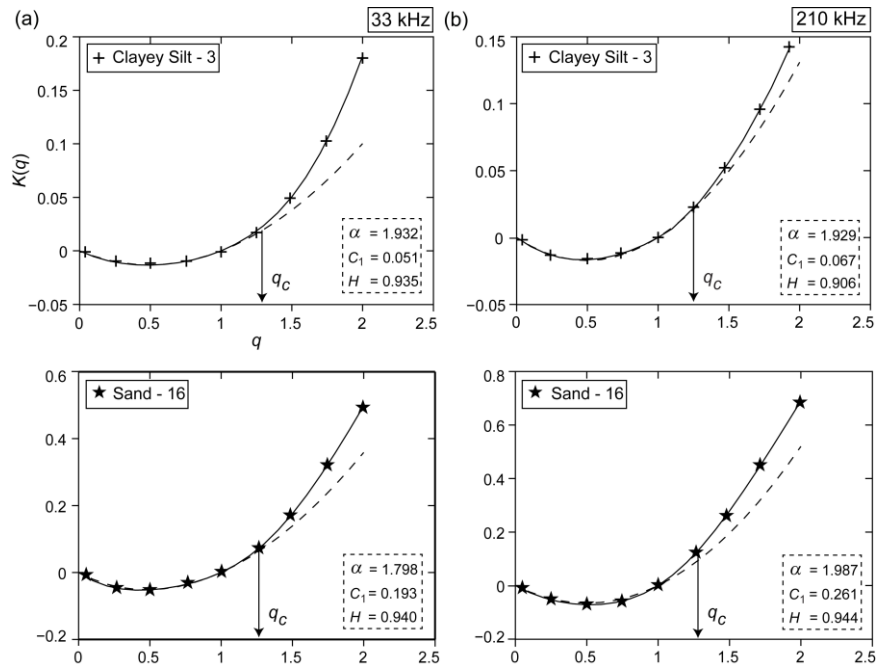


Fig. 6.9 Comparison between the empirical (solid curve) and theoretical (dash curve) moment scaling function $K(q)$ as a function of q . The empirical $K(q)$ values of the representative clayey silt and sand substrates are determined from the logarithmic slopes of trace moments illustrated in Figure 6.8. The theoretical $K(q)$ values are calculated using Eq. (6.4) based on the computed α and C_1 . The linear deviation of theoretical curves beyond $q \geq q_c > 1.25$ is indicative of a first-order multifractal phase transition, caused by the rare and violent singularities in the dual-frequency data.

6.9.3 The universal multifractal parameters

The dual frequency universal multifractal parameters were analyzed along with the ground truth values of the mean grain size (M_ϕ) to understand their relationships. The C_1 values are negatively correlated with the measured M_ϕ , having correlation coefficients of -0.96 and -0.92 , respectively at 33 and 210 kHz (Fig. 6.10). The C_1 values decreases with increasing weight percentage of both silt and clay fraction (with $M_\phi > 4$). Concurrently, the C_1 values increases linearly with increasing percentage content of sand fraction (with $M_\phi < 4$). The range of C_1 values associated with coarse and fine sediments vary between 0.171–0.249 and 0.035–0.089 and between 0.180–0.294 and 0.051–0.090, respectively at 33 and 210 kHz. Moreover, in coarse sediment region, the average C_1 values are restricted to values around 0.203 ± 0.0222 and 0.209 ± 0.0372 , respectively at 33 and 210 kHz. In fine sediment region, the average C_1 values are found to be within 0.066 ± 0.0162 and 0.0722 ± 0.0115 , respectively at 33 and 210 kHz. In brief, the C_1 values are well clustered at both the acoustic frequencies with fewer fluctuations for the fine sediment as compared to the coarse sediment region found at deeper depths (Fig. 6.10). The relatively low C_1 values attributed to the fine sediment region indicate that the field values (pressure values) are close to the mean values.

Table 6. 1 Summary of universal multifractal parameters.

Sediment	β		α		C_1		H	
	33 kHz	210 kHz	33 kHz	210 kHz	33 kHz	210 kHz	33 kHz	210 kHz
Clayey Silt	2.74	2.64	1.91	1.91	0.064	0.068	0.92	0.87
	\pm 0.074	\pm 0.085	\pm 0.056	\pm 0.029	\pm 0.019	\pm 0.011	\pm 0.031	\pm 0.038
Silt	2.68	2.51	1.93	1.95	0.067	0.079	0.91	0.86
	\pm 0.017	\pm 0.061	\pm 0.040	\pm 0.035	\pm 0.006	\pm 0.009	\pm 0.010	\pm 0.051
Silty Sand	2.32	2.43	1.89	1.94	0.189	0.232	0.92	0.94
	\pm 0.09	\pm 0.032	\pm 0.037	\pm 0.046	\pm 0.013	\pm 0.048	\pm 0.044	\pm 0.037
Sand	2.34	2.39	1.91	1.93	0.212	0.226	0.95	0.95
	\pm 0.090	\pm 0.220	\pm 0.075	\pm 0.034	\pm 0.023	\pm 0.032	\pm 0.023	\pm 0.018

The α values of the dual frequency echo-envelopes show identical trend (≈ 1.93), expressing similar degree of multifractality in coarse and fine sediment provinces (Fig. 6.11 and Fig. 6.12). The H values signifying the degree of smoothness of the data associated with coarse and fine sediments vary between 0.857–0.999 and 0.888–0.984 and between 0.887–0.986 and 0.804–0.913, respectively at 33 and 210 kHz. The scatter diagram (Fig. 6.12) of H values at 33 and 210 kHz reveals that the values computed at 210 kHz are confined within 0.874 ± 0.0406 in fine sediments and within 0.951 ± 0.0268 in coarse sediments. However, at 33 kHz the calculated H values do not exhibit any apparent trend distinguishing between the fine and coarse sediment provinces. The obtained results provide a construal that is similar to the previously estimated sediment geoacoustic inversion results (discussed in the Chapter 3). Generally, the dual frequency universal multifractal parameters among the coarse and fine sediments shows subtle difference in α and H , whereas the codimension parameter C_1 representing the sparseness of the data is varying (Fig. 6.12 and Table 6.1). This suggests that the physics of scattering mechanism responsible for the variation in C_1 is different.

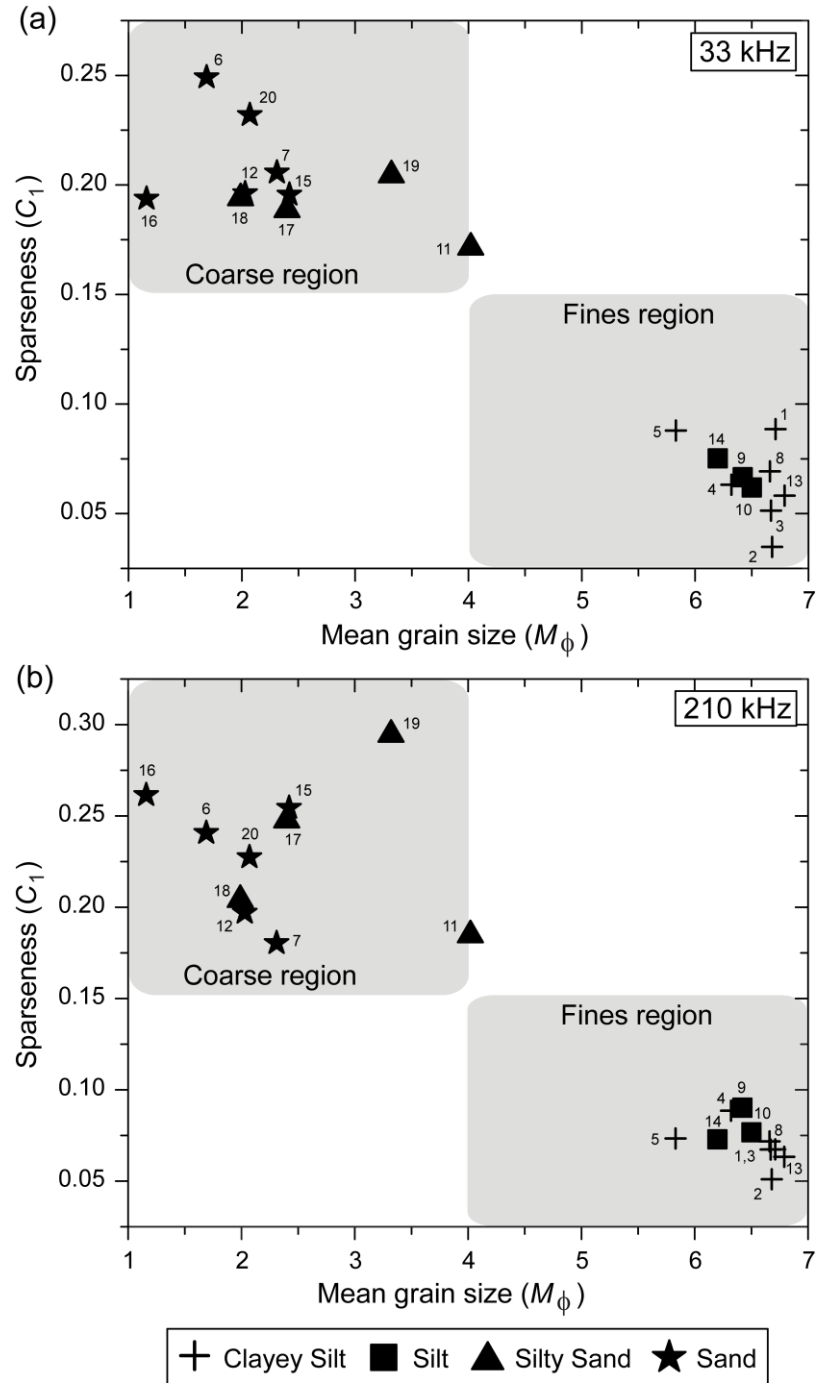


Fig. 6.10 Frequency wise scatter plot of the measured M_ϕ and computed codimension parameter C_1 at 33 and 210 kHz. The shaded region demarcates the boundaries of C_1 in coarse and fine sediment provinces.

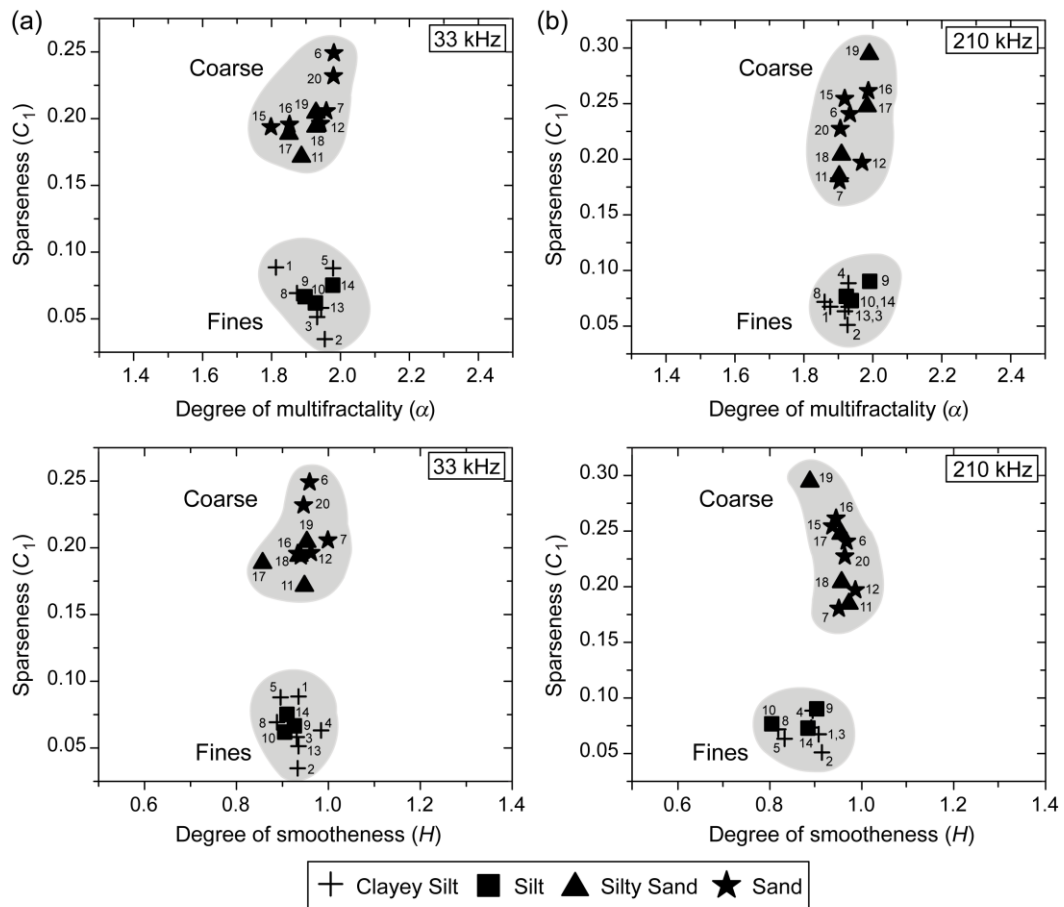


Fig. 6.11 A quantitative comparison between the scale invariant multifractal parameters (α , C_1 , and H) at 33 and 210 kHz. The shaded region represents the coarse and fine sediment provinces.

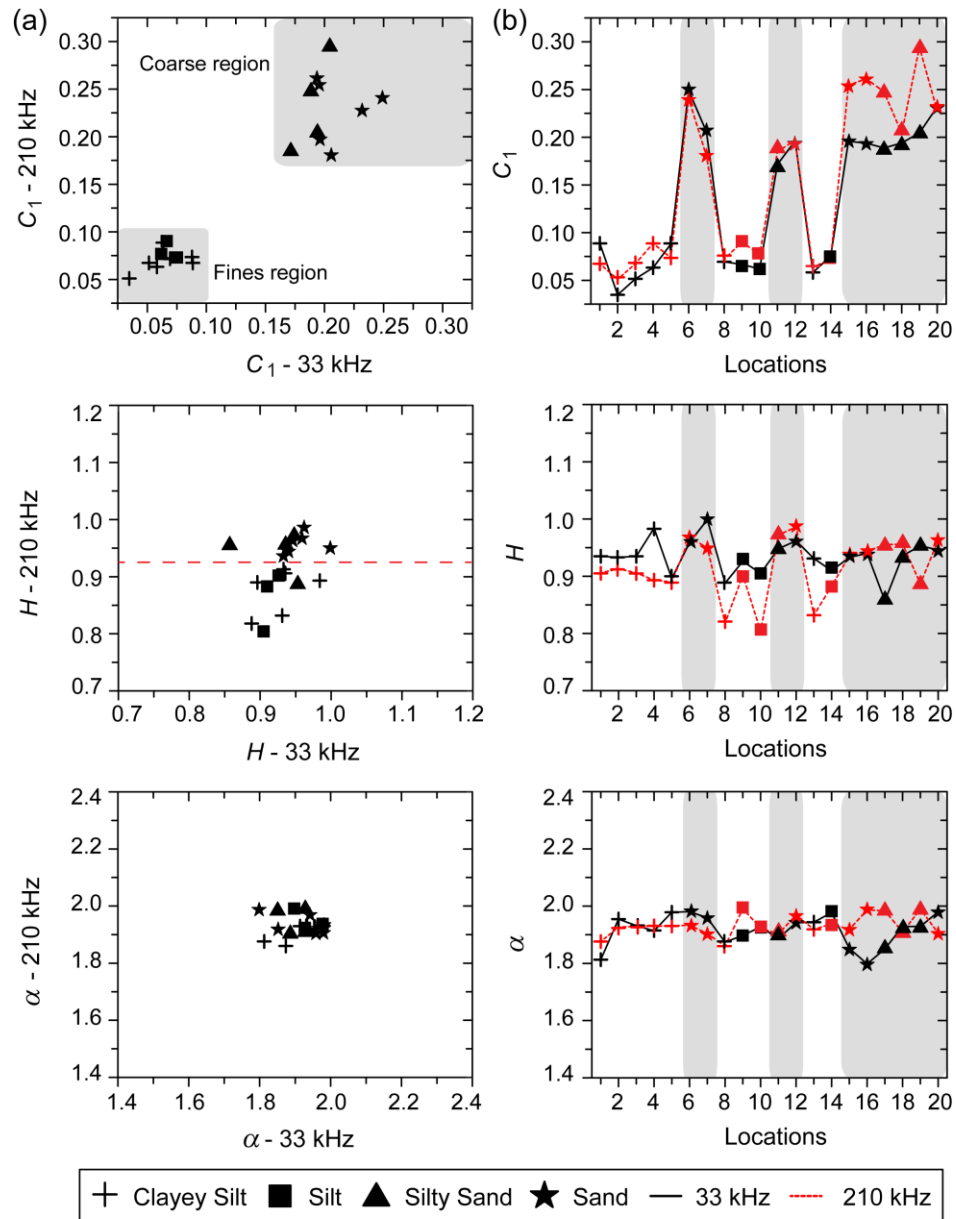


Fig. 6.12 Panel (a) shows the comparison of the computed multifractal parameters (α , C_1 , and H) at frequencies 33 and 210 kHz. The C_1 values are well clustered, demarcating the coarse and fine sediment provinces. The horizontal dash line (red) demarcates the H values at 210 kHz in fine and coarse sediment provinces. The variations of multifractal parameters for different frequencies with the same sediment types at each location are represented in panel (b), the shaded region corresponds to coarse sediment locations.

6.9.4 Possible influence of seafloor backscattering process

The backscattering from the seabed can be generally attributed to two contributing factors namely, interface and volume scattering (Sternlicht and de Moustier, 2003a). The strength of the backscattered signal is primarily controlled by the acoustic frequency, the acoustic impedance contrast between water and sediment, the contributions from seafloor interface roughness, as well as the sediment volume heterogeneity. The interface scattering is governed by the microscale roughness of the seafloor facets coupled with the acoustic impedance. A part of the transmitted acoustic energy penetrates the sediments and reflected back by the volume heterogeneities. Such scattering mechanism is normally referred to as volume scattering (mainly due to the coarse sand particles, shells, gas bubbles, benthic organisms and sediment layers).

The shape of the echo-envelope has two distinct parts, the initial part and the tail part. The initial part of the data represents the reflection from the water-sediment interface (interface scattering), and the tail portion corresponds to the backscatter from the sediment volume (volume scattering). A significant contribution, due to the volume scattering (in addition to the interface scattering) from various scatterers is expected to be dominant for acoustically soft sediments such as mixtures of clayey-silt and silt. Accordingly, the contribution of sub-bottom scattering becomes prominent near the tail portion of the echo-envelope from the soft sediments (De and Chakraborty, 2011). Besides, acoustically soft sediments are penetrated more deeply by the acoustic signal and produce longer and corrugated echoes than hard sediments. The scattering process takes place exclusively at the surface for acoustically hard sediments, i.e. mixtures of silty-sand and sand sediments. The scattering processes described herein determine the statistical and geometrical properties of the data, resulting in the variation of the estimated C_1 parameter.

6.9.5 Relationship with fractal dimension

Several studies while comparing the fractal dimension of the echo-envelopes to the ground truth sediment have concluded that the fractal dimension (as a measure of

complexity and roughness) is a good descriptor of a bottom type in the investigated area (Tegowski and Lubniewski, 2000; Tegowski *et al.*, 2003; Tegowski, 2005; van Walree *et al.*, 2005; De and Chakraborty, 2009). The fractal dimension describes the statistical and geometrical properties of the data. Variations in the fractal dimension of the echo-envelope carry information concerning the fractal structure of the sediment layers signifying the hardness of the seabed. The fractal dimension of the echo-envelopes reflected from the fine seafloor has been found to be higher as compared to the coarse sediment region (Tegowski and Lubniewski, 2000). The low values of fractal dimension in coarse region have been controlled by the dominant interface scattering due to limited bottom penetration of the acoustic signals. Besides, the fine region reflects the environment with deeper acoustic penetration and the fractal structure of the sediment layers are more apparent in the recorded echo, indicating higher fractal dimension values.

The C_1 parameter represents the codimension of the set of points that give the dominant contribution to the mean of the conserved multifractal flux. The corresponding fractal dimension can be expressed as $d-C_1$, where d denotes the standard dimension of the space (Lovejoy *et al.*, 2001). The relatively high C_1 values correspond to a very sparse process. The field values contributing to the mean behaviour in such instance is violent and confined to a very sparse set signifying low fractal dimension. Conversely, a low C_1 implies a more uniform and less extreme process. Appropriately, the relatively low values of C_1 attributed to the fine sediment region (with higher fractal dimension) indicate that the field values (pressure values) are close to the mean values as compared to the coarse sediment region (Fig. 6.10).

The stochastic based multifractal analysis followed herein has several advantages over standard statistical approaches as it characterizes the local scale properties of the data in addition to its global properties. Correspondingly, it is possible to quantify the statistical distribution of the local singularities (i.e. local multifractal exponents) present in the data (see Lovejoy *et al.*, 2009a).

6.9.6 Comparison with inversion results

The acoustic backscatter data obtained from the echo-sounding systems can be matched with theoretical scattering models to interpret the information embedded in the data (Jackson *et al.*, 1986). The numerical approach employed for extracting information from the data is commonly referred to as “inversion modeling” (discussed in Chapter 3). The inversion modeling primarily involves physics based inversion of echo-sounding data to obtain the upper-layer seafloor roughness parameters, namely the sediment mean grain size (M_ϕ); spectral parameters at the water-seafloor interface (γ_2 , w_2); and sediment volume parameter (σ_2), that can be used to examine the fine scale seafloor processes (Sternlicht and de Moustier, 2003a, b; De and Chakraborty, 2011; Haris *et al.*, 2011).

The seafloor “roughness power spectrum” estimated from the echo data characterizes the size and periodicity of the seafloor height fluctuations as a function of the spatial frequency. The roughness power spectrum is often parameterized using a power law by slope and intercept of a linear regression line through the points of the periodogram estimate in log-log space. Indeed, the parameters γ_2 and w_2 used in the scattering models are the slope and intercept respectively, of the 2D roughness power spectrum, which are estimated from the 1D power-law values (Haris *et al.*, 2011). A wide range of 2D roughness power spectrum parameters of the study area are available (De and Chakraborty, 2011) and offer an opportunity to determine their relationship with the presently estimated universal multifractal parameters.

The parameter H describing the height statistics of the data has been empirically determined from the spectral slope β and $K(2)$ using the relation $\beta=1+2H-K(2)$ (Table 6.1). The differences in H principally reflect variations in the spectral slopes (Lovejoy *et al.*, 2001) (and thereby the corresponding γ_2 values). With reference to the inversion modeling study carried out by De and Chakraborty (2011), in coarse sediment region, the average γ_2 values were restricted to values around 3.23 ± 0.071 and 3.16 ± 0.047 respectively at 33 and 210 kHz. In fine sediment region, the average γ_2 values were found to be within 3.22 ± 0.074 and 3.30 ± 0.037 respectively for 33 and

210 kHz. The scatter diagram [Fig. 3b of De and Chakraborty (2011)] between the estimated mean values of M_ϕ and γ_2 at 210 kHz indicated that the values of γ_2 were confined within 3.21–3.4 in fine sediments and within 3.0–3.21 in coarse sediments. In contrast, the estimated mean values of γ_2 at 33 kHz inversions did not exhibit any apparent trend to discriminate between the fine and coarse sediment provinces. The subtle difference in the computed γ_2 (or the spectral slope β) between coarse and fine sediments conform to the meager variation in the computed H parameter (Fig. 6.12), particularly at 33 kHz.

The scatter diagram between the estimated mean values of M_ϕ and w_2 [Fig. 3a of De and Chakraborty (2011)] revealed that, in coarse sediment region, the average w_2 values were restricted to values around 0.00356 ± 0.00047 and 0.00365 ± 0.00101 respectively at 33 and 210 kHz. But in fine sediments, the average w_2 values were found to be varying between 0.000461 ± 0.00013 and 0.000605 ± 0.000042 , respectively at 33 and 210 kHz. The computed w_2 (or intercept) values were well clustered at both the acoustic frequencies, having fewer fluctuations for the fine sediment as compared to the coarse sediment region. Likewise, the parameter C_1 revealing the noise statistics of the data are well clustered at both the acoustic frequencies with fewer fluctuations for the fine sediment as compared to the coarse sediment region. It is observed that the relatively higher values of w_2 and C_1 are associated with coarse sediments, while the lower values of w_2 and C_1 are the characteristics of fine sediments (Fig. 6.13).

As pointed out in the introduction, the model-based methods can help interpret echo signal of the seafloor sediment properties (M_ϕ) and micro roughness parameters (γ_2 , w_2). However, the calculation of correct set of geoaoustic parameters gets convoluted by the large number of good fits existing in the multidimensional search space. Accordingly, it is possible to obtain convincing model-data fits in the search space that do not necessarily correspond to the correct set of geoaoustic parameters (Sternlicht and de Moustier, 2003b). Moreover, the physics based models are valid

only for a certain range of frequencies and sediment types⁴ (Amiri-Simkooei *et al.*, 2011), such that the direct inversion of acoustic signal is unlikely without setting the limits of geoaoustic parameters for a known seabed sediment. In contrast the statistical based empirical methods rely on the analyses of certain echo signal features that are correlated with sediment properties. These methods are relatively easy to implement in view of computation time involved. However proper ground-truth measurements are imperative to validate and interpret the results.

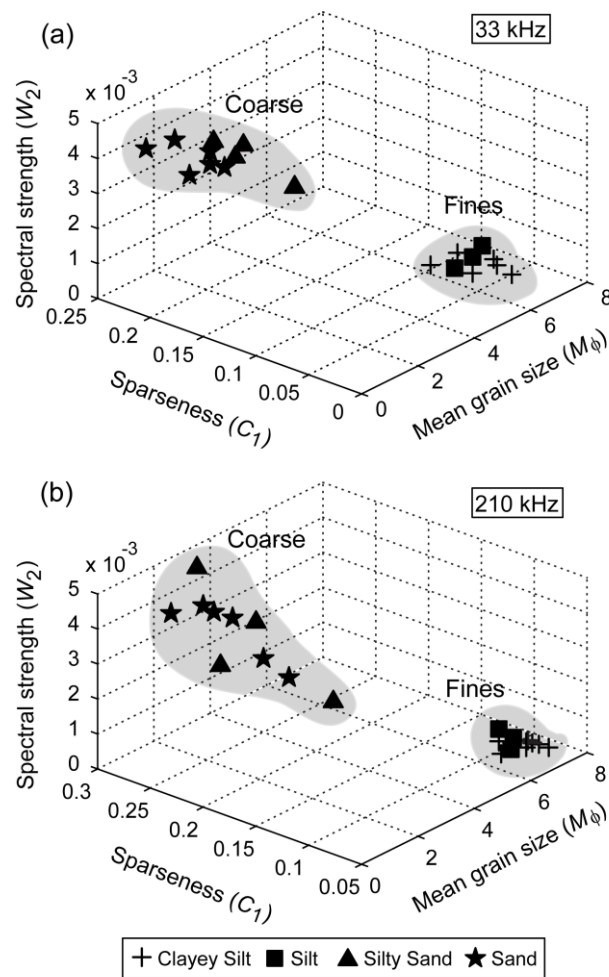


Fig. 6.13 3D scatter diagram showing clustering among M_ϕ , C_1 and w_2 at 33 and 210 kHz. Regions comprising of coarse and fine sediments can be seen clearly delineated.

⁴ See Appendix A for the validity of the composite-roughness approximation.

6.10 Concluding remarks

The scaling and multifractality of the SBES echo-envelopes (at 33 and 210 kHz) have been demonstrated using stochastic based universal multifractal framework. The variations in the three fundamental scale invariant parameters (α , C_1 , and H) and their behaviour with respect to the ground truth sediment information can delineate different bottom types in the investigated area. The evidence for the first-order multifractal phase transition (with the divergence of higher order statistical moments) further reveals the hierarchy of multiplicative cascade dynamics associated with the echo-envelopes.

The universal multifractal parameters among the coarse and fine sediments show subtle difference in α and H , whereas the codimension parameter C_1 representing the sparseness of the data is varying. The C_1 values are well clustered at both the acoustic frequencies, demarcating the coarse and fine sediment provinces. The computed α values show identical trend (≈ 1.93), expressing similar degree of multifractality in coarse and fine sediment region. The minute variation in the H parameter ascribed to the coarse and fine sediment location is well corroborated with the previously estimated sediment geoacoustic inversion results. In the context of multifractal analyses the 210 kHz appears to be marginally better as compared to 33 kHz. This could be due to the fact that the lower acoustic frequencies penetrate relatively more in the substrates whereas higher frequencies have a better resolving capability. The final outcome of the multifractal analyses underpins the hitherto-applied model based seafloor characterization and help foster research on the empirical method based feature discrimination.

Chapter 7

Summary

The thesis highlights the technological approach and relevance to remote acoustic seafloor characterization using high-frequency echo-sounding systems. The geoacoustic inversion results obtained using multi-frequency MBES and SBES data provide important information that can be utilized for acoustic seafloor characterization. The generation of benthic habitat maps has ever more underpinned a relationship among the benthic habitat attributes, the acoustic backscatter and the sediment texture that exist in the study area. The multifractal techniques utilized in the work is a first-time endeavor to analyze and statistically characterize the patchiness of the seafloor using high resolution MBES backscatter and bathymetry data. The outcome of stochastic formalism based multifractal analyses of SBES data underpins the hitherto applied model-based seafloor characterization and helps foster research on the empirical method-based feature discrimination.

In Chapter 3, the angular backscatter data acquired using MBES have been matched with the composite roughness scattering model to interpret the fine scale seafloor roughness information embedded in the data. The seafloor parameters (M_φ , γ_2 , w_2 , and σ_2) are derived employing 4D inversion approach at 95 kHz acoustic frequency. Distinct interclass separations between the sediment provinces are evident from the spatial variability of computed inversion results, particularly the sediment mean grain size (M_φ) and sediment-water interface roughness (w_2), substantiating the

multi-frequency inversion results. In the absence of measured roughness data, the computed multi-frequency γ_2 and w_2 values are assessed with reference to the available published information, displaying subtle variations among 33, 95, and 210 kHz. The seafloor parameters derived from the 95 kHz MBES data are consistent with the ground-truth data as well as with the inversion results obtained using 33 and 210 kHz SBES data at the same locations.

The acoustic data acquired using SBES and MBES operable at 33/210 kHz and 95 kHz, respectively, have been further utilized to demonstrate the correlation among the derived backscatter, grain size, geoacoustic inversion results and benthic macro-fauna abundance (Chapter 4 and 5). The corresponding benthic habitat maps conveniently illustrate the nature, distribution and extent of the distinct sedimentary environment and the associated species communities along the central part of the WCMI. The preferences of deposit feeders (soft body benthic macro-fauna) in the fine-sediment regions and filter feeders (hard body benthic macro-fauna) in coarse sediment regions reveal the influence of sediment texture and total organic carbon on the feeding behavior of the organisms. The results presented here accentuates the versatility of SBES and MBES for generating benthic habitat maps across large areas of seafloor.

The attainment of the model-based inversion procedure (Chapter 3) for seafloor characterization fundamentally depends on the scattering theory employed in the forward backscatter model and requires detailed understanding of the scattering mechanism. The study of sound interaction with the seafloor and the corresponding inversion modeling impose a challenging task, particularly if the physical structure of the seafloor and the associated benthic communities with its diversity coexists (Chapter 4 and 5). Therefore, expounding on the established power law behaviour of seafloor bathymetry and backscatter data, we have developed nonlinear statistical based multifractal techniques to elucidate the spatial and temporal seafloor heterogeneities (Chapter 6). Two distinct multifractal formalisms (strange attractors and stochastic) have been applied in this context to further expand the seafloor characterization procedure. The final outcome of the two multifractal analyses

underscores the advantages of nonlinear techniques to substantiate the hitherto applied numerical inversion based characterization and the soft computational technique based classification of the seafloor sediments along the WCMI.

The time lapse remote sensing of seabed processes using high-frequency SBES\MBES\Stereo photography\X-ray tomography\Underwater laser scanner can generate unique data to facilitate multidisciplinary studies of the ocean environment and associated physical and biological activities. Advanced studies, with the support of concurrent environmental measurements (including the hydrodynamic and biological activities), can be envisioned to examine the suitability of scaling analyses based multifractal techniques for uncovering dominant roughness creating processes on the seafloor over a wide range of spatio-temporal scales.

Appendix

A. Validity of the composite-roughness approximation

The attainment of the composite-roughness approximation used to model scattering by the sea surface (McDaniel and Gorman, 1982) intrigued Jackson *et al.* (1986) for the corresponding application to seafloor scattering. The bottom line of this approximation is the division of the seafloor roughness into large- and small-scale components (as illustrated in Fig. 13.16 of Jackson and Richardson, 2007). In terms of the spectrum of seafloor roughness, the small-scale (shorter-wavelength) roughness causes scattering, while the large-scale (longer-wavelength) roughness virtually tilts the seafloor, altering the grazing angle and resulting in acoustic shadowing. The division of the seafloor roughness into large and small scale is based on the “cutoff” wavenumber (K_c) that can be expressed as (Jackson and Richardson, 2007):

$$K_c = \left(\frac{8\pi w_2 k_w^2}{\gamma_2 - 2} \right)^{1/(\gamma_2 - 2)} \quad (\text{A.1})$$

where k_w is the acoustic wavenumber¹, w_2 the spectral strength, and γ_2 the spectral exponent².

With reference to Jackson and Richardson (2007), the composite-roughness approximation is applicable only if the cutoff wavenumber (K_c) is less than the Bragg

¹ The acoustic wavenumber is given as: $k_w = 2\pi / \lambda a = 2\pi f / c$, where λa is the acoustic wavelength, f the acoustic frequency, and c the sound speed in water.

² See Figure 3.5 in Chapter 3.

wavenumber (ΔK). In the specific case of seafloor backscattering, the Bragg wavenumber follows the simple form:

$$\Delta K = 2k_w \cos(\theta_g) \quad (\text{A.2})$$

where θ_g is the grazing angle.

The validity condition ($K_c < \Delta K$) restricts the application of the composite-roughness approximation to certain “valid” grazing angles that need to be precisely defined during the inversion modeling. For a given value of K_c , the valid grazing angles can be obtained by assuming $\Delta K = K_c$ and solving Eq. (A.2) for θ_g . The value of K_c is dependent on the spectral strength w_2 and the spectral exponent γ_2 (Eq. A.1). Therefore, for a particular acoustic frequency, it is possible to compute the valid θ_g as a function of w_2 (Fig. A.1). The value of γ_2 has been assigned as 3.25 in the calculation procedure irrespective of the sediment type.

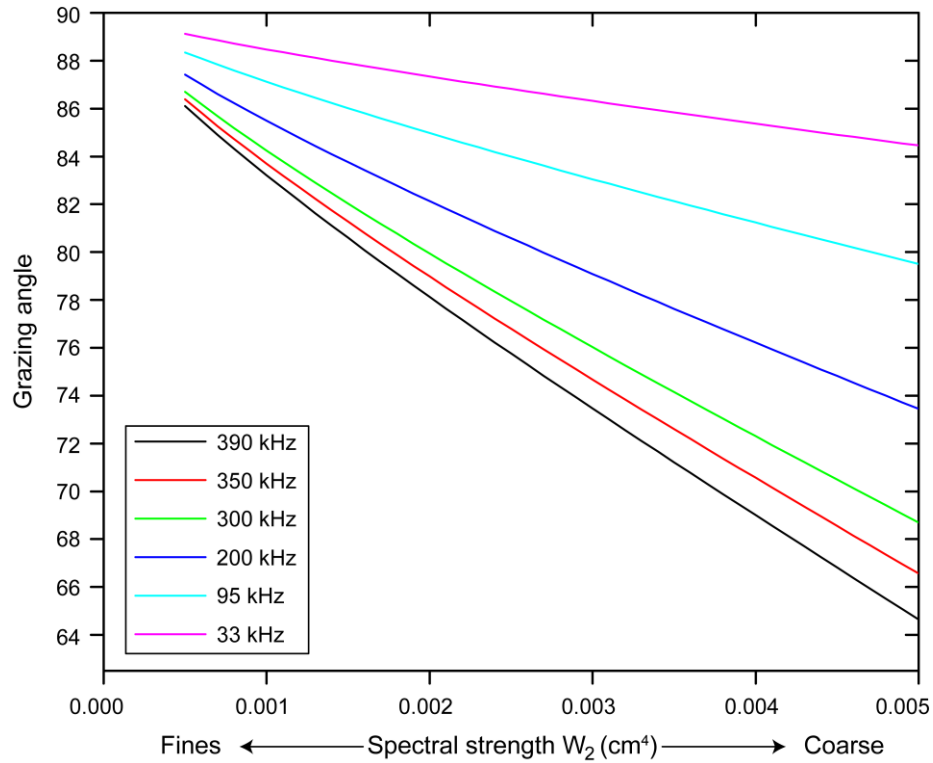


Fig. A.1 The figure depicts the validity of the composite-roughness approximation as a function of the acoustic frequency and spectral strength w_2 .

Bibliography

- Alexandrou, D. and Pantartzis, D.: A methodology for acoustic seafloor classification, *IEEE J. Ocean. Eng.*, 18, 81–86, 1993.
- Amiri-Simkooei, A. R., Snellen, M., and Simons, D. G.: Principal component analysis of single-beam echo-sounder signal features for seafloor classification, *IEEE J. Ocean. Eng.*, 36, 259–271, 2011.
- Anderson, J. T., Gregory, R. S., and Collins, W. T.: Acoustic classification of marine habitats in coastal Newfoundland, *ICES J. Mar. Sci.*, 59, 156–167, 2002.
- Anderson, J. T., Holliday, D. V., Kloser, R., Reid, D. G., and Simard, Y.: Acoustic seabed classification: current practice and future directions, *ICES J. Mar. Sci.*, 65, 1004–1011, 2008.
- Ansari, Z. A., Parulekar, A. H., Harkantra, S. N., and Ayyappan, N.: Shallow water macrobenthos of the central west coast of India, *Mahasagar–Bulletin National Institute of Oceanography*, 10, 123–127, 1977.
- Applied Physics Laboratory: High frequency ocean environmental acoustic models handbook, Technical Report APL-UW TR9407, AEAS 9501, University of Washington, 1994.
- Bak, P., Tang, C., and Wiesenfeld, K.: Self-Organized Criticality: An Explanation of $1/f$ Noise, *Phys. Rev. Lett.*, 59, 381–384, 1987.

- Bhattacharya, G. C. and Chaubey, A. K.: Western Indian Ocean—a glimpse of the tectonic scenario, in: *The Indian Ocean – A Perspective*, edited by: SenGupta, R. and Desa, E., Oxford-IBH, New Delhi, 691–729, 2001.
- Briggs, K. B.: Microtopographical roughness of shallow-water continental shelves, *IEEE J. Ocean. Eng.*, 14, 360–367, 1989.
- Briggs, K. B., Lyons, A. P., Pouliquen, E., Mayer, L. A., and Richardson, M. D.: Seafloor roughness, sediment grain size, and temporal stability, in *Proceedings of the International Conference on Underwater Acoustical Measurements: Technol. Results*, edited by J. P. Papadakis and L. Bjørnø, Heraklion, Crete, 337–344, 2005.
- Brown, C. J. and Blondel, P.: Developments in the application of multibeam sonar backscatter for seafloor habitat mapping, *App. Acoust.*, 70, 1242–1247, 2009a.
- Brown, C. J. and Blondel, P.: Guest editorial: the application of underwater acoustics to seabed habitat mapping, *App. Acoust.*, 70, 1241, 2009b.
- Brown, C. J., Todd, B. J., Kostylev, V. E., and Pickrill, R. A.: Image-based classification of multibeam sonar backscatter data for objective surficial sediment mapping of Georges Bank, Canada, *Cont. Shelf Res.*, 31, S110–S119, 2011.
- Chakraborty, B., Schenke, H. W., Kodagali, V., and Hagen, R.: Sea bottom characterization using multibeam echosounder angular backscatter: An application of the composite roughness theory, *IEEE Trans. Geosci. Remote Sens.*, 38, 2419–2422, 2000.
- Chakraborty, B., Kaustubha, R., Hegde, A., and Pereira, A.: Acoustic seafloor sediment classification using self organizing feature maps, *IEEE Trans. Geosci. Remote Sens.*, 39, 2722–2725, 2001.
- Chakraborty, B., Kodagali, V., and Baracho, J.: Seafloor classification using multibeam echo sounder angular backscatter data: A real time approach employing hybrid neural network architecture, *IEEE J. Oceanic Eng.*, 28, 121–128, 2003.

- Chakraborty, B., Mahale, V., De Sousa, C., and Das, P.: Seafloor classification using echo-waveforms: a method employing hybrid neural network architecture, *IEEE Geosci. Remote Sens. Lett.*, 1, 196–200, 2004.
- Chakraborty, B., Mahale, V., Navelkar, G., Rao, B. R., Prabhudesai, R. G., Ingole, B. S., and Janakiraman, G.: Acoustic characterization of seafloor habitats on the western continental shelf of India, *ICES J. Mar. Sci.*, 64, 551–558, 2007.
- Chakraborty, B., Haris, K., Latha, G., Maslov, N., and Menezes, A.: Multifractal Approach for Seafloor Characterization, *IEEE Geosci. Remote Sens. Lett.*, 11, 54–58, 2014.
- Chakraborty, B., Menezes, A., Dandapath, S., Fernandes, W. A., Karisiddaiah, S. M., Haris, K., and Gokul, G. S.: Application of hybrid techniques (self organizing map and fuzzy algorithm) using backscatter data for segmentation and fine-scale roughness characterization of seepage related seafloor along the western continental margins of India, *IEEE J. Ocean. Eng.*, 40, 3–15, 2015.
- Chhabra, A. B. and Jensen, R. V.: Direct determination of the $f(\alpha)$ singularity spectrum, *Phys. Rev. Lett.*, 62, 1327–1330, 1989.
- Dandapath, S., Chakraborty, B., Karisiddaiah, S. M., Menezes, A., Ranade, G., Fernandes, W., Naik, D. K., and Prudhvi Raju, K. N.: Morphology of pockmarks along the western continental margin of India: employing multibeam bathymetry and backscatter data, *Mar. Petrol. Geol.*, 27, 2107–2117, 2010.
- Dandapath, S., Chakraborty, B., Maslov, N., Karisiddaiah, S. M., Ghosh, D., Fernandes, W., and Menezes, A.: Characterization of seafloor pockmark seepage of hydrocarbons employing fractal: A case study from the western continental margin of India, *Mar. Petrol. Geol.*, 29, 115–128, 2012.
- De, C. and Chakraborty, B.: Acoustic characterization of seafloor sediment employing a hybrid method of neural network architecture and fuzzy algorithm, *IEEE Geosci. Remote Sens. Lett.*, 6, 743–747, 2009.

- De, C. and Chakraborty, B.: Preference of echo features for classification of seafloor sediments using neural networks, *Mar. Geophys. Res.*, 31, 215–221, 2010.
- De, C. and Chakraborty, B.: Model-based acoustic remote sensing of seafloor characteristics, *IEEE Trans. Geosci. Remote Sens.*, 49, 3868–3877, 2011.
- De, C. and Chakraborty, B.: Estimation of mean grain size of seafloor sediments using neural network, *Mar. Geophys. Res.*, 33, 45–53, 2012.
- De, C.: Characterization and classification of seafloor by acoustic method using model-based and model-free techniques, PhD thesis, Goa University, 2010.
- De Falco, G., Tonielli, R., Martino, G. D., Innangi, S., Simeone, S., and Parnum, I.M.: Relationships between multibeam backscatter, sediment grain size and Posidonia oceanic seagrass distribution, *Cont. Shelf Res.*, 30, 1941–1950, 2010.
- de Moustier, C. and Alexandrou, D.: Angular dependence of 12-kHz seafloor acoustic backscatter, *J. Acoust. Soc. Am.*, 90, 522–531, 1991.
- de Moustier, C. and Matsumoto, H.: Seafloor acoustic remote sensing with multibeam echo-sounders and bathymetric sidescan sonar systems, *Mar. Geophys. Res.*, 15, 27–42, 1993.
- Diaz, R. J., Cutter, G. R., and Rhoads, D. C.: The importance of bioturbation to continental slope sediment structure and benthic processes, *Deep-Sea Res. Pt II*, 41, 719–734, 1994.
- Dziak, R. P., Matsumoto, H., and Fox, C. G.: Estimation of seafloor roughness spectral parameters from multi-beam sonar acoustic backscatter data: Axial seamount, Juan de Fuca Ridge, *Geophys. Res. Lett.*, 20, 1863–1866, 1993.
- Fernandes, W. A. and Chakraborty, B.: Multi-beam backscatter image data processing techniques employed to EM 1002 system, in *Proceedings of the International Symposium on Ocean Electronics*, Kochi, India, 93–99, 2009.
- Ferrini, V. L. and Flood, R. D.: The effects of fine-scale surface roughness and grain size on 300 kHz multibeam backscatter intensity in sandy marine sedimentary environments, *Mar. Geol.*, 228, 153–172, 2006.

- Fox, C. G. and Hayes, D. E.: Quantitative methods for analyzing the roughness of the seafloor, *Rev. Geophys.*, 23, 1–48, 1985.
- Freitas, R., Silva, S., Quintino, V., Rodrigues, A. M., Rhynas, K., and Collins, W. T.: Acoustic seabed classification of marine habitats: studies in the western coastal-shelf area of Portugal, *ICES J. Mar. Sci.*, 60, 599–608, 2003.
- Gagnon, J. -S., Lovejoy, S., and Schertzer, D.: Multifractal earth topography, *Nonlin. Processes Geophys.*, 13, 541–570, 2006.
- Garrido, P., Lovejoy, S., and Schertzer, D.: Multifractal processes and self-organized criticality in the large-scale structure of the universe, *Physica A*, 225, 294–311, 1996.
- Gires, A., Tchiguirinskaia, I., Schertzer, D., and Lovejoy, S.: Development and analysis of a simple model to represent the zero rainfall in a universal multifractal framework, *Nonlin. Processes Geophys.*, 20, 343–356, 2013.
- Goff, J. A. and Jordan, T. H.: Stochastic modeling of seafloor morphology: Inversion of sea beam data for second-order statistics, *J. Geophys. Res.*, 93, 13589–13608, 1988.
- Goff, J. A., Kraft, B. J., Mayer, L. A., Schock, S. G., Sommerfield, C. K., Olson, H. C., Gulick, S. P. S., and Nordfjord, S.: Seabed characterization on the New Jersey middle and outer shelf: correlatability and spatial variability of seafloor sediment properties, *Mar. Geol.*, 209, 147–172, 2004.
- Halsey, T. C., Jensen, M. H., Kadanoff, L. P., Procaccia, I., and Shraiman, B. I.: Fractal measures and their singularities: The characterization of strange sets, *Phys. Rev. A*, 33, 1141–1151, 1986.
- Hamilton, L. J. and Parnum, I.: Acoustic seabed segmentation from direct statistical clustering of entire multibeam sonar backscatter curves, *Cont. Shelf Res.*, 31, 138–148, 2011.
- Hammerstad, E.: EM technical note: Backscattering and seabed image reflectivity, Horten, Norway: Kongsberg Maritime AS, p. 5, 2000.

- Haris, K., Chakraborty, B., De, C., Prabhudesai, R. G., and Fernandes, W. A.: Model-based seafloor characterization employing multi-beam angular backscatter data – A comparative study with dual-frequency single beam, *J. Acoust. Soc. Am.*, 130, 3623–3632, 2011.
- Haris, K., Chakraborty, B., Ingole, B. S., Menezes, A., and Srivastava, R.: Seabed habitat mapping employing single and multibeam backscatter data: A case study from the western continental shelf of India, *Cont. Shelf Res.*, 48, 40–49, 2012.
- Haris, K. and Chakraborty, B.: Stochastic formalism-based seafloor feature discrimination using multifractality of time-dependent acoustic backscatter, *Nonlin. Processes Geophys.*, 21, 101–113, 2014.
- Haris, K., Chakraborty, B., Menezes, A., Fernandes, W. A., and Naik, M.: Seafloor micro-roughness, benthic macro-fauna, and sediment substrate: A study of their interrelationship using high-frequency echo-sounding systems, *Indian J. Mar. Sci.*, in press, 2015.
- Hentschel, H. G. E. and Procaccia, I.: The infinite number of generalized dimensions of fractals and strange attractors, *Physica D*, 8, 435–444, 1983.
- Holliday, D. V., Greenlaw, C. F., Rines, J. E. B., and Thistle, D.: Diel variations in acoustical scattering from a sandy seabed, in *Proceedings of the ICES Conference on 22–25 September 2004*, Vigo, 2004.
- Holliday, D. V.: Theory of sound scattering from the seabed, *ICES Coop. Res. Rep.*, 286, 7–28, 2007.
- Hooge, C., Lovejoy, S., Schertzer, D., Pecknold, S., Malouin, J. -F., and Schmitt, F.: Multifractal phase transitions: the origin of self-organized criticality in earthquakes, *Nonlin. Processes Geophys.*, 1, 191–197, 1994.
- Hovland, M. and Judd, A. G.: Seabed Pockmarks and Seepages: Impact on Geology, Biology and the Marine Environment, Graham & Trotman, London, 1988.
- Ierodiaconou, D., Monk, J., Rattray, A., Laurenson, L., and Versace, V. L.: Comparison of automated classification techniques for predicting benthic

- biological communities using hydroacoustics and video observations, *Cont. Shelf Res.*, 31, S28–S38, 2011.
- Ingole, B. S., Rodrigues, N., and Ansari, Z. A.: Macrobenthic communities of the coastal waters of Dhabol, west coast of India, *Indian J. Mar. Sci.*, 31, 93–99, 2002.
- Ingole, B. S., Sautya, S., Sivadas, S., Singh, R., and Nanajkar, M.: Macrofaunal community structure in the western Indian continental margin including the oxygen minimum zone, *Mar. Ecol-Evol Persp.*, 31, 148–166, 2010.
- Ivakin, A. N. and Sessarego, J.-P.: High frequency broad band scattering from water-saturated granular sediments: Scaling effects, *J. Acoust. Soc. Am.*, 122, EL165–EL171, 2007.
- Ivanov, P. C., Nunes Amaral, L. A., Goldberger, A. L., Havlin, S., Rosenblum, M. G., Struzik, Z. R., and Stanley, H. E.: Multifractality in human heartbeat dynamics, *Nature*, 399, 461–465, 1999.
- Jackson, D. R., Winebrenner, D. P., and Ishimaru, A.: Application of the composite roughness model to high-frequency bottom backscattering, *J. Acoust. Soc. Am.*, 79, 1410–1422, 1986.
- Jackson, D. R. and Briggs, K. B.: High-frequency bottom backscattering: Roughness vs. sediment volume scattering, *J. Acoust. Soc. Am.*, 92, 962–977, 1992.
- Jackson, D. R., Briggs, K. B., Williams, K. L., and Richardson, M. D.: Test of models for high-frequency seafloor backscatter, *IEEE J. Ocean. Eng.*, 21, 458–470, 1996a.
- Jackson, D. R., Williams, K. L., and Briggs, K. B.: High-frequency acoustic observations of benthic spatial and temporal variability, *Geo-Mar. Lett.*, 16, 212–218, 1996b.
- Jackson, D. R. and Richardson, M. D.: High-Frequency Seafloor Acoustics, Springer-Verlag, New York, 2007.

- Jayaraj, K. A., Jayalakshmi, K. V., and Saraladevi, K.: Influence of environmental properties on macrobenthos in the northwest Indian shelf, *Environ. Monit. Assess.*, 127, 459–475, 2007.
- Jayaraj, K. A., Sheeba, P., Josia Jacob, J., Revichandran, C., Arun, P. K., Praseeda, K. S., Nisha, P. A., and Rasheed, K. A.: Response of infaunal macrobenthos to the sediment granulometry in a tropical continental margin-southwest coast of India, *Estuar. Coast. Shelf S.*, 77, 743–754, 2008.
- Jones, C. D. and Jackson, D. R.: Scattering due to bioturbation in marine sediments, *J. Acoust. Soc. Am.*, 104, 1813–1813, 1998.
- Jumars, P. A., Jackson, D. R., Gross, T. F., and Sherwood, C.: Acoustic remote sensing of benthic activity: a statistical approach, *Limnol. Oceanogr.*, 41, 1220–1241, 1996.
- King, L. H. and MacLean, B.: Pockmarks on the Scotian shelf, *Geol. Soc. Am. Bull.*, 81, 3141–3148, 1970.
- Kloser, R. J., Bax, N. J., Ryan, T., Williams, A., and Barker, B. A.: Remote sensing of seabed types in the Australian South East Fishery; development and application of normal incident acoustic techniques and associated ‘ground truthing’, *Mar. Freshwater Res.*, 52, 475–489, 2001.
- Kloser, R. J., Penrose, J. D., and Butler, A. J.: Multi-beam backscatter measurements used to infer seabed habitats, *Cont. Shelf Res.*, 30, 1772–1782, 2010.
- Kogure, K. and Wada, M.: Impacts of macro-benthic bioturbation in marine sediment on bacterial metabolic activity, *Microbes Environ.*, 20, 191–199, 2005.
- Lovejoy, S. and Schertzer, D.: Multifractal, universality classes, satellite and radar measurements of clouds and rain, *J. Geophys. Res.*, 95, 2021–2034, 1990.
- Lovejoy, S., Currie, W. J. S., Tessier, Y., Claereboudt, M. R., Bourget, E., Roff, J. G., and Schertzer, D.: Universal multifractals and ocean patchiness: phytoplankton, physical fields and coastal heterogeneity, *J. Plankton Res.*, 23, 117–141, 2001.

- Lovejoy, S. and Schertzer, D.: Scale, scaling and multifractals in geophysics: Twenty years on, *Nonlin. Dynam. Geosci.*, 311–337, 2007a.
- Lovejoy, S. and Schertzer, D.: Scaling and multifractal fields in the solid earth and topography, *Nonlin. Processes Geophys.*, 14, 465–502, 2007b.
- Lovejoy, S., Agterberg, F., Carsteanu, A., Cheng, Q., Davidsen, J., Gaonac’h, H., Gupta, V., L’Heureux, I., Liu, W., Morris, S. W., Sharma, S., Shcherbakov, R., Tarquis, A., Turcotte, D., and Uritsky, V.: Nonlinear Geophysics: Why We Need It, *Eos Trans. AGU*, 90, 455–456, 2009a.
- Lovejoy, S., Schertzer, D., Allaire, V., Bourgeois, T., King, S., Pinel, J., and Stolle, J.: Atmospheric complexity or scale by scale simplicity, *Geophys. Res. Lett.*, 36, 1–6, 2009b.
- Lurton, X., Dugelay, S., and Augustin, J. M.: Analysis of multibeam echosounder signals from the deep seafloor, in *Proceedings of IEEE Oceans ’94*, Brest, France, 213–218, 1994.
- Lurton, X.: An Introduction to Underwater Acoustics: Principle and Applications, PRAXIS, Chichester, 2002.
- Madricardo, F., Tegowski, J., and Donnici, S.: Automated detection of sedimentary features using wavelet analysis and neural networks on single beam echosounder data: A case study from the Venice Lagoon, Italy, *Cont. Shelf Res.*, 43, 43–54, 2012.
- Malinverno, A.: Segmentation of topographic profiles of the seafloor based on a self-affine model, *IEEE J. Ocean. Eng.*, 14, 348–358, 1989.
- Mandelbrot, B. B.: How long is the coastline of Britain? Statistical self-similarity and fractional dimension, *Science*, 155, 636–638, 1967.
- Mandelbrot, B. B.: Multifractal measures, especially for the geophysicist, *Pageoph*, 131, 5–42, 1989.
- Manly, B. F. J.: Multivariate Statistical Methods, Chapman & Hall, 1994.

- Matsumoto, H., Dziak, R. P., and Fox, C. G.: Estimation of seafloor microtopographic roughness through modeling of acoustic backscatter data recorded by multi-beam systems, *J. Acoust. Soc. Am.*, 94, 2776–2787, 1993.
- McDaniel, S. T. and Gorman, A. D.: Acoustic and radar sea surface backscatter, *J. Geophys. Res.*, 87, 4127–4136, 1982.
- McGonigle, C., Brown, C., Quinn, R., and Grabowski, J.: Evaluation of image-based multibeam sonar backscatter classification for benthic habitat discrimination and mapping at Stanton Banks, UK., *Estuar. Coast. Shelf S.*, 81, 423–437, 2009.
- Michalopoulou, Z. H., Alexandrou, D., and de Moustier, C.: Application of neural and statistical classifiers to the problem of seafloor characterization, *IEEE J. Ocean. Eng.*, 20, 190–197, 1995.
- Mortensen, P. B., Dolan, M., and Buhl-Mortensen, L.: Prediction of benthic biotopes on a Norwegian offshore bank using a combination of multivariate analysis and GIS classification, *ICES J. Mar. Sci.*, 66, 2026–2032, 2009.
- Parulekar, A. H.: Quantitative distribution of benthic fauna on the inner shelf of central west coast of India, *Indian J. Mar. Sci.*, 2, 113–115, 1973.
- Pouliquen, E. and Lurton, X.: Sea-bed identification using echo-sounder signals, in *European Conference on Underwater Acoustics*, edited by M. Weydert (Elsevier Applied Science, London), 535–538, 1992.
- Pouliquen, E. and Lyons, A. P.: Backscattering from bioturbated sediments at very high frequency, *IEEE J. Ocean. Eng.*, 27, 388–402, 2002.
- Pouliquen, E.: Depth dependence correction for normal incidence echo sounding, in *Proceedings of the Seventh European Conference on Underwater Acoustics, ECUA 2004*, Delft, The Netherlands, 2004.
- Quintino, V., Freitas, R., Mamede, R., Ricardo, F., Rodrigues, A. M., Mota, J., Pe´rezRuzafa, A´., and Marcos, C.: Remote sensing of underwater vegetation using single-beam acoustics, *ICES J. Mar. Sci.*, 67, 594–605, 2009.

- Sanders, H. L.: Benthic studies in Buzzards Bay. I. Animal–sediment relationships, *Limnol. Oceanogr.*, 3, 245–258, 1958.
- Schertzer, D. and Lovejoy, S.: Physical modeling and analysis of rain and clouds by anisotropic scaling multiplicative processes, *J. Geophys. Res.*, 92, 9693–9714, 1987.
- Schertzer, D. and Lovejoy, S.: Nonlinear geodynamical variability: multiple singularities, universality and observables, in: *Nonlinear Variability in Geophysics*, edited by: Schertzer, D. and Lovejoy, S., Kluwer Academic Publishers, Netherlands, 41–82, 1991.
- Schertzer, D. and Lovejoy, S.: Hard and soft multifractal processes, *Physica A*, 185, 187–194, 1992.
- Schertzer, D., Lovejoy, S., and Lavalée, D.: Generic multifractal phase transitions and self-organized criticality, in: *Cellular Automata: Prospects in Astrophysical Application*, edited by: Perchang, J. M. and Lejeune, A., World Scientific, Singapore, 216–227, 1993.
- Schertzer, D. and Lovejoy, S.: Universal multifractals do exist!, *J. Appl. Meteorol.*, 36, 1296–1303, 1997.
- Schmitt, F., Schertzer, D., Lovejoy, S., and Brunet, Y.: Empirical study of multifractal phase transitions in atmospheric turbulence, *Nonlin. Processes Geophys.*, 1, 95–104, 1994.
- Seuront, L., Schmitt, F., Lagadeuc, Y., Schertzer, D., and Lovejoy, S.: Universal multifractal analysis as a tool to characterize multiscale intermittent patterns: Example of phytoplankton distribution in turbulent coastal waters, *J. Plankton Res.*, 21, 877–922, 1999.
- Seuront, L. and Spilmont, N.: Self-organized criticality in intertidal microphytobenthos patch patterns, *Physica A*, 313, 513–539, 2002.
- Seuront, L.: *Fractals and Multifractals in Ecology and Aquatic Science*, New York, USA, CRC Press, 2010.

- Shepard, F. P.: Nomenclature based on sand–silt–clay ratios, *J. Sediment. Petrol.*, 24, 151–158, 1954.
- Simons, D. G. and Snellen, M.: A Bayesian approach to seafloor classification using multi-beam echo-sounder backscatter data, *App. Acoust.*, 70, 1258–1268, 2009.
- Snellen, M., Siemes, K., and Simons, D.: Model-based sediment classification using single-beam echosounder signal, *J. Acoust. Soc. Am.*, 129, 2878–2888, 2011.
- Snellen, M., Eleftherakis, D., Amiri-Simkooei, A., Koomans, R. L., and Simons, D. G.: An inter-comparison of sediment classification methods based on multi-beam echo-sounder backscatter and sediment natural radioactivity data, *J. Acoust. Soc. Am.*, 134, 959–970, 2013.
- Stanic, S., Briggs, K. B., Fleischer, P., Sawyer, W. B., and Ray, R. I.: High-frequency acoustic backscattering from a coarse shell ocean bottom, *J. Acoust. Soc. Am.*, 85, 125–136, 1989.
- Stanley, H. E., Amral, L. A. N., Goldberger, A. L., Havlin, S., Ivanov, P. Ch., and Peng, C. -K.: Statistical physics and physiology: Monofractal and multifractal approaches, *Physica A*, 270, 309–324, 1999.
- Stanton T. K., Chu D., Wiebe P. H., Eastwood R. L., and Warren J. D.: Acoustic scattering by benthic and planktonic shelled animals, *J. Acoust. Soc. Am.*, 108, 535–550, 2000.
- Sternlicht, D. D. and de Moustier, C. P.: Temporal modeling of high frequency (30–100 kHz) acoustic seafloor backscatter: Shallow water results, in *Proceedings of High Frequency Acoustics in Shallow Water*, edited by N. G. Pace, E. Poliquen, O. Bergen, and A. P. Lyons (NATO SACLANT Undersea Res. Ctr., La Spezia, Italy), 509–516, 1997.
- Sternlicht, D. D. and de Moustier, C. P.: Time dependent seafloor acoustic backscatter (10–100 kHz), *J. Acoust. Soc. Am.*, 114, 2709–2725, 2003a.

- Sternlicht, D. D. and de Moustier, C. P.: Remote sensing of sediment characteristics by optimized echo-envelope matching, *J. Acoust. Soc. Am.*, 114, 2727–2743, 2003b.
- Stewart, R. A. and Chotiros, N. P.: Estimation of sediment volume scattering cross section and absorption loss coefficient, *J. Acoust. Soc. Am.*, 91, 3242–3247, 1992.
- Stolle, J., Lovejoy, S., and Schertzer, D.: The stochastic multiplicative cascade structure of deterministic numerical models of the atmosphere, *Nonlin. Processes Geophys.*, 16, 607–621, 2009.
- Sutherland, T. F., Galloway, J., Loschiavo, R., Levings, C. D., and Hare, R.: Calibration techniques and sampling resolution requirements for groundtruthing multibeam acoustic backscatter (EM3000) and QTC VIEW classification technology, *Estuar. Coast. Shelf S.*, 75, 447–458, 2007.
- Szczepaniak, A. and Macek, W. M.: Asymmetric multifractal model for solar wind intermittent turbulence, *Nonlin. Processes Geophys.*, 15, 615–620, 2008.
- Tegowski, J. and Łubniewski, Z.: The use of fractal properties of echo signals for acoustic classification of bottom sediments, *Acta Acust.*, 86, 276–282, 2000.
- Tegowski, J., Gorska, N., and Klusek Z.: Statistical analysis of acoustic echoes from underwater meadows in the eutrophic Puck Bay, *Aquat. Living Resour.*, 16, 215–221, 2003.
- Tegowski, J.: Acoustical classification of the bottom sediments in the southern Baltic Sea, *Quatern. Int.*, 130, 153–161, 2005.
- Telesca, L., Colangelo, G., Lapenn, V., and Macchiato, M.: Monofractal and multifractal characterization of geoelectrical signals measured in southern Italy, *Chaos Solition Fract.*, 18, 385–399, 2003.
- Thorsos, E. I., Williams, K. L., Chotiros, N. P., Christoff, J. T., Commander, K. W., Greenlaw, C. F., Holliday, D. V., Jackson, D. R., Lopes, J. L., McGehee, D. E., Piper, J. E, Richardson, M. D., and Tang, D.: An overview of SAX99: Acoustic measurements, *IEEE J. Ocean. Eng.*, 26, 4–25, 2001.

- Urlick, R. J.: Principles of Underwater Sound, McGraw-Hill, New York, 1983.
- van Walree, P. A., Tegowski, J., Laban, C., and Simons, D. G.: Acoustic seafloor discrimination with echo shape parameters: a comparison with the ground truth, *Cont. Shelf Res.*, 25, 2273–2293, 2005.
- van Walree, P. A., Ainslie, M. A., and Simons, D. G.: Mean grain size mapping with single-beam echo sounders, *J. Acoust. Soc. Am.*, 120, 2555–2566, 2006.
- Williams, K. L., Jackson, D. R., Thorsos, E. I., Tang, D., and Briggs, K. B.: Acoustic backscattering experiments in a well characterized sand sediments: Data/model comparisons using sediment fluid and Biot models, *IEEE J. Ocean. Eng.*, 27, 376–387, 2002.
- Williams, K. L., Jackson, D. R., Tang, D., Briggs, K. B., and Thorsos, E. I.: Acoustic backscattering from a sand and a sand/mud environment: Experiments and data/model comparisons, *IEEE J. Ocean. Eng.*, 34, 388–398, 2009.
- Williams, K. L., Thorsos, E. I., Jackson, D. R., and Hefner, B. T.: Thirty years of sand acoustics: A perspective on experiments, models and data/model comparisons, in *ADVANCES IN OCEAN ACOUSTICS: Proceedings of the 3rd International Conference on Ocean Acoustics (OA2012)*, AIP Conf. Proc. No. 1495, 166–192, 2012.